Radiometric Adjustment of Aerial Imagery

Miriam MN Nærum

Kongens Lyngby 2014
DTU Compute-M.Sc.-2014

Technical University of Denmark
Department of Applied Mathematics and Computer Science
Matematiktorvet, Building 303B, DK-2800 Kongens Lyngby, Denmark
Phone +45 45253031, Fax +45 45881399
reception@compute.dtu.dk
www.compute.dtu.dk DTU Compute-M.Sc.

Abstract

The goal of this thesis is to develop a colour correction to a number of overlapping aerial photographs.

Maps created from aerial photographs are used for many practical purposes, for instance environmental investigations and city planning. In order to make maps of large areas, a mosaic from several photographs is created, and therefore the colours in the images should match to avoid visible seamlines between them.

COWI A/S has provided 22 overlapping orthophotos from aerial photos, which are used to investigate different methods of radiometric colour correction.

Three different methods are investigated: Global histogram matching, global pixelwise matching, and global gradual matching.

In histogram matching the histograms in two neighbouring orthophotos are matched, and a linear transformation is estimated for each of the 22 orthophotos simultaneously in global histogram matching.
Then global pixelwise matching, where linear transformations are estimated by simple pixelwise correspondence, is investigated.
The third method described is global gradual matching, where the colour correction is performed under the assumption that there is a gradual change in colours over each orthophoto. In global gradual matching the results are improved by using boundary conditions and change detection.

Change detection is used to remove pixels that contain e.g. moving objects, or tall objects photographed from different angles, from the model estimation. In all three models a regularization term is added, such that a colour transformation, which is too large, does not occur.

In order to evaluate the quality of the results three measures are defined: The seamline measure, the saturation, and the contrast.

Experiments are performed to determine the optimal regularization, which show that it should be chosen as a trade-off, between making the seamlines less distinct, and obtaining a too low contrast for global histogram matching and global pixelwise matching. For global gradual matching the connection between the regularization of the model coefficients, the regularization used on the colour change in the boundary, and change detection is investigated.

The experiments show that the best results are obtained, when global gradual matching is used with boundary conditions and change detection.

Resumé

Målet med dette speciale er at udvikle metoder til farvekorrektion til flere overlappende luftfotos.

Kort dannet ved hjælp af luftfotos bliver brugt til mange praktiske formål, for eksempel til miljøundersøgelser og byplanlægning. For at lave kort over større områder, dannes en mosaik ud fra flere fotografier, og derfor bør farverne i billederne matche for at undgå synlige seamlines mellem dem.

COWI A/S har stillet 22 overlappende ortofotos fra luftfotos til rådighed til brug for undersøgelserne i projektet.

Tre forskellige metoder undersøges: Global histogrammatching, global pixelvis matching og global gradvis matching.

I histogrammatching matches histogrammerne i to nabobilleder, og en lineær transformation bliver estimeret for hvert af de 22 ortofotos samtidigt, og dette er grundlaget for den første metode, global histogrammatching.
Den næste metode, der undersøges, er global pixelvis matching, hvor lineære transformationer estimeres ud fra en simpel pixel-til-pixel matching.
Den tredje metode, der er beskrevet, er global gradvis matching, hvor farvekorrektionen udføres under antagelse af, at der er en gradvis farveovergang i hvert ortofoto. I global gradvis matching bliver resultaterne forbedret ved brug af randbetingelser og change detection.

Change detection bruges til at fjerne pixels, som indeholder for eksempel objekter, der flytter sig, eller høje objekter der fotograferes fra forskellige vinkler, så der ses bort fra disse pixels i estimeringen af modellen. I alle tre modeller tilføjes regulering, således at der ikke opstår for stor farvetransformation.

For at bestemme kvaliteten af resultaterne defineres tre mål: Seamline measure, saturation, og kontrast.

Den optimale regulering bestemmes ved hjælp af en række eksperimenter, som viser, at reguleringen bør vælges som et kompromis mellem at gøre seamlines mindre synlige, mod at kontrasten bliver for lav ved global histogrammatching og ved global pixelvis matching. For global gradvis matching bliver sammenhængen mellem reguleringen af modellens koefficienter, reguleringen fra randbetingelserne og change detection undersøgt.

Eksperimenterne viser, at de bedste resultater findes, når global gradvis matching benyttes med randbetingelser og change detection.

Preface

This thesis was prepared at Department of Applied Mathematics and Computer Science at the Technical University of Denmark in fulfilment of the requirements for acquiring an M.Sc. in Mathematical Modelling and Computing. The thesis was produced in collaboration with COWI A/S, Parallelvej 2, DK-2800 Kongens Lyngby.

The thesis deals with radiometric colour adjustment in orthophotos developed from aerial photos.

The thesis is structured as follows: There is an introduction in Chapter 1, Chapter 2 contains a description of previous work, and in Chapter 3 there is a description of the used data. Then follows Chapter 4 with the theory of the methods for colour correction. In Chapter 5 these methods are investigated by performing several experiments, and the results are then discussed in Chapter 7. In Chapter 6 some suggestions for future development are presented. The conclusions are listed in Chapter 8. Finally at the end of the thesis is the appendix and the bibliography.

Lyngby, 02-January-2014

Miriam MN Nærum

Acknowledgements

I would like to thank my supervisor associate professor Henrik Aanæs and associate professor Anders Bjorholm Dahl from Department of Applied Mathematics and Computer Science. I would also like to thank chief specialist Søren Andersen, engineer, consultant, coordinator Regin Møller Sørensen, and project director Søren Vosgerau Jespersen from COWI A/S, technical director David Child from COWI Mapping UK, and geospatial software developer Lars Hansen from CDT3 Ltd.

Contents

Chapter 1

Introduction

In many situations it is relevant to use a graphical map showing details of an area. Graphical maps are used for instance by local authorities to find unauthorized buildings as house extensions, sheds etc., for construction of roads and railways, by farmers to document field boundaries, to measure vegetation e.g. rosehip or hogweed for removing weed, and investigations to protect the environment. Furthermore the graphical maps provides basis for construction of technical maps and aerial maps. [16] [8]

A graphical map is created from a number of aerial photographs. These photographs are taken from a plane, flying over the desired area a number of times, taking a number of overlapping photos. The different light and weather conditions during the flight cause large changes in the colours in the aerial photographs, and when they are combined, some will have different colours than others, although they may cover some of the same area as illustrated in Figure 1.1. The differences will be seen as distinct lines, called seamlines, between neighbouring photographs. Furthermore, the differences may be seen as different shadows in images showing the same area, see Figure 1.3. Another problem is that moving objects may not have the same position in two overlapping images, see Figure 1.2.

(a) *Orthophoto 3*

(b) *Orthophoto 11*

(c) *Orthophoto 3 and 11*

Figure 1.1: *The figure shows the seamline between two orthophotos in a small area of the graphical map. The black area in (a) is outside orthophoto 3.*

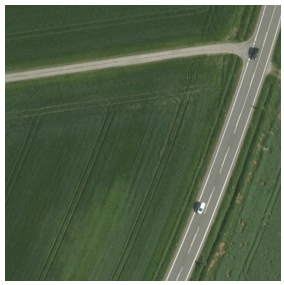

(a) *Orthophoto 5*

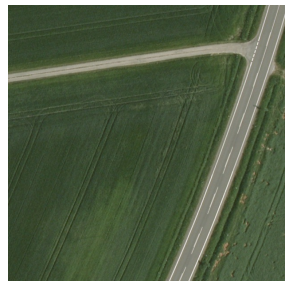

(b) *Orthophoto 6*

Figure 1.2: *Small area of two images showing a moving object.*

(a) *Orthophoto 18* **(b)** *Orthophoto 20*

Figure 1.3: *Small area of two images showing trees photographed from different angles.*

In this thesis, a number of methods for correcting the colours, in order to remove the differences between the photos, will be investigated. Only radiometric colour correction is investigated, i.e. the colour correction is only estimated from the pixels in the images and no information about e.g. the time of day, the position of the air plane, weather, etc. is taken into account. Some colour correction have been performed on the data initially by COWI A/S, based on non-radiometric information.

Before correcting the colours in the images, an orthorectification is performed. This is a process, in which the aerial photos are transformed into orthophotos, which have the property that in every pixel the photo appears to be taken from directly above [5]. Each orthophoto is also georeferenced, which means that the geographical positions of the orthophotos are found [20]. The overlapping orthophotos are then combined into a single image of the entire area by using a mosaicking method.

In this thesis the used colour correction methods are based on evaluation of the overlap between neighbouring orthophotos. An algorithm is used to exclude some of the overlaps to reduce the necessary amount of data, using either 4 or 8 neighbouring orthophotos for each orthophoto. A method is presented, which uses the colour histogram in the overlaps to match neighbouring orthophotos.

The global histogram matching algorithm is presented, as an algorithm which matches all the used overlaps simultaneously. This algorithm is compared to an algorithm called global pixelwise matching. Global pixelwise matching matches each pair of pixels in the overlaps instead. The third algorithm presented is based on the assumption that there is a linear change in the light from one side

of an orthophoto to the other caused by the position of the sun. This means that the correction is performed by transformation of the colour values, using a bilinear function for each orthophoto.

In order to be able to compare the results a quantification method is developed, by using three measures consisting of a measure to quantify visibility of seamlines, a measure of the saturation, and a measure of the contrast. Another measure, residuals, is provided in order to quantify the colour differences locally. This is a spatial measure of the colour differences, based on the standard deviation.

In the correction methods change detection is used to remove objects that have moved, and therefore have different positions in different orthophotos. Furthermore boundary conditions can be added to global gradual matching.

The results are computed using aerial photographs, taken over a small area of Bornholm, provided by COWI A/S.

Figure 1.4: *The original test area*

Chapter 2

Previous Work

Colour correction of aerial photographs has been investigated in earlier projects and scientific papers.

A number of requirements to ensure acceptable orthophotos is stated by a task group under Geoforum Denmark in [2] and by Ordnance Survey in [10]. There are demands for e.g. the size of the overlap between the images, geometric quality, the contrast, and the resolution. In [2] there is also a description of the basic methods used for mosaicking and feathering.
A colour transformation from RGB (Red, Green, and Blue) to HSV (Hue, Saturation, and Value) is presented by Naoum et al. in [9] and Tsai et al. in [18] as a tool used for different methods of image colour enhancement.

The change detection method, Iterative Reweighted Multivariate Alteration Detection (IR-MAD), which uses canonical correlation analysis to maximize the difference between overlapping images, has been described by Aasbjerg Nielsen in [11]. A linear multivariate alteration detection transformation is created, which highlights the areas with low correlation. For each pixel, the probability that a change has occurred, is calculated and used as a weight for each pixel. The weights are updated in each iteration of the IR-MAD algorithm. The method is invariant to linear transformations between the colours of the overlapping images caused by e.g. weather, sunlight, or other changes.

Mosaicking is used to merge orthophotos to form a mosaic, such that the seamlines between overlapping orthophotos are as indistinct as possible. Different mosaicking methods are discussed by Ødegaard Nielsen in [12]. Ødegaard Nielsen also describes a method of feathering to decrease the visibility of seam-

lines.

Colour adjustment of overlapping orthophotos has previously been investigated by Ødegaard Nielsen in [12] by matching the histograms of a pair of overlapping orthophotos. The overlapping areas are transformed by matching their histograms to obtain a linear transformation. Rasmussen has extended the method in [15] to match a grid of overlapping orthophotos iteratively. A further extension is presented namely global histogram matching by matching a number of overlapping images simultaneously. Regularization is used to prevent the images from changing too much compared to the original colours. An example is presented, which proposes to use image segmentation, and make different colour transformations for the different classes to obtain a higher saturation. It is also suggested to let the transformation vary over each orthophoto.
In order to determine the quality of the results from colour correction a panel test is used to evaluate the results manually in [15].

A method for removing scan-angle distortion caused by different illumination, atmospheric conditions and reflective properties of objects is proposed by Palubinskas et al. in [13]. The method is a correction algorithm, which is used for line scanner images made with a wide field of view. A model is presented that calculates the radiance of an object as a function of the scan angle. The image is initially classified using an unsupervised classification method, and linear regression is performed from the resulting clustering in order to estimate the needed parameters.

An approach to find the optimal seamline between two images has been investigated by Sadeghi et al. [17]. Different weight functions have been tested and the best candidate is for each pixel p given by

$$W(p) = \|\nabla X_{ij}(p) - \nabla X_{ji}(p)\|_1^1 \quad , \tag{2.1}$$

where X_{ij} is the overlap between orthophoto i and j in orthophoto i and X_{ji} is the corresponding overlap in orthophoto j. This weight function is preferred since it is robust even if orthophoto i and j have different light conditions.
A method for making a colour correction in the overlap is presented. A correction function on the overlapping area is estimated by solving Poisson's Equation with different boundary conditions.

Chapter 3

Data

This section contains a description of the data provided by COWI A/S. There is a definition of the used notation and an overview of the provided orthophotos. Furthermore, some challenges with aerial photography are presented, due to e.g. flight position and shadows.

Throughout this thesis a number of images are used to test the different approaches in order to adjust the colours to form a geographical map. These images are provided by COWI A/S and consist of 22 orthophotos. The orthophotos are constructed by performing orthorectification, where geometric distortion is removed and a topographic relief is used to make a planimetric geometry [5]. This means that any area of an orthophoto appears to be photographed from orthogonally above.

The data is provided in 4361 RGB images of 625 by 625 pixels called tiles. The tiles are placed in a chess board pattern with no overlaps. Each orthophoto consists of a number of tiles as shown in Figure 3.1.

Figure 3.1: *The figure shows orthophoto no. 2 with the tiles marked by a dark red grid. The tiles outside the orthophoto are marked in black.*

In this project the following definitions will be used:

- Orthophoto no. i is defined as X_i
- The overlap between orthophoto i and j in orthophoto i is defined as X_{ij}
- The overlap between orthophoto i and j in orthophoto j is defined as X_{ji}

as illustrated in Figure 3.2. Orthophoto i is represented by a $3 \times n_i$ matrix X_i, where each row contains the pixel values of one of the three colour bands, and n_i is the number of pixels in orthophoto i. X_{ij} is a $3 \times n_{ij}$ matrix, where n_{ij} is the number of pixels in the overlap.

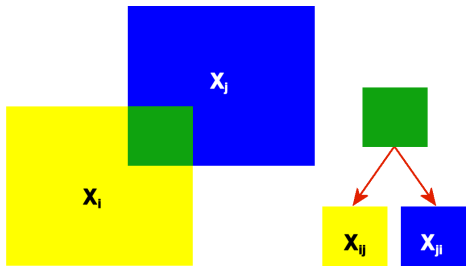

Figure 3.2: *The figure illustrates the definitions of variables that define orthophotos and the corresponding overlaps.*

3.1 Data Overview

In order to get an overview of the provided data it is investigated which orthophotos the data set consists of. For this purpose a 3D-matrix $D \in \mathbb{N}^{n_r \times n_c \times n_v}$ is constructed, where $n_r \times n_c$ denotes the size of the area, denoted in tiles, and n_v is the number of orthophotos. From this matrix it is observed that there are 22 orthophotos, and they are situated as shown in Figure 3.3. In the figure each orthophoto is represented by a colour, and consequently the overlaps are shown with colours, which are combinations of these colours. In this example parts of the tiles are not covered by the orthophoto, and they are therefore black or white. This will be taken into consideration in the calculations by using masks to exclude these areas.

It is deduced from the figure that the data is a segment of the route of an air plane, and that the data consists of 3 parallel lanes, as shown by the arrows in Figure 3.4.

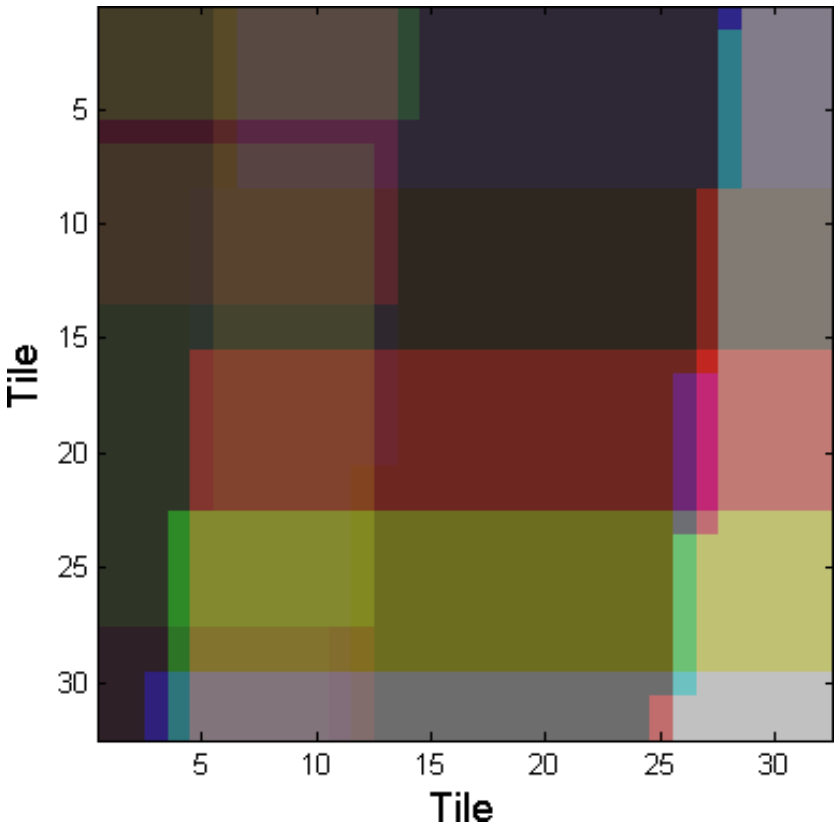

Figure 3.3: *The figure shows how the* 32×32 *tiles are situated in different orthophotos. Each colour marks a different orthophoto.*

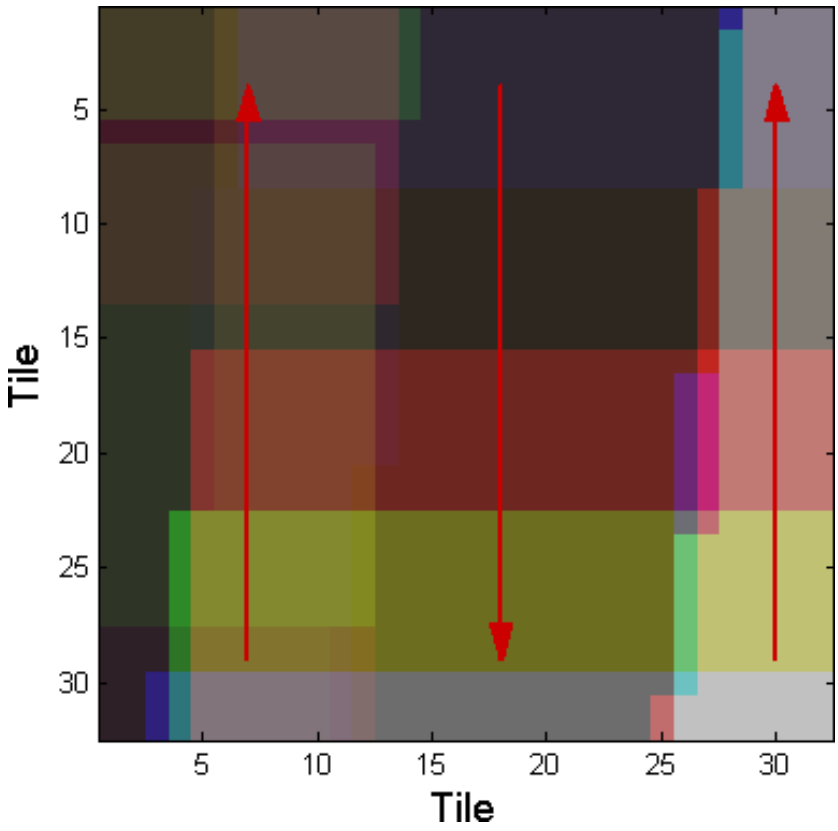

Figure 3.4: *The figure shows how the tiles are situated in different orthophotos. Each colour marks a different orthophoto and the direction of the 3 lanes in the route of the air plane is shown in red arrows.*

3.2 Aerial Photos

In order to construct graphical maps, a number of aerial photos are taken by flying over the desired area a number of times, taking a number of overlapping photos. These overlapping photos are then transformed into orthophotos, which have the property that in every pixel the photo appears to be taken from directly above, as described at the beginning of this chapter. The overlapping orthophotos are then combined into a single image of the entire area by using a mosaicking method, as described in Section 4.1.
Orthophotos are taken at different times of the day and different times of the

year, and under different weather conditions. This means that some orthophotos are brighter than others that cover the same area. For this reason the combined graphical map will clearly show the borders between the different orthophotos. The photographs are taken, such that there is a large overlap between images within the same lane, and a smaller overlap between images in different lanes. Different demands can be set for the quality. For instance it is specified by Ordnance Survey [10] that they require a minimum of 55% within flight lanes, and a minimum of 20% between flight lanes.

The time of day can have much effect on the colours in orthophotos. The only light source used for the imaging is the sun, and therefore the colours in the image are dependent on the relative angle to the sun. Different angles relative to the sun will change the overall brightness of the image.

An object with a reflective surface will appear brighter, when the air plane is positioned, such that the angle of incidence, i.e. the angle between the line from the sun to a reflective object and the normal of the object surface, is equal to the angle of reflection, i.e. the angle between the line from the plane to the reflective object and the normal of the object surface. Therefore such an object will appear differently, depending on the position of the plane. An example of such an object could e.g. be a tin roof, which is highly reflective and not parallel to the ground. [12]

A similar problem can arise, if a tall object, e.g. a building or a tree, is photographed from different angles. From one angle the object will cover more of its shadow and the ground than from another angle. This is illustrated in Figure 3.5.

(a) *Orthophoto 19* **(b)** *Orthophoto 9*

Figure 3.5: *A single tile from two different orthophotos taken at different angles.*

Another part of the colour adjustment is that it is important to avoid over- and underexposed areas. If a reflective surface becomes so bright that the structure is indistinguishable or if a shadow becomes so dark that it is impossible to observe any details on the ground, the image is not acceptable [8]. An example of too dark a shadow is shown in Figure 3.6 where it is very difficult to distinguish the ground from the part of the roof that lies in shadow.

Figure 3.6: *A small part of orthophoto 11 where the shadow on the roof and on the rightmost part of the courtyard are indistinguishable*

Chapter 4

Method

In this chapter the theory for some methods for radiometric colour correscion are described.

Initially the theory of mosaicking and histogram matching is presented as a tool for the three developed colour correction methods: Global histogram matching, global pixelwise matching, and global gradual matching. The theory behind each of these methods is described, and two methods, used to improve the results, are specified. Finally some quality measures are presented.

4.1 Mosaicking

Mosaicking has a large influence on the quality of the resulting graphical map, since it determines the position of the seamlines. For practical use minimum cost methods are used to place the seamlines, and feathering is used to disguise seamlines, but in this thesis a crude mosaicking algorithm is used without feathering. The mosaicking in this thesis is performed using masks that determines the position of the data in the tiles. The computational time is reduced by downsampling the tiles.

In order to make a map of a large area, a number of orthophotos are combined. This process is called mosaicking, and it has great influence on the result. If there is too large a difference between two orthophotos, where the seamline is placed, it will become very distinct. This can be limited by placing the seamlines

where the differences are small. At COWI A/S a minimum cost algorithm is used to find the optimal positions of the seamlines. However, sometimes it is not possible for the algorithm to find a suitable position, and some of the seamlines are therefore placed manually. This is done by placing seamlines at roads, streams, and along field boundaries. It is important that seamlines are not placed too close to buildings and other tall objects, since a tall object seen from different angles, may be covered by different pixels, and may therefore be shown twice. [8], [2], [6]

When the seamlines have been placed, the visibility of the seamlines is reduced by using feathering. This is a process, where the colour difference between each side of the seamline is reduced by smoothing a small surrounding area at both sides of the seamline. In city areas the feathering is performed on a narrow area, contrary to a wider area used in fields and forests. [8], [2]

In this thesis feathering is not performed, and a simple mosaicking algorithm is used. Each orthophoto is simply added to the graphical map by a user specified order, such that the first orthophoto has the highest priority, and the second is added only in the area that is not covered by the first orthophoto. The third orthophoto is placed, where the area is not covered by either the first or the second orthophotos, etc.

As each orthophoto is placed in the graphical map, the area it covers is recorded in a reference map. The reference map can therefore be used to specify where each of the orthophotos in the graphical map is visible. The algorithm is summarised in Algorithm 1 and an example of the mosaicking of the test area and the corresponding reference map are shown in Figure 4.1. In this case the orthophoto priority list is given by

$$P = (1, 2, 3, 4, 5, 6, 7, 15, 16, 17, 18, 19, 20, 21, 22, 8, 9, 10, 11, 12, 13, 14) \quad . \quad (4.1)$$

The orthophotos have been given this order to ensure that a large number of orthophotos are visible, since this provides more visible seamlines. Figure 4.1b shows that 17 of the available 22 orthophotos are visible.

The chosen order in the sequence can have large influence on the result, since it determines how much of an orthophoto is shown in the resulting graphical map.

Algorithm 1 Simple mosaicking algorithm

Require: Orthophoto priority list P **and** Transformation boolean T
1: Define G: Graphical map, size of photographed area
2: Define R: Reference map, size of photographed area
3: **for all** Orthophotos $\in P$ **do**
4: **if** T **then**
5: Insert orthophoto $A_i \cdot P_i$ where G is empty
6: **else**
7: Insert orthophoto P_i where G is empty
8: **end if**
9: Insert the position of orthophoto P_i into R
10: **end for**
11: **return** G **and** R

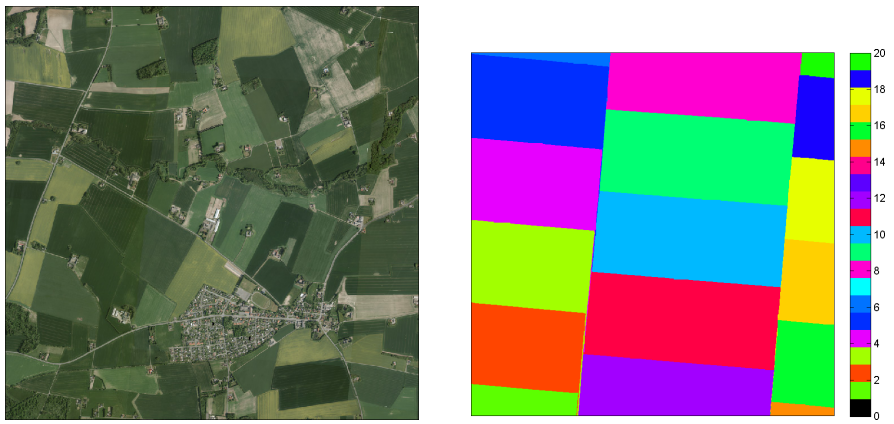

(a) (b)

Figure 4.1: *The figure shows (a) the original test area and (b) the corresponding reference map.*

4.1.1 Downsampling

In order to decrease the necessary computational time all the tiles are downsampled before the computations are performed. The images are downsampled to a smaller number of pixels by using bicubic interpolation, i.e. the pixels in the downsampled image are computed as a weighted average of the neighbouring pixels in the original image.

If a tile is only partly covered by an orthophoto, the rest of the image is black or white. Therefore a mask is created that removes these parts of the image. However, due to rounding errors and the interpolation used in the downsampling process, a part of the resulting graphical map will contain undefined small white or black parts near the border of the orthophoto. This is removed by performing different morphological operations.

Downsampling is discussed further in Section 4.11.

4.2 Neighbourhood

In order to reduce the computational time, model estimation is performed only on a selected set of overlaps. Since the images are approximately placed in a grid, 4-neighbourhood and 8-neighbourhood are used to exclude some of the overlaps.

In some cases there are a lot of overlaps between the orthophotos dependent on how they are produced. In this case the photographs are taken with relatively small intervals as described in section 3. Therefore there are 109 overlaps between the 22 orthophotos. A high number of overlaps can be an advantage since each overlap adds some information to the algorithm, which makes the model more precise. However, it is not practical to use so many overlaps, because the great number of matchings is very time consuming. The linear system of equations would also be less sparse, and therefore more computational power will be necessary.

Therefore only a selected number of overlaps are used in the implementation. Since the orthophotos have been made from an air plane, they are aligned in three parallel lanes, approximately equidistantly. This means that the centers of the orthophotos are approximately situated in a grid as illustrated in Figure 4.2. Due to the fact that the orthophotos are situated in lanes, each orthophoto should be dependent on information in its own lane and in neighbouring lanes.

Figure 4.2a shows how neighbouring pairs of orthophotos are selected by using 4-neighbourhood (also called city-block/Manhatten neighbourhood). Each orthophoto that does not lie on the boarder has 4 neighbours, and this method only uses 34 of the possible 109 overlaps. In Figure 4.2b neighbouring orthophotos are selected using 8-neighbourhood (also called checkerboard neighbourhood). In this method each orthophoto that is not on the boarder has 8 neighbours, and there are therefore more overlaps between the three lanes. This method uses 58 overlaps of the possible 109.

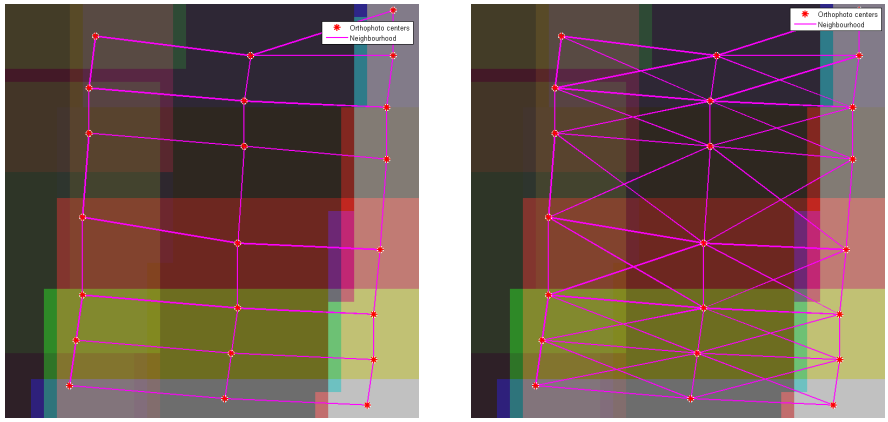

(a) (b)

Figure 4.2: *The figure shows (a) 4-neighbourhood and (b) 8-neighbourhood of the orthophoto centres.*

In Section 5.2 some experiments have been made to show the effect of using 4-neighbourhood and 8-neighbourhood using global histogram matching.

If 8-neighbourhood is chosen the model estimation is based on more overlaps, but the computational time will also be higher than if 4-neighbourhood is used.

4.3 Histogram Matching

Histogram matching is a method that uses the overlap between two images to give neighbouring orthophotos matching colours. This is done by matching the two colour histograms in the overlap, and use the result to estimate a linear transformation. Histogram matching is basis for the first colour correction method in this thesis, global histogram matching.

Histogram matching is uset for colour correction, since it is invariant to possible errors in orthorectification and georeferencing [15].

Initially histogram matching has been performed as described in [15] and [3]. In histogram matching a model is estimated to ensure that the histograms of two images match in the overlap. This means that the two images will have

approximately the same amount of each colour. The model is defined by [3] as

$$c_m(v_{out}) = c(v_{in}) \quad , \tag{4.2}$$

where $c(v_{in})$ is the cumulative histogram of the input image v_{in} and $c_m(v_{out})$ is the cumulative model histogram of the output image v_{out}. In order to find the output image the combined process is performed

$$v_{out} = c_m^{-1}\left(c(v_{in})\right) \quad . \tag{4.3}$$

Since the images consist of a discrete number of colours the inverse of the cumulative model histogram is found by making a lookup table, where each entry t is defined by

$$v_{out} = \min_t |c_m(t) - c(v_{in})| \tag{4.4}$$

This process is illustrated by the sketch in Figure 4.3. The figure illustrates that for each colour value c_i in the cumulative histogram of the input image the corresponding colour c_j in the cumulative histogram of the output image, which is approximately at the same number of pixels in the cumulative histogram is found. This is done for all 256 colour values for each band red, green, and blue in the input image, and the results are inserted into the lookup table.[12]

An example of the histograms in the overlap between orthophoto 1 and 2 is shown in Figure 4.4a, and the histograms after the matching process is shown in Figure 4.4b. It can be observed from the figure that in the resulting histograms some peaks have been added where the original histograms should be higher, and some intensities have been removed to make the original histograms lower.

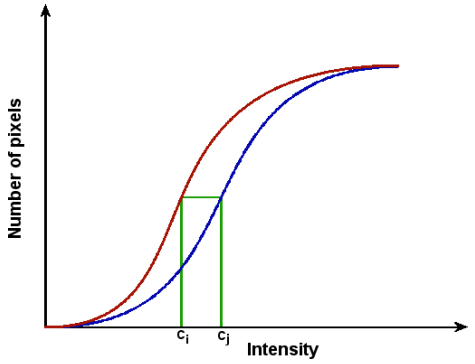

Figure 4.3: *The figure shows a sketch of the process used to create the lookup table. For each colour value c_i in the cumulative histogram of the input image (marked in red) the corresponding colour c_j in the cumulative histogram of the output image (marked in blue), which is approximately at the same number of pixels in the cumulative histogram is found.*

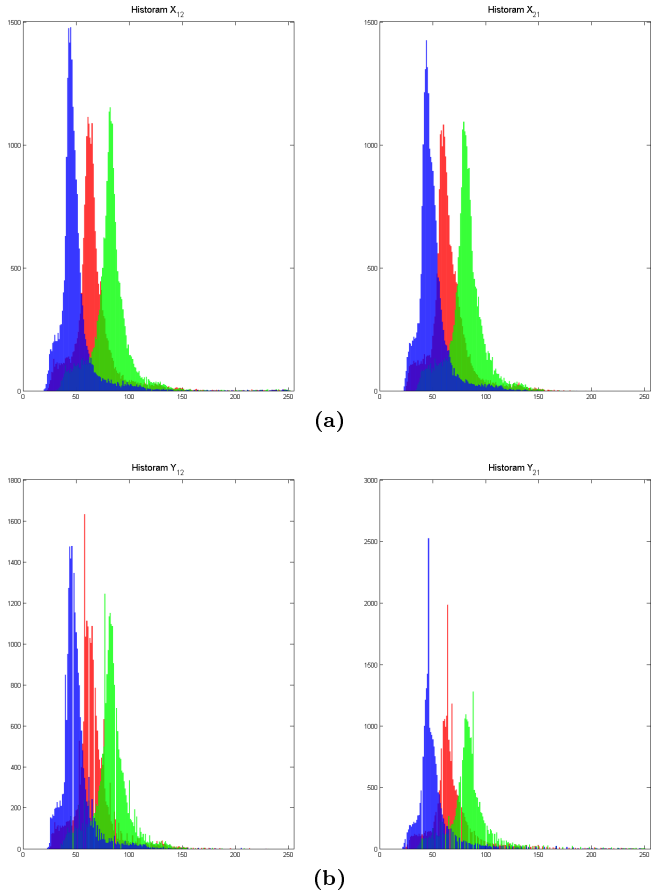

Figure 4.4: *Histograms of the overlap between orthophoto 1 and 2 (a) before and (b) after the histogram matching*

Once the histogram matching has been performed, a model which describes the colour transformation is estimated. This is done such that the model can be applied for the entire overlapping orthophoto. For this a linear model is used, based on a least squares estimate.

Rasmussen has suggested three different linear colour correction models in [15]. All three have the general form

$$AI_1 = I_2 \ , \tag{4.5}$$

where the $3 \times n$ matrix I_1 is the image to be transformed, the $3 \times n$ matrix I_2

is the reference image it is matched to, and n is the total number of pixels. In one of the models A is simply given by a full matrix

$$A = \begin{bmatrix} a & b & c \\ d & e & f \\ g & h & i \end{bmatrix} \quad . \tag{4.6}$$

The least squares estimate is then defined by

$$A = I_2 I_1^T (I_1 I_1^T)^{-1} \quad . \tag{4.7}$$

The second model presented is similar, but with an offset inserted such that

$$A = \begin{bmatrix} a & b & c & \alpha \\ d & e & f & \beta \\ g & h & i & \gamma \end{bmatrix} \quad . \tag{4.8}$$

The third model is a diagonal model given by

$$A = \begin{bmatrix} \alpha & 0 & 0 \\ 0 & \beta & 0 \\ 0 & 0 & \gamma \end{bmatrix} \quad . \tag{4.9}$$

The first diagonal element in the transformation matrix is estimated by $\alpha = \frac{mean(R_2)}{mean(R_1)}$, where R_1 and R_2 are the pixel values in the red band in I_1 and I_2, respectively, and similar estimations are made for the green and the blue band, respectively.

The two models in Equation (4.6) and (4.8) respectively, suggested by Rasmussen in [15] are models that include off-diagonal elements. However, since the histogram matching has been performed bandwise, any possible dependency between the three bands has been removed. Therefore only the diagonal model should be used. However, since this was discovered late in the project, the following derivations have been performed using the model shown in Equation (4.6). The results show that the estimated off-diagonal elements are close to zero, and they have therefore little importance.

The histogram matching is extended for later use in the method global histogram matching, where it is used globally, in order to histogram match all the orthophotos to their neighbouring images simultaneously.

4.4 Global Histogram Matching

In histogram matching one image is transformed to match another image by using the histograms of the overlap between them. A global histogram matching algorithm is used to find the colour transformation of all the orthophotos simultaneously. Initially a reference image is used, but later in this secdtion regularization is used to penalize the transformation to ensure that the colour transformation is not too large.

The colour correction of all orthophotos simultaneously can be done by matching overlapping images in pairs succeedingly, but this is dependent on the sequence of images in the computation, and can lead to inconsistencies. Therefore a global histogram matching algorithm, as described in [15], is used. This algorithm computes the transformations between all image pairs simultaneously by computing the least squares solution to a linear system of equations.

The global histogram matching algorithm described in [15] is used to find a transformation matrix A_i for each orthophoto i, which is represented by a $3 \times n_i$ matrix X_i, where each row is the pixel values of the three colour bands, and n_i is the number of pixels in the orthophoto. The pixels in the overlap between orthophoto i and orthophoto j is denoted X_{ij}, which is a $3 \times n_{ij}$ matrix, where n_{ij} is the number of pixels in the overlap. In order to compute all the transformation matrices simultaneously, the algorithm attempts to solve the optimization problem, which minimizes the expression given by

$$F = \sum_i \sum_{j \in \mathcal{N}(i)} G_{ij} \tag{4.10}$$

$$= \sum_i \sum_{j \in \mathcal{N}(i)} \|A_i X_{ij} - A_j Y_{ij}\|_F^2 \quad , \tag{4.11}$$

where $\mathcal{N}(i)$ is the set of neighbours to orthophoto i and $\|\cdot\|_F^2$ is the Frobenious norm, which is defined by $\|M\|_F^2 = \sum_i \sum_j m_{ij}^2 = tr(MM^T)$, and X_{ij} and Y_{ij} is the overlap between orthophoto i and j as shown in Figure 3.2 in Chapter 3 before and after the histogram matching, respectively.

As the expression states, the algorithm attempts to minimize the sum of all $G_{ij} = \|A_i X_{ij} - A_j Y_{ij}\|_F^2$. In other words, the goal is to minimize the difference between the transformed original orthophoto i in the overlap and the transformed histogram matching of the other orthophoto j in the overlap. The expression in (4.11) is differentiated and set equal to zero, which yields a linear system of equations.

If all orthophotos overlap, the linear system of equations is given by [15][1]

$$\begin{bmatrix} K_{12}+K_{13}+\dots & -L_{12} & -L_{13} & \cdots \\ -L_{21} & K_{21}+K_{23}+\dots & -L_{23} & \cdots \\ -L_{31} & -L_{32} & K_{31}+K_{32}+\dots & \cdots \\ \vdots & \vdots & \vdots & \ddots \end{bmatrix} \begin{bmatrix} A_1^T \\ A_2^T \\ A_3^T \\ \vdots \end{bmatrix} = 0 \quad (4.12)$$

where $K_{ij} = 2X_{ij}X_{ij}^T + 2Y_{ji}Y_{ji}^T$ and $L_{ij} = 2X_{ij}Y_{ij}^T + 2Y_{ji}X_{ji}^T$. If a pair of orthophotos do not overlap, the corresponding K_{ij} and L_{ij} are simply 0.

This system of linear equations can simply be solved by setting all transformation matrices $A_i = 0$. This is of course not a viable option and it is avoided by letting one or more orthophotos be reference images. This means that they are not transformed and the corresponding transformation matrix should therefore be the identity matrix. This is ensured by simply letting the left and the right side be identity matrices. If e.g. orthophoto 1 is a reference image, the linear system of equations is modified to [15]

$$\begin{bmatrix} I & 0 & 0 & \cdots \\ 0 & K_{21}+K_{23}+\dots & -L_{23} & \cdots \\ 0 & -L_{32} & K_{31}+K_{32}+\dots & \cdots \\ \vdots & \vdots & \vdots & \ddots \end{bmatrix} \begin{bmatrix} A_1^T \\ A_2^T \\ A_3^T \\ \vdots \end{bmatrix} = \begin{bmatrix} I \\ L_{21} \\ L_{31} \\ \vdots \end{bmatrix} . \quad (4.13)$$

The global histogram matching algorithm is implemented as described in Algorithm 2.

[1] There is a correction to the system of linear equations in [15], such that the transformation matrices are written as A_i^T instead of A_i. This is explained further in appendix A.1

Algorithm 2 Global histogram matching [15]

1: For each pair of overlapping images i and j extract the overlapping pixels X_{ij} and X_{ji} and find the corresponding histogram matchings Y_{ij} and Y_{ji}
2: Set the right hand side values RHS to 0 and construct left hand side matrix LHS as follows:
3: **for all** images i **do**
4: Add 3 rows LHS_i to LHS, constructed as follows:
5: **for all** neighbours j **do**
6: Add K_{ij} to the columns corresponding to A_i
7: Add $-L_{ij}$ to the columns corresponding to A_j
8: **end for**
9: **end for**
10: **for all** reference images i **do**
11: Replace the image's 3 rows with $IA_i^T = I$ and move all other values in the columns for A_i to the right hand side while negating them.
12: **end for**
13: Find transformations $A = \begin{bmatrix} A_1^T \\ A_2^T \\ A_3^T \\ \vdots \end{bmatrix}$ as solution to

$$LHS \cdot A = RHS \Rightarrow A = (LHS^T LHS)^{-1} LHS^T RHS \tag{4.14}$$

14: Apply transformations to images

In global histogram matching all the transformation matrices are estimated for all the orthophotos simultaneously by finding the least squares solution of a system of linear equations. The algorithm for doing this minimizes the differences between the histograms in each overlap.

4.4.1 Reference Image

The global histogram matching algorithm is greatly influenced by the choice of reference image. This is due to the fact that the histograms of all orthophotos are matched to each other, and as the histogram of the reference image does not change, then all other histograms must change.

The influence of the choice of reference image is been illustrated in Figure 4.5. The result of global histogram matching using orthophoto 10 as reference image

is shown in Figure 4.5b. It can be observed that the image contains more yellow colours, and that some of the seamlines are more distinct, compared to the result using orthophoto 1 as reference image in Figure 4.5a.

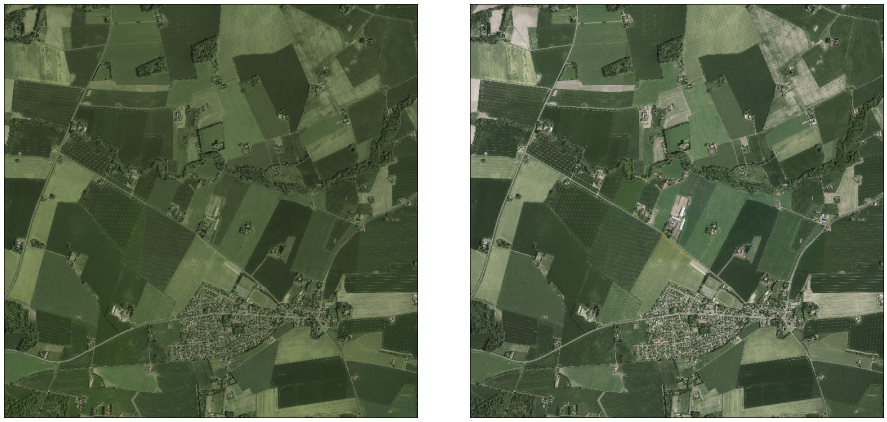

(a) (b)

Figure 4.5: *The figure shows (a) the result of a global histogram matching using orthophoto 1 as reference image and (b) the result of a global histogram matching using orthophoto 10 as reference image. Both computations are made using 4-neighbourhood.*

The observations extracted from Figure 4.5 can be confirmed by calculating the three quantification measures. The measures for the two graphical maps are computed and shown in Table 4.1. The seamline measures in the table state that the seamlines are more distinct in the result shown in Figure 4.5b. This confirms the previous statement from the observations of the figure.
The measures in the table also state that the saturation is higher when reference image 1 is used. This is confirmed by the figure since it can be observed that Figure 4.5b has more grey colours than Figure 4.5a. It can also be observed that the contrast in Figure 4.5b is higher than in Figure 4.5a. This is in accordance with the contrast measures in the table.

	Reference image 1	Reference image 10
Seamline measure	11.24	14.16
Saturation	0.353	0.268
Contrast	0.0885	0.127

Table 4.1: *The table shows the three measures for two results of the global histogram matching with different reference images. Both examples are computed using 4-neighbourhood.*

4.4.2 Regularization

The example in Section 4.4.1 shows that when a reference image is used it has a large influence on the result. The colours of the additional orthophotos are forced to match the colours of the reference image, but it is only necessary that the orthophotos match each other.

Therefore a regularization term is introduced to replace the use of a reference image [15]. A damping parameter λ is used to penalize the sum of squared differences between the transformation matrix and the identity matrix, thus penalizing too large changes in the colours. This means that the regularization term is given by

$$\lambda \left\| I - A_i \right\|_2^2 \quad , \tag{4.15}$$

where $\lambda \geq 0$.

In order to prevent the dependency on choice of reference image the model is altered such that all images have equal importance. Then the linear system of equations is given by [15]

$$\begin{bmatrix} 2\lambda I + K_{12} + K_{13} \dots & -L_{12} & -L_{13} & \cdots \\ -L_{21} & 2\lambda I + K_{21} + K_{23} \dots & -L_{23} & \cdots \\ -L_{31} & -L_{32} & 2\lambda I + K_{31} + K_{32} \dots & \cdots \\ \vdots & \vdots & \vdots & \ddots \end{bmatrix} \begin{bmatrix} A_1^T \\ A_2^T \\ A_3^T \\ \vdots \end{bmatrix} = \begin{bmatrix} 2\lambda I \\ 2\lambda I \\ 2\lambda I \\ \vdots \end{bmatrix} \tag{4.16}$$

where $K_{ij} = 2X_{ij}X_{ij}^T + 2Y_{ji}Y_{ji}^T$ and $L_{ij} = 2X_{ij}Y_{ij}^T + 2Y_{ji}X_{ji}^T$. If a pair of orthophotos do not overlap, the corresponding K_{ij} and L_{ij} are simply 0.

In this altered model no image is chosen as reference image, but the colours of all images are moving as close to each other as possible, minimizing the difference in the colour histograms between the overlapping orthophotos.

The results obtained using regularization vary depending on the choice of damping parameter. A number of examples have been made to investigate this effect. The examples are described in Section 5.6.1. The examples confirm that with a large value of the damping parameter only a small change is permitted, and with a small value of the damping parameter there are large changes in the colours.

It should be noted that too small values of the damping parameter may result in negative pixel values. An example is described in Section 5.6.2.2.

It is seen that global histogram matching is very dependent on the choice of reference image. Therefore regularization is used to penalize the amount of colour transformation. The regularization is dependent on the choice of a damping parameter λ.

4.5 Global Pixelwise Matching

Pixelwise matching is developed as a method, where each pair of pixels are matched directly.

In pixelwise matching each pixel in an overlap from orthophoto i is matched directly to the pixel in the corresponding position in orthophoto j. In order to avoid some of the possible errors of orthorectification and georeferencing, a blurring of the image should be performed initially. Blurring is a process where the colour of a pixel is changed, such that it is influenced by the neighbouring pixels [7]. However, since the implementation in this thesis uses downsampling to reduce the computational time, the blurring is already performed by the downsampling process.

In this case the pixelwise matching is done by selecting all pixels of the same colour in orthophoto i, and calculating the mean colour of the corresponding pixels in orthophoto j for each band red, green, and blue.

The reason for choosing this pixelwise matching method is that there are on average $2.43 \cdot 10^7$ pixels in an overlap, and only 256 levels of each colour band. Because of this the probability that each colour is fairly represented in each overlap is relatively high. This means that the probability that there are only a few outliers of the corresponding pixels in orthophoto j is relatively high. The pixelwise matching is implemented in a global pixelwise matching algorithm corresponding to the global histogram matching algorithm.

A regularization term is added to the optimization problem, which penalizes the distance between the transformation matrices and the identity matrix. This is done similarly to the regularization for global histogram matching in Section 4.4.2.

Some experiments have been performed, and the result of the global pixelwise matching algorithm is compared to the result of the global histogram matching

algorithm in Section 5.7.

Global pixelwise matching minimizes the sum of squared differences between pixels in an overlap, unlike global histogram matching. As for global histogram matching, global pixelwise matching is very dependent on the choice of the damping parameter λ. The experiments show that there is not much difference between results of the two methods for this test area. However, the computational time is smaller for pixelwise matching, and this method allows the colour transformation to take dependencies between the colour bands into account.

4.6 Global Gradual Matching

In Section 4.4 global histogram matching is used to compute a transformation matrix for each of the 22 orthophotos. However, since each of the orthophotos cover a large area, there may be other light conditions in one end of the photo than in the other. Therefore it would be prudent to change the model, such that it is able to take the local variation into account.

Five different models are investigated, which lead to: The interpolation method, the multiplication method, the addition method, the logarithm method, and the division method. Only the multiplication method and the division method are used for experiments in this thesis.

4.6.1 Interpolation Method

In this method the linear colour transformations, estimated by global histogram matching or global pixelwise matching, are used to make an interpolation between the transformation of the neighbouring orthophotos.

With histogram and pixelwise matching, a transformation matrix is obtained for each orthophoto. Therefore, it may be prudent to calculate 4 or 8 (depending on the neighbourhood) different transformations and make an interpolation between them. This is done by computing a distance transformation and using it to weigh the different transformations in the interpolation. This ensures that the pixels in an overlap only use the transformation found at the given overlap, and that the weight of this transformation is decreased the further away it is from the overlap.[15]

The purpose of using gradual transformation is to allow local variation within

each orthophoto. In order to model the local variation it is no longer sufficient to compute a single linear transformation for an entire orthophoto. The local variation can be modelled by letting each of the neighbouring orthophotos have different linear models obtained from the their respective overlaps.

Initially histogram matching is performed for each overlap as described in section 4.3. Once the linear models for the respective overlaps have been obtained, models should be found for the rest of the pixels in the orthophoto. It seams plausible to make an interpolation between the obtained linear models. The interpolation is performed such that if a pixel is close to overlap k, the model of the pixel has a large component from the model of the closest overlap A_k. The interpolation in pixel j is given by [4]

$$y_j = \alpha_1 A_1 x_j + \alpha_2 A_2 x_j + \ldots + \alpha_P A_P x_j \ , \tag{4.17}$$

where P is the number of overlaps, α_r, where $r \in \{1, 2, \ldots, P\}$ denotes the interpolation coefficients, A_r is the transformation matrix computed as shown in Equation (4.16) for the respective overlaps, and x_j is the pixel colour values in the orthophoto in question.

The interpolation coefficients are found by making a distance transformation of each overlap. This method is performed by using a binary image. In this case the overlap will have value 1, and the rest of the orthophoto will have value 0. A distance transformation is performed such that for each pixel in the orthophoto the Euclidian distance to the pixels with the value 1 is calculated. In this case the distance transformation is used to assign coefficients in the interpolation, and therefore the results are reversed, such that the values decrease, the further the pixels are from the overlap. Afterwards the results are normalized between the orthophotos.
The algorithm is summarized in Algorithm 3

Algorithm 3 Gradual Transformation

for all images i **do**
  Find the neighbours $\mathcal{N}(i)$ using e.g. 4- or 8-neighbourhood
  Locate the overlap between each pair i and $j \in \mathcal{N}(i)$
  for all overlaps X_{ij} **do**
    Perform a histogram matching between X_{ij} and X_{ji} and estimate a linear model
    Make a distance transformation D_{ij} from X_{ij}
    Normalize D_{ij}
  end for
  Make an interpolation between the transformation matrices obtained with each $k \in \mathcal{N}(i)$
  Apply the obtained transformation to i
end for

The downside of using interpolation between previously created transformation matrices is that during the estimation of the matrices, the spatial nature of the algorithm is not taken into account. This means that the coefficients in each transformation matrix are already determined, and as the distance from each pixel to the neighbouring orthophotos is initially determined, the model no longer gives a gradual estimation. Therefore this model was not investigated any further.

4.6.2 Multiplication Method

In the multiplication method a bilinear function is estimated and multiplied on each colour band. The function is estimated, such that the sum of squared differences in the overlap is minimized. A regularization term is added to prevent too large differences.

The bandwise linear model, described in Section 4.3, given by

$$A = \begin{bmatrix} \alpha & 0 & 0 \\ 0 & \beta & 0 \\ 0 & 0 & \gamma \end{bmatrix} , \tag{4.18}$$

uses the same colour model, with constant α, β, and γ, for all the pixels in an orthophoto. The coefficients can be computed by utilising that $\alpha = \frac{mean(R_y)}{mean(R_x)}$ for the red channel R in the original image R_x and the histogram matched image R_y, respectively. Similar computations can be performed to obtain β and γ [15].

In order to take the position of each pixel into account, the colour model is changed, such that the three components α, β, and γ depend on the coordinates (x, y) of each pixel. The three components in the colour model are computed using a bilinear model, depending on the position, which for the red colour band, is given by

$$\alpha(x, y) = ax + by + c \ , \tag{4.19}$$

where a, b, and c are constant for each orthophoto, and (x, y) is the pixel position. Other models could be used, but this model is the simplest method that is dependent on the pixel position, and it will make the computations relatively simple. This expression is used to compute the component for the red band, and similar computations are performed for the green and the blue band.

In order to perform a gradual transformation the three coefficients a, b, and c are estimated, such that the sum of squared differences between orthophoto i and orthophoto j after the transformation is minimized for the pixels in each overlap. This means that initially the overlap in orthophoto i is matched to the overlap in orthophoto j, which is held constant. The minimization problem is then given by

$$\min_{\beta} f = \sum_{k=1}^{n} \left(r_i^{(k)} (a x^{(k)} + b y^{(k)} + c) - r_j^{(k)} \right)^2 \tag{4.20}$$

$$= \sum_{k=1}^{n} \left(r_i^{(k)} a x^{(k)} + r_i^{(k)} b y^{(k)} + r_i^{(k)} c - r_j^{(k)} \right)^2 \tag{4.21}$$

$$= \| R_i \beta - r_j \|_2^2 \ , \tag{4.22}$$

where

$$R_i = \begin{bmatrix} r_i^{(1)} x^{(1)} & r_i^{(1)} y^{(1)} & r_i^{(1)} \\ \vdots & \vdots & \vdots \\ r_i^{(k)} x^{(k)} & r_i^{(k)} y^{(k)} & r_i^{(k)} \\ \vdots & \vdots & \vdots \\ r_i^{(n)} x^{(n)} & r_i^{(n)} y^{(n)} & r_i^{(n)} \end{bmatrix} \tag{4.23}$$

$$\beta = \begin{bmatrix} a \\ b \\ c \end{bmatrix} \ , \tag{4.24}$$

and r_i and r_j are vectors containing the values in the red band in the pixels of the overlap in orthophoto i and j, respectively, and n is the number of pixels in the overlap. β is in this context the three coefficients in $\alpha(x, y)$ and should not be confused with β in Equation (4.18).

4.6.2.1 Global Gradual Matching for Multiplication Method

With the method described in the previous section it is possible to compute a linear model depending on the pixel position for an entire orthophoto. However, since each overlap is used in the calculations, the orthophoto is close to matching each of the overlaps, but not necessarily the neighbouring orthophotos. This is due to the fact that other linear models are applied to the neighbouring orthophotos. Therefore, a global method should be developed to estimate all the coefficients at once, as was done with the global histogram matching described in Section 4.4 [15].

Since the transformation from global gradual matching is estimated by using several orthophotos, a new variable, similar to R_i in Equation (4.23), for overlap X_{ij} is denoted

$$R_{ij} = \begin{bmatrix} r_{ij}^{(1)} x_{ij}^{(1)} & r_{ij}^{(1)} y_{ij}^{(1)} & r_{ij}^{(1)} \\ \vdots & \vdots & \vdots \\ r_{ij}^{(k)} x_{ij}^{(k)} & r_{ij}^{(k)} y_{ij}^{(k)} & r_{ij}^{(k)} \\ \vdots & \vdots & \vdots \\ r_{ij}^{(n)} x_{ij}^{(n)} & r_{ij}^{(n)} y_{ij}^{(n)} & r_{ij}^{(n)} \end{bmatrix} . \tag{4.25}$$

The subscript on the position coordinates (x, y) are due to the fact that the position in each pixel is relative to its orthophoto. This means that origo is at the bottom left corner of the orthophoto. This will have the effect that the coefficients of the linear model in each orthophoto are of the same order of magnitude. The linear function is created for each orthophoto with the coefficient vector, similar to β in Equation (4.24), defined by

$$\beta_i = \begin{bmatrix} a_i \\ b_i \\ c_i \end{bmatrix} . \tag{4.26}$$

The optimal solution will make a gradual transformation for each orthophoto which minimizes the difference between the orthophotos in their respective overlaps. Since both orthophotos i and j are transformed, the squared difference in the overlap between them must be given by

$$G_{ij} = \|R_{ij}\beta_i - R_{ji}\beta_j\|_2^2 . \tag{4.27}$$

The total sum of the differences in the overlaps is given by

$$F = \sum_i \sum_{j \in \mathcal{N}(i)} G_{ij} \tag{4.28}$$

$$G_{ij} = \|R_{ij}\beta_i - R_{ji}\beta_j\|_2^2 \tag{4.29}$$

$$= (R_{ij}\beta_i - R_{ji}\beta_j)^T (R_{ij}\beta_i - R_{ji}\beta_j) \tag{4.30}$$

$$= \beta_i^T R_{ij}^T R_{ij}\beta_i - \beta_i^T R_{ij}^T R_{ji}\beta_j - \beta_j^T R_{ji}^T R_{ij}\beta_i + \beta_j^T R_{ji}^T R_{ji}\beta_j \tag{4.31}$$

$$= \beta_i^T R_{ij}^T R_{ij}\beta_i + \beta_j^T R_{ji}^T R_{ji}\beta_j - 2\beta_i^T R_{ij}^T R_{ji}\beta_j \tag{4.32}$$

$$= \beta_i^T K_{ij}\beta_i + \beta_j^T K_{ji}\beta_j - 2\beta_i^T L_{ij}\beta_j \ , \tag{4.33}$$

where

$$K_{ij} = R_{ij}^T R_{ij} \tag{4.34}$$

$$L_{ij} = R_{ij}^T R_{ji} \ . \tag{4.35}$$

It should be noticed that K_{ij} is symmetric, which means that $K_{ij} = K_{ij}^T$.

In order to find the optimal value of the expression in Equation (4.28), the derivative of the quadratic program is calculated, such that [14]

$$\frac{\partial G_{ij}}{\partial \beta_i} = (K_{ij} + K_{ij}^T)\beta_i - 2L_{ij}\beta_j \tag{4.36}$$

$$= 2K_{ij}\beta_i - 2L_{ij}\beta_j \tag{4.37}$$

$$\frac{\partial G_{ji}}{\partial \beta_i} = 2K_{ij}\beta_i - 2L_{ij}\beta_j \tag{4.38}$$

$$\frac{\partial F}{\partial \beta_i} = \sum_{j \in \mathcal{N}(i)} 2K_{ij}\beta_i - 2L_{ij}\beta_j - 2L_{ij}\beta_j + 2K_{ij}\beta_i \tag{4.39}$$

$$= \sum_{j \in \mathcal{N}(i)} 4K_{ij}\beta_i - 4L_{ij}\beta_j \ . \tag{4.40}$$

In order to minimize F the derivative is set equal to zero, such that

$$\frac{\partial F}{\partial \beta_i} = 0 \Rightarrow \tag{4.41}$$

$$\sum_{j \in \mathcal{N}(i)} 4K_{ij}\beta_i - 4L_{ij}\beta_j = 0 \ . \tag{4.42}$$

The second order derivative is given by

$$\frac{\partial^2 F}{\partial \beta_i^2} = \sum_{j \in \mathcal{N}(i)} 4K_{ij} > 0 \tag{4.43}$$

Since it is assumed that the pixel values are positive, the second order derivative is positive, which means that the solution to Equation (4.42) is a minimum.

Equation (4.40) is solved for all orthophotos simultaneously by using a linear system of equations similar to Equation (4.12) in Section 4.4, such that

$$\begin{bmatrix} \sum_j 4K_{1j} & -4L_{12} & \cdots & -4L_{1n} \\ -4L_{21} & \sum_j 4K_{2j} & \cdots & -4L_{2n} \\ \vdots & \vdots & \ddots & \vdots \\ -4L_{n1} & -4L_{n2} & \cdots & \sum_j 4K_{nj} \end{bmatrix} \begin{bmatrix} \beta_1 \\ \beta_2 \\ \vdots \\ \beta_n \end{bmatrix} = \begin{bmatrix} 0 \\ 0 \\ \vdots \\ 0 \end{bmatrix} , \tag{4.44}$$

where n is the number of orthophotos in the test data.

The system of linear equations can be solved simply by setting $\beta_i = \begin{bmatrix} 0 \\ 0 \\ 0 \end{bmatrix}$ for all i. This is not a useful solution, so a regularization term must be inserted similarly to the regularization term in global histogram matching Equation (4.16) in Section 4.4. The used regularization term is defined, such that

$$Q = \left\| \begin{bmatrix} w_a & 0 & 0 \\ 0 & w_b & 0 \\ 0 & 0 & w_c \end{bmatrix} \begin{bmatrix} a \\ b \\ c \end{bmatrix} - \begin{bmatrix} 0 \\ 0 \\ w_c \end{bmatrix} \right\|_2^2 \tag{4.45}$$

$$= \|W\beta - v\|_2^2 , \tag{4.46}$$

where $W = \begin{bmatrix} w_a & 0 & 0 \\ 0 & w_b & 0 \\ 0 & 0 & w_c \end{bmatrix}$ and $v = \begin{bmatrix} 0 \\ 0 \\ w_c \end{bmatrix}$.

The regularization term defined in Equation (4.46) has three parameters, w_a, w_b, and w_c. The three parameters are used to set a damping of each of the parts in the model, $\alpha(x, y) = ax + by + c$. w_a is used to put a damping on the ax term. This insures that the variation between the left and the right part of the orthophoto does not become too large. Similarly is w_b used to insure that the vertical variation does not become too large.
The third parameter w_c is used in Equation (4.46) to form the term

$$w_c c - w_c = w_c(c - 1) . \tag{4.47}$$

This means that w_c is used to penalize how far c can go from 1. This is done due to the fact that the closer c is to one, the closer the orthophoto is to the original orthophoto.

The regularization term is inserted for each orthophoto, such that

$$\begin{bmatrix} \sum_j 4K_{1j} & -4L_{12} & \cdots & -4L_{1n} \\ -4L_{21} & \sum_j 4K_{2j} & \cdots & -4L_{2n} \\ \vdots & \vdots & \ddots & \vdots \\ -4L_{n1} & -4L_{n2} & \cdots & \sum_j 4K_{nj} \\ W & 0 & \cdots & 0 \\ 0 & W & \cdots & 0 \\ \vdots & \vdots & \ddots & \vdots \\ 0 & 0 & \cdots & W \end{bmatrix} \begin{bmatrix} \beta_1 \\ \beta_2 \\ \vdots \\ \beta_n \end{bmatrix} = \begin{bmatrix} 0 \\ 0 \\ \vdots \\ 0 \\ v \\ v \\ \vdots \\ v \end{bmatrix} . \tag{4.48}$$

This overdetermined system of linear equations is solved by finding the least squares solution. The calculations in this section are shown only for the red colour band and are similar for the green and blue colour bands, respectively.

In order to illustrate how the method works, two one dimensional signals are constructed by using 100 random values between 0 and 1, and multiplying with the signal magnitudes given by $0.1x + 2$ for signal A and $0.3x + 5$ for signal B, where $x = 1, \ldots, 100$. The two signals and their transformed signals are shown in Figure 4.6a. In Figure 4.6b the signal magnitudes are shown with the magnitude of the respective transformed signals.

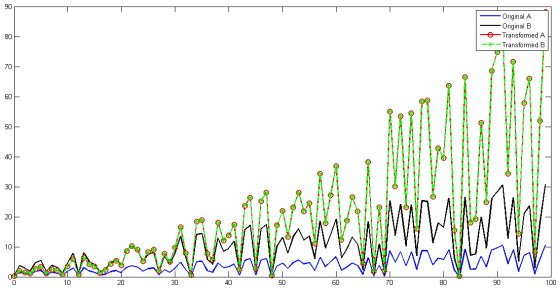

(a)

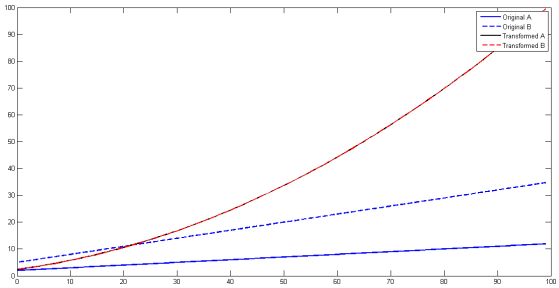

(b)

Figure 4.6: *The figure shows (a) the two signals A and B, and their transformed signals using the gradual multiplication method, and (b) the signal magnitude for signal A, B, and their transformed signals.*

Figure 4.6 shows that although the two transformed signals are in the same position, their signal magnitudes are not linear but parabolic. This is due to the fact that since the gradual change in lighting is modelled by multiplying the colours with a linear function, multiplying another linear function will result in a parabola, such that

$$\begin{aligned} & r(ux+vy+w)(ax+by+c) \\ = \; & r(aux^2+buxy+cux+avxy+bvy^2+cvy+awx+bwy+cw) \; . \end{aligned}$$

From this equation it is seen that the linear function can not be removed by multiplying with another linear function.

An example of global gradual matching with the multiplication method is shown in Section 5.8.1 for a constructed example.

The consequence of the parabolic shape of the transformed images is that it

can lead to extreme colour values outside the acceptable range, and the distance between the darkest and brightest colours can become very high. Another downside is that although the two images match at the parabola, it will be difficult to match a third image.

4.6.3 Addition Method

The addition method is based on the assumption that the gradual change that occurs, due to the sun position, is modelled by adding a linear function to the colours. The model coefficients are estimated by minimizing the sum of the quadratic differences in the overlaps.

This means that the colour r in the pixel at the position (x, y) in the image is given by

$$r = \rho + \mu(x, y) \tag{4.49}$$
$$= \rho + ux + vy + w \ , \tag{4.50}$$

where ρ is the colour that would be obtained under equally distributed light conditions, $\mu(x, y) = ux + vy + w$, and u, v, and w are unknown constants. In order to remove the unknown added linear function, the function should be subtracted. In order to estimate the coefficients of $\mu(x, y)$, an approximation is made, by a linear function, $\alpha(x, y)$, which gives the minimum difference between each pair of orthophotos when it is added to the colour values.

For the overlap between orthophoto i and orthophoto j the resulting colour after the transformation is for every pixel given by

$$r'_{ij} = \rho_{ij} + \mu_i(x, y) + \alpha_i(x, y) \tag{4.51}$$
$$= r_{ij} + \begin{bmatrix} x^{(1)} & y^{(1)} & 1 \\ x^{(2)} & y^{(2)} & 1 \\ \vdots & \vdots & \vdots \\ x^{(n)} & y^{(n)} & 1 \end{bmatrix} \begin{bmatrix} a_i \\ b_i \\ c_i \end{bmatrix} \ , \tag{4.52}$$

where the vector r_{ij} is the original colour values in each pixel in the overlap between orthophoto i and orthophoto j, (x, y) is the pixel position, the coefficients of orthophoto i are denoted $\beta_i = \begin{bmatrix} a_i \\ b_i \\ c_i \end{bmatrix}$, and $Z_{ij} = \begin{bmatrix} x^{(1)} & y^{(1)} & 1 \\ x^{(2)} & y^{(2)} & 1 \\ \vdots & \vdots & \vdots \\ x^{(n)} & y^{(n)} & 1 \end{bmatrix}$ contains the pixel positions in the overlap between orthophoto i and orthophoto j. Here

$(x^{(p)}, y^{(p)})$ is the pixel position in the p'th pixel. It should be noted that in order to remove an added linear function, a linear function should be subtracted, but here $\alpha_i(x, y)$ is added. This means that the estimated coefficients will have the opposite sign, than if it was subtracted.

In order to determine the coefficients for each orthophoto, the squared differences in each overlap are minimized similarly to Equation (4.29). The sum of squared differences between orthophoto i and j is given by

$$\begin{aligned} G_{ij} &= ||(r_{ij} + Z_{ij}\beta_i) - (r_{ji} + Z_{ij}\beta_j)||_2^2 && (4.53)\\ &= ||r_{ij} + Z_{ij}\beta_i - r_{ji} - Z_{ij}\beta_j||_2^2 && (4.54)\\ &= (r_{ij} + Z_{ij}\beta_i - r_{ji} - Z_{ij}\beta_j)^T(r_{ij} + Z_{ij}\beta_i - r_{ji} - Z_{ij}\beta_j) && (4.55)\\ &= r_{ij}^T r_{ij} + r_{ij}^T Z_{ij}\beta_i - r_{ij}^T r_{ji} - r_{ij}^T Z_{ij}\beta_j \\ &\quad +\beta_i^T Z_{ij}^T r_{ij} + \beta_i^T Z_{ij}^T Z_{ij}\beta_i - \beta_i^T Z_{ij}^T r_{ji} - \beta_i^T Z_{ij}^T Z_{ij}\beta_j \\ &\quad -r_{ji}^T r_{ij} - r_{ji}^T Z_{ij}\beta_j + r_{ji}^T r_{ji} + r_{ji}^T Z_{ij}\beta_j \\ &\quad -\beta_j^T Z_{ij}^T r_{ij} - \beta_j^T Z_{ij}^T Z_{ij}\beta_i + \beta_j^T Z_{ij}^T r_{ji} + \beta_j^T Z_{ij}^T Z_{ij}\beta_j \ . && (4.56) \end{aligned}$$

In order to be able to solve the optimization problem G_{ij} is differentiated with respect to β_i

$$\frac{\partial G_{ij}}{\partial \beta_i} = 2Z_{ij}^T r_{ij} + 2Z_{ij}^T Z_{ij}\beta_i - 2Z_{ij}^T r_{ji} - 2Z_{ij}^T Z_{ij}\beta_j \ , \quad (4.57)$$

and G_{ji} with respect to β_i

$$\frac{\partial G_{ji}}{\partial \beta_i} = 2Z_{ij}^T r_{ij} + 2Z_{ij}^T Z_{ij}\beta_i - 2Z_{ij}^T r_{ji} - 2Z_{ij}^T Z_{ij}\beta_j \ . \quad (4.58)$$

The sum of squared differences is similarly to Equation (4.28) given by

$$F = \sum_i \sum_{j \in \mathcal{N}(i)} G_{ij} \ , \quad (4.59)$$

where $\mathcal{N}(i)$ is the set of neighbours of orthophoto i. In order to find the optimal solution the sum of the squared differences is differentiated with respect to β_i

$$\begin{aligned} \frac{\partial F}{\partial \beta_i} &= 4Z_{ij}^T r_{ij} + 4Z_{ij}^T Z_{ij}\beta_i - 4Z_{ij}^T r_{ji} - 4Z_{ij}^T Z_{ij}\beta_j && (4.60)\\ &= 4k_{ij} + 4K_{ij}\beta_i - 4k_{ji} - 4K_{ij}\beta_j \ , && (4.61) \end{aligned}$$

where $K_{ij} = Z_{ij}^T Z_{ij}$, and $k_{ij} = Z_{ij}^T r_{ij}$.

The optimization problem is solved, setting the derivative equal to zero, such that

$$\begin{aligned} \frac{\partial F}{\partial \beta_i} &= 0 \Rightarrow && (4.62)\\ 4k_{ij} + 4K_{ij}\beta_i - 4k_{ji} - 4K_{ij}\beta_j &= 0 \ . && (4.63) \end{aligned}$$

The resulting equation is solved similarly to Equation (4.44) by solving the following system of linear equations

$$\begin{bmatrix} \sum_j 4K_{1j} & -4K_{21} & \cdots & -4K_{n1} \\ -4K_{12} & \sum_j 4K_{2j} & \cdots & -4K_{n2} \\ \vdots & \vdots & \ddots & \vdots \\ -4K_{1n} & -4K_{2n} & \cdots & \sum_j 4K_{nj} \end{bmatrix} \begin{bmatrix} \beta_1 \\ \beta_2 \\ \vdots \\ \beta_n \end{bmatrix} = \begin{bmatrix} \sum_i 4k_{i1} - 4k_{1i} \\ \sum_i 4k_{i2} - 4k_{2i} \\ \vdots \\ \sum_i 4k_{in} - 4k_{ni} \end{bmatrix}$$

The problem with the addition method is that it is assumed that the gradual change in lighting is added to the image, which is not the case. A gradual change in lighting from the position of the sun will result in a function multiplied with the colours in the image [1]. Therefore this method will only be used as part of the logarithm method described in Section 4.6.4.

4.6.4 Logarithm Method

The simplest way to model the gradual change in lighting is to use a linear model, and according to theories of reflection of light, described in [1], the colours in the orthophoto can be modelled by multiplying the actual colours in the area with a linear expression. The model coefficients are estimated by minimizing the sum of the quadratic differences in the overlaps.

A natural way to remove a linear function that is multiplied on the pixel values, is to divide by the same function. However, a non-linearity arises, when the problem is minimized. Therefore the logarithm is used to rewrite the problem to an addition problem, which then can be solved as described in Section 4.6.3.

The colours r of a pixel with position (x, y) in an orthophoto is modelled by

$$r = \rho\mu(x, y) \tag{4.64}$$
$$= \rho(ux + vy + w) \ , \tag{4.65}$$

where ρ is the colour that would be obtained, if the lighting was equally distributed, $\mu(x, y) = ux + vy + w$, and u, v, and w are unknown constants.

Since the coefficients in Equation (4.65) are unknown, some coefficients must be estimated by minimizing the sum of squared differences in the overlaps.

An approximation of the actual colour is given by

$$\frac{\rho\mu(x, y)}{\alpha(x, y)} = \frac{\rho(ux + vy + w)}{ax + by + c} \ , \tag{4.66}$$

where $\alpha(x, y) = ax + by + c$ is the estimated function.

The approximation is done by minimizing the term

$$\min_{\theta} F = \sum_{i} \sum_{j \in \mathcal{N}(i)} G_{ij} \ , \tag{4.67}$$

where $\mathcal{N}(i)$ is the set of neighbours of orthophoto i, and

$$G_{ij} = \left\| \frac{r_{ij}}{\alpha_i(x, y)} - \frac{r_{ji}}{\alpha_j(x, y)} \right\|_2^2 \tag{4.68}$$

$$\theta = \begin{bmatrix} \beta_1 \\ \beta_2 \\ \vdots \\ \beta_n \end{bmatrix} \ , \tag{4.69}$$

where the two fractions are computed elementwise, and r_{ij} is a vector with the colour of each pixel in the corresponding positions (x, y) in orthophoto i in the overlap, r_{ji} is a vector of the colour of each pixel in the corresponding position (x, y) in orthophoto j in the overlap, $\alpha_i(x, y)$ is the correction function for each pixel in orthophoto i, and $\alpha_j(x, y)$ is the correction function for each pixel in orthophoto j, and n is the number of orthophotos.

The expression in Equation (4.68) is non-linear and therefore difficult to solve. However, the addition method described in Section 4.6.3 is solvable under the condition that the gradual change in colours in the images are added to the actual colours. Therefore it seams evident to use the logarithm function to turn the division problem into an addition problem. This means that the model is changed to

$$\ln\left(\frac{\rho\mu(x, y)}{\alpha(x, y)}\right) = \ln\left(\rho\mu(x, y)\right) - \ln\left(\alpha(x, y)\right) \tag{4.70}$$

$$= \ln\left(\rho(ux + vy + w)\right) - \ln\left(ax + by + c\right) \ . \tag{4.71}$$

The problem with the logarithm method is that it cannot be solved by using the addition method, unless the change in lighting is so small that the logarithm can be approximated by a linear function. This is due to the fact that the model in the addition method shown in Equation (4.51) assumes a linear function is added, whereas the logarithm method requires that the logarithm of a linear function is added. The non-linearity of the logarithm function makes it impossible to rewrite the addition model to a matrix product as shown in Equation (4.52).

4.6.5 Division Method

As described in Section 4.6.4 the gradual change in lighting is modelled as a bilinear function, multiplied on the actual colour values, and a natural way to remove this change is to divide the pixel values by the same bilinear function. In this section the solution is found by changing the problem into a multiplication problem for the reciprocal problem. The model coefficients are estimated by minimizing the sum of squared differences in the overlaps. A regularization term is added to penalize a too large change in the pixel values.

Some of the colour differences in neighbouring orthophotos are caused by the position of the sun. If the sun is not placed directly above the area, there may be a gradual change in the lighting of the photographed area. The simplest way to model this gradual change is to use a linear model, and according to theories of reflection of light, described in [1], the colours in the orthophoto can be modelled by multiplying the actual colours in the area with a linear expression.

The colour r of a pixel with position (x, y) in an orthophoto is modelled as in Section 4.6.4 by

$$\begin{aligned} r &= \rho\mu(x,y) && (4.72)\\ &= \rho(ux+vy+w) \ , && (4.73) \end{aligned}$$

where ρ is the colour that would be obtained, if the lighting was equally distributed, $\mu(x, y) = ux + vy + w$, and u, v, and w are unknown constants.

As mentioned in Section 4.6.4 a natural way to remove the gradual change in lighting is to divide the colour values in the orthophoto by a linear expression with the same coefficients as the expression in Equation (4.73). This gives again that some coefficients must be estimated by minimizing the sum of squared differences in the overlaps.

An approximation of the actual colour is given by

$$\frac{\rho\mu(x,y)}{\alpha(x,y)} = \frac{\rho(ux+vy+w)}{ax+by+c} \ , \qquad (4.74)$$

where $\alpha(x, y) = ax + by + c$ is the estimated function.

The approximation is done by minimizing the term

$$\min_{\theta} F = \sum_i \sum_{j \in \mathcal{N}(i)} G_{ij} \ , \qquad (4.75)$$

where $\mathcal{N}(i)$ is the set of neighbours of orthophoto i, and

$$G_{ij} = \left\| \frac{r_{ij}}{\alpha_i(x,y)} - \frac{r_{ji}}{\alpha_j(x,y)} \right\|_2^2 \tag{4.76}$$

$$\theta = \begin{bmatrix} \beta_1 \\ \beta_2 \\ \vdots \\ \beta_n \end{bmatrix} , \tag{4.77}$$

where the two fractions are computed elementwise, and r_{ij} is a vector with the colour of each pixel in the corresponding positions (x, y) in orthophoto i in the overlap, r_{ji} is a vector of the colour of each pixel in the corresponding position (x, y) in orthophoto j in the overlap, $\alpha_i(x, y)$ is the correction function for each pixel in orthophoto i, and $\alpha_j(x, y)$ is the correction function for each pixel in orthophoto j, and n is the number of orthophotos. Since the term in Equation (4.76) is non-linear, the reciprocal values are used instead since they have the same position of extrema. Therefore the new optimization problem is given by

$$\min_{\theta} \widetilde{F} = \sum_i \sum_{j \in \mathcal{N}(i)} \widetilde{G}_{ij} \tag{4.78}$$

$$\widetilde{G}_{ij} = \left\| \frac{\alpha_i(x,y)}{r_{ij}} - \frac{\alpha_j(x,y)}{r_{ji}} \right\|_2^2 \tag{4.79}$$

$$= \| \widetilde{r}_{ij} \alpha_i(x,y) - \widetilde{r}_{ji} \alpha_j(x,y) \|_2^2 \tag{4.80}$$

$$= \left\| \widetilde{R}_{ij} \beta_i - \widetilde{R}_{ji} \beta_j \right\|_2^2 , \tag{4.81}$$

where $\widetilde{r}_{ij} = \frac{1}{r_{ij}}$ and $\widetilde{r}_{ji} = \frac{1}{r_{ji}}$, and for the n pixels in the overlap

$$\widetilde{R}_{ij} = \begin{bmatrix} \widetilde{r}_{ij}^{(1)} x^{(1)} & \widetilde{r}_{ij}^{(1)} y^{(1)} & \widetilde{r}_{ij}^{(1)} \\ \widetilde{r}_{ij}^{(2)} x^{(2)} & \widetilde{r}_{ij}^{(2)} y^{(2)} & \widetilde{r}_{ij}^{(2)} \\ \vdots & \vdots & \vdots \\ \widetilde{r}_{ij}^{(n)} x^{(n)} & \widetilde{r}_{ij}^{(n)} y^{(n)} & \widetilde{r}_{ij}^{(n)} \end{bmatrix} . \tag{4.82}$$

Then

$$\widetilde{G}_{ij} = \left\| \widetilde{R}_{ij} \beta_i - \widetilde{R}_{ji} \beta_j \right\|_2^2 \tag{4.83}$$

$$= (\widetilde{R}_{ij} \beta_i - \widetilde{R}_{ji} \beta_j)^T (\widetilde{R}_{ij} \beta_i - \widetilde{R}_{ji} \beta_j) \tag{4.84}$$

$$= \beta_i^T \widetilde{R}_{ij}^T \widetilde{R}_{ij} \beta_i - \beta_i^T \widetilde{R}_{ij}^T \widetilde{R}_{ji} \beta_j - \beta_j^T \widetilde{R}_{ji}^T \widetilde{R}_{ij} \beta_i + \beta_j^T \widetilde{R}_{ji}^T \widetilde{R}_{ji} \beta_j \tag{4.85}$$

$$= \beta_i^T \widetilde{R}_{ij}^T \widetilde{R}_{ij} \beta_i + \beta_j^T \widetilde{R}_{ji}^T \widetilde{R}_{ji} \beta_j - 2 \beta_i^T \widetilde{R}_{ij}^T \widetilde{R}_{ji} \beta_j \tag{4.86}$$

$$= \beta_i^T \widetilde{K}_{ij} \beta_i + \beta_j^T \widetilde{K}_{ji} \beta_j - 2 \beta_i^T \widetilde{L}_{ij} \beta_j , \tag{4.87}$$

where

$$\widetilde{K}_{ij} = \widetilde{R}_{ij}^T \widetilde{R}_{ij} \tag{4.88}$$

$$\widetilde{L}_{ij} = \widetilde{R}_{ij}^T \widetilde{R}_{ji} \ . \tag{4.89}$$

It should be noticed that $\widetilde{K}_{ij}$ is symmetric, which means that $\widetilde{K}_{ij} = \widetilde{K}_{ij}^T$.

In order to find the optimal value, the derivative of the quadratic program is given by [14]

$$\frac{\partial \widetilde{G}_{ij}}{\partial \beta_i} = (\widetilde{K}_{ij} + \widetilde{K}_{ij}^T)\beta_i - 2\widetilde{L}_{ij}\beta_j \tag{4.90}$$

$$= 2\widetilde{K}_{ij}\beta_i - 2\widetilde{L}_{ij}\beta_j \tag{4.91}$$

$$\frac{\partial \widetilde{G}_{ji}}{\partial \beta_i} = 2\widetilde{K}_{ij}\beta_i - 2\widetilde{L}_{ij}\beta_j \tag{4.92}$$

$$\frac{\partial \widetilde{F}}{\partial \beta_i} = \sum_{j \in \mathcal{N}(i)} 2\widetilde{K}_{ij}\beta_i - 2\widetilde{L}_{ij}\beta_j - 2\widetilde{L}_{ij}\beta_j + 2\widetilde{K}_{ij}\beta_i \tag{4.93}$$

$$= \sum_{j \in \mathcal{N}(i)} 4\widetilde{K}_{ij}\beta_i - 4\widetilde{L}_{ij}\beta_j \ . \tag{4.94}$$

In order to solve the optimization problem, the derivative is set equal to zero, such that

$$\frac{\partial \widetilde{F}}{\partial \beta_i} = 0 \Rightarrow \tag{4.95}$$

$$\sum_{j \in \mathcal{N}(i)} 4\widetilde{K}_{ij}\beta_i - 4\widetilde{L}_{ij}\beta_j = 0 \ . \tag{4.96}$$

The second order derivative is given by

$$\frac{\partial^2 \widetilde{F}}{\partial \beta_i^2} = \sum_{j \in \mathcal{N}(i)} 4\widetilde{K}_{ij} > 0 \ . \tag{4.97}$$

Since it is assumed that the pixel values are positive, the second order derivative is positive, which means that a minimum is found.

Equation (4.94) can be solved for all orthophotos simultaneously by solving a system of linear equations similar to Equation (4.12) given by [15]

$$\begin{bmatrix} \sum_j \overline{K}_{1j} & -\overline{L}_{12} & \cdots & -\overline{L}_{1n} \\ -\overline{L}_{21} & \sum_j \overline{K}_{2j} & \cdots & -\overline{L}_{2n} \\ \vdots & \vdots & \ddots & \vdots \\ -\overline{L}_{n1} & -\overline{L}_{n2} & \cdots & \sum_j \overline{K}_{nj} \end{bmatrix} \begin{bmatrix} \beta_1 \\ \beta_2 \\ \vdots \\ \beta_n \end{bmatrix} = \begin{bmatrix} 0 \\ 0 \\ \vdots \\ 0 \end{bmatrix} \ , \tag{4.98}$$

where n is the number of orthophotos, $\overline{K}_{ij} = 4\widetilde{K}_{ij}$, $\overline{L}_{ij} = 4\widetilde{L}_{ij}$, and $\overline{K}_{ij} = 0$ and $\overline{L}_{ij} = 0$ if there is no overlap between orthophoto i and orthophoto j.

As in Section 4.6.2.1 the system of linear equations can be solved simply by setting $\beta_i = \begin{bmatrix} 0 \\ 0 \\ 0 \end{bmatrix}$ for all orthophotos i. This is not a useful solution, so a regularization term must be inserted as done in Equation (4.16). The used regularization term is defined in Equation (4.46), such that

$$Q = \left\| \begin{bmatrix} w_a & 0 & 0 \\ 0 & w_b & 0 \\ 0 & 0 & w_c \end{bmatrix} \begin{bmatrix} a \\ b \\ c \end{bmatrix} - \begin{bmatrix} 0 \\ 0 \\ w_c \end{bmatrix} \right\|_2^2 \tag{4.99}$$

$$= \|W\beta - v\|_2^2 \ , \tag{4.100}$$

where $W = \begin{bmatrix} w_a & 0 & 0 \\ 0 & w_b & 0 \\ 0 & 0 & w_c \end{bmatrix}$ and $v = \begin{bmatrix} 0 \\ 0 \\ w_c \end{bmatrix}$.

The regularization term defined in Equation (4.100) has three parameters, w_a, w_b, and w_c. The three parameters are used to set a damping on each of the coefficients in the model, $\alpha(x, y) = ax + by + c$. w_a is used to put a damping on the ax term. This insures that the variation between the left and the right part of the orthophoto does not become too large. Similarly w_b is used to insure that the vertical variation does not become too large.
The third parameter w_c is used in Equation (4.100) to form the term

$$w_c c - w_c = w_c(c - 1) \tag{4.101}$$

This means that w_c is used to penalize how far c can go from 1. This is done due to the fact that the closer c is to one, the closer the orthophoto is to the original orthophoto.

The regularization term should be inserted for each orthophoto, such that

$$\begin{bmatrix} \sum_j \overline{K}_{1j} & -\overline{L}_{12} & \cdots & -\overline{L}_{1n} \\ -\overline{L}_{21} & \sum_j \overline{K}_{2j} & \cdots & -\overline{L}_{2n} \\ \vdots & \vdots & \ddots & \vdots \\ -\overline{L}_{n1} & -\overline{L}_{n2} & \cdots & \sum_j \overline{K}_{nj} \\ W & 0 & \cdots & 0 \\ 0 & W & \cdots & 0 \\ \vdots & \vdots & \ddots & \vdots \\ 0 & 0 & \cdots & W \end{bmatrix} \begin{bmatrix} \beta_1 \\ \beta_2 \\ \vdots \\ \beta_n \end{bmatrix} = \begin{bmatrix} 0 \\ 0 \\ \vdots \\ 0 \\ v \\ v \\ \vdots \\ v \end{bmatrix} . \tag{4.102}$$

Some experiments with global gradual matching with the division method are computed and discussed in Section 5.8.2.

A way to estimate a correction method for a bilinear change in colours over each orthophoto has been developed. For the division method there are three damping parameters: w_a, w_b, and w_c, which denote the damping of the slope in the x-direction and the y-direction, and the general level of the pixel values, respectively.

The global gradual matching method is being implemented in a test version of the production system at COWI A/S.

4.7 Boundary

An addition to global gradual matching is created, which penalizes the changes in the colours at the boundary of the area. This means that another regularization term is added to the regularization described in Section 4.6.5.

The gradual transformation is estimated by minimizing the sum of squared differences in the overlaps between orthophotos. This can cause a problem in the orthophotos at the boundary of the graphical map, since one or more of the possible neighbouring orthophotos does not exist. This can lead to extreme results at the boundary, and therefore some boundary conditions are used to limit, how much the pixels at the boundary are allowed to change. This means that another term is inserted in the optimization problem, which penalizes the changes at the boundary.

The number of pixels across the boundary is defined by the boundary width $\delta \geq 0$.

The transformed pixel values of the boundary are expressed using the coefficients of the linear model β_i for each orthophoto i. The original pixel values are subtracted and the sum of squared differences $\widehat{F}$ is minimized. This is similar to the derivation in Section 4.6.2, such that

$$\begin{aligned}
\min_{\theta} \widehat{F} &= \sum_i \widehat{G_i} && (4.103)\\
\widehat{G_i} &= \|B_i\beta_i - b_i\|_2^2 && (4.104)\\
&= (B_i\beta_i - b_i)^T(B_i\beta_i - b_i) && (4.105)\\
&= \beta_i^T B_i^T B_i\beta_i - \beta_i^T B_i^T b_i - {b_i}^T B_i\beta_i - {b_i}^T b_i && (4.106)\\
&= \beta_i^T B_i^T B_i\beta_i - 2\beta_i^T B_i^T b_i - {b_i}^T b_i \ , && (4.107)
\end{aligned}$$

where

$$\theta = \begin{bmatrix} \beta_1 \\ \beta_2 \\ \vdots \\ \beta_n \end{bmatrix} , \tag{4.108}$$

and b_i is a vector, containing all the pixel values of the boundary, β_i is the usual coefficients of the linear model, and B_i is given by

$$B_i = \begin{bmatrix} b_{i1}x_{i1} & b_{i1}y_{i1} & b_{i1} \\ b_{i2}x_{i2} & b_{i2}y_{i2} & b_{i2} \\ \vdots & \vdots & \vdots \\ b_{im}x_{im} & b_{im}y_{im} & b_{im} \end{bmatrix} , \tag{4.109}$$

where x_{ik} and y_{ik} are the positions of each boundary pixel, and m is the number of pixels on the boundary. In order to solve the minimization problem the expression obtained in (4.107) is differentiated

$$\frac{\partial \widehat{G_i}}{\partial \beta_i} = (\widehat{K_i} + \widehat{K_i}^T)\beta_i - 2\widehat{L_i} \tag{4.110}$$

$$= 2\widehat{K_i}\beta_i - 2\widehat{L_i} , \tag{4.111}$$

where $\widehat{K_i} = B_i^T B_i$ and $\widehat{L_i} = B_i^T b_i$.

It should be noticed that $\widehat{K_i}$ is symmetric, which means that $\widehat{K_i} = \widehat{K_i}^T$.

The minimum can then be found by solving the following equation

$$\frac{\partial \widehat{F}}{\partial \beta_i} = 2\widehat{K_i}\beta_i - \widehat{L_i} = 0 \Rightarrow \tag{4.112}$$

$$2\widehat{K_i}\beta_i = 2\widehat{L_i} . \tag{4.113}$$

Since the boundary conditions are used as another regularization term, a damping parameter is multiplied to the computed expressions. Then the expression, along with the corresponding damping parameter $w_B \geq 0$ is inserted in the system of linear equations for the gradual transformation, such that

$$\begin{bmatrix} \sum_j \overline{K}_{1j} & -\overline{L}_{12} & \cdots & -\overline{L}_{1n} \\ -\overline{L}_{21} & \sum_j \overline{K}_{2j} & \cdots & -\overline{L}_{2n} \\ \vdots & \vdots & \ddots & \vdots \\ -\overline{L}_{n1} & -\overline{L}_{n2} & \cdots & \sum_j \overline{K}_{nj} \\ W & 0 & \cdots & 0 \\ 0 & W & \cdots & 0 \\ \vdots & \vdots & \ddots & \vdots \\ 0 & 0 & \cdots & W \\ w_B\widehat{K_1} & 0 & \cdots & 0 \\ 0 & w_B\widehat{K_2} & \cdots & 0 \\ \vdots & \vdots & \ddots & \vdots \\ 0 & 0 & \cdots & w_B\widehat{K_n} \end{bmatrix} \begin{bmatrix} \beta_1 \\ \beta_2 \\ \vdots \\ \beta_n \end{bmatrix} = \begin{bmatrix} 0 \\ 0 \\ \vdots \\ 0 \\ v \\ v \\ \vdots \\ v \\ w_B\widehat{L_1} \\ w_B\widehat{L_2} \\ \vdots \\ w_B\widehat{L_n} \end{bmatrix} . \quad (4.114)$$

A number of experiments have been performed using global gradual matching with the division method and boundary conditions, described in Section 5.8.2.

Boundary conditions can be used to improve the results from global gradual matching, since it adds another type of regularizarion. It is dependent on two parameters: The boundary width δ and the boundary damping parameter w_B. These parameters should be tuned with the damping parameters w_a, w_b, and w_c in the regularization term, used in the multiplication method or the division method.

4.8 Change Detection

It can occur that some pixels in two overlapping orthophotos do not represent the same object. Therefore these pixels should be removed from the model estimation. This is done by finding the pixels that have changed the most. This is based on canonical correlation analysis. In this section change detection is described in connection with global histogram matching, but can be used as well for global pixelwise matching and global gradual matching.

The change in the objects between orthophotos can have an effect on the histogram matching. For instance if the observation angle of the air plane causes more shadow to be seen in one overlap X_{ij} than in the other overlap X_{ji}, the histogram of overlap X_{ij} will also contain more shadow pixels than the histogram of overlap X_{ji}, see Figure 3.5. This means that the histograms contain

pixels, which represent different objects, and therefore pixels, which should not be compared. Another example is a car in different positions in two overlapping orthophotos. This effect can be avoided by simply removing the pixels in question from both histograms before the histogram matching is done. The pixels are found using change detection.

Change detection is a method to find the pixels that represent objects, which are different in two overlapping images. There are different change detection methods. In this case iteratively reweighted multivariate alteration detection (IR-MAD) is used, as described by [11]. IR-MAD is an extension of multivariate alteration detection (MAD), which is based on canonical correlation analysis (CCA). An advantage of using IR-MAD is that it is invariant to affine transformations, which means that it is unaffected to the influence of weather and light conditions on the colours of the images, which is highly relevant in this case.

In change detection a linear transformation is found which maximizes the variance of the difference between the images. This means that the pixels where there is a change between the two images are enhanced. The pixels with the largest change between two images are then found by simple thresholding. Since the images in this case are not colour adjusted, it is prudent to use IR-MAD, because a different linear combination of the spectral bands is made for each of the overlapping images. The two linear combinations, which highlights the changes between the images, are found by maximizing the variance of the difference between them. The variance is given by

$$V\{a^T X_{ij} - b^T X_{ji}\} \ , \tag{4.115}$$

where a and b are the coefficients of the two linear combinations, and $V\{a^T X_{ij}\} = V\{b^T X_{ji}\} = 1$. The maximum is found by using CCA, which finds a number of different pairs of linear combinations, where the first pair has the highest canonical correlation. The second pair, which is orthogonal to the first pair, has the second highest canonical correlation, and so on. The correlation is found by using the variance-covariance matrices of X_{ij} denoted as Σ_{11}, X_{ji} denoted as Σ_{22}, and the covariance between them denoted as Σ_{12}. The correlation is given by $\rho = Corr\{a^T X_{ij}, b^T X_{ji}\}$, which results in the Rayleigh quotient [11]

$$\rho^2 = \frac{a^T \Sigma_{12} \Sigma_{22}^{-1} \Sigma_{21} a}{a^T \Sigma_{11} a} \tag{4.116}$$

$$= \frac{b^T \Sigma_{21} \Sigma_{11}^{-1} \Sigma_{12} b}{b^T \Sigma_{22} b} \ . \tag{4.117}$$

The results are found by calculating the eigenvalues of $\Sigma_{12}\Sigma_{22}^{-1}\Sigma_{21}$ with respect to Σ_{11}. The eigenvalues are denoted $\rho_1^2 \geq \cdots \geq \rho_p^2 \geq 0$ and the corresponding

eigenvectors are given by $a_1, \cdots, a_p$, where p is the number of spectral bands, in this case 3. The corresponding results for X_{ji} are found by using the eigenvalues of $\Sigma_{21}\Sigma_{11}^{-1}\Sigma_{12}$ with respect to Σ_{22}, which are identical to the eigenvalues calculated before. The corresponding eigenvectors are given by $b_1, \ldots, b_p$.

From the results of the canonical correlation analysis the MAD transformation is defined as

$$\begin{bmatrix} X_{ij} \\ X_{ji} \end{bmatrix} \rightarrow \begin{bmatrix} a_p^T X_{ij} - b_p^T X_{ji} \\ \vdots \\ a_1^T X_{ij} - b_1^T X_{ji} \end{bmatrix} \ . \tag{4.118}$$

The MAD variates are defined such that MAD variate 1 is a difference between the highest order canonical pairs of linear combinations, which means the ones with the least canonical correlation. In order to distinguish the areas in the overlapping images that have changed from the rest, MAD variate 1 which represents the lowest canonical correlation, computed above, is used.

In change detection the goal is to label every pixel to either "changed" or "unchanged". This is done by using a χ^2-distribution to determine the probability of the event that a pixel is "changed". The variance of the MAD variates is then given by

$$\sigma^2_{MAD_i} = 2(1 - \rho_{p-i+1}) \ . \tag{4.119}$$

The χ^2-distribution is introduced by the expression

$$T_j = \sum_{i=1}^{p} \left(\frac{MAD_{ij}}{\sigma_i} \right)^2 \sim \chi^2(p) \ . \tag{4.120}$$

In IR-MAD this method is expanded by iteratively assigning weights w_j to pixel j, such that pixels that have changed have a low weight. The weights are chosen as the probability of finding a greater value of T_j defined in (4.120) [11]

$$w_j = P\{T_j > t\} \approx P\{\chi^2(p) > t\} \ . \tag{4.121}$$

The weights are used in the calculations of the MAD variates, by calculating the weighted means of X_{ij} and X_{ji} and the variance-covariance matrices of X_{ij} and X_{ji}. In this way the MAD variates are updated iteratively, until the change in the Rayleigh quotient is sufficiently small, i.e. smaller than the change detection convergence limit $\epsilon \geq 0$. The weights are then used to assign labels to the pixels by simple thresholding, such that all pixels with a weight smaller than the change detection threshold $\alpha \in [0; 1]$ are removed.

Some experiments have been performed in order to investigate the effect of the change detection for different values of the threshold parameter α and the change detection convergence limit ϵ in Section 5.3.

With change detection the pixels that have changed the most between a pair of overlapping orthophotos, are found by maximizing the variance of the difference between them. Change detection depends on two parameters: The change detection threshold α and the change detection convergence limit ϵ.

4.9 Quantification

The object of the colour correction methods is that the orthophotos appear to be part of one big continuous image. Problems can arise, since observers are different, and therefore the colours are perceived differently for each person. This is described in [15], where a panel test has been performed, although only with a small number of people. Due to the subjective nature of colour observation three measures are presented here, which can be used to quantify the quality of the developed results.

4.9.1 Gradient Based Quantification of Seamlines

A measure is created, which determines the visibility of seamlines. This is done based on the gradients at the seamline.

In order to make a graphical map more uniform, the colours should be adjusted, such that the seamlines are as invisible as possible, while keeping the colours as natural as possible. Several methods to obtain this result are investigated. Therefore it is useful to have a way of measuring the quality of the results by evaluating the visibility of the seamlines with a quantitative measure.

In this gradient based quantification method the gradient is first computed between the two sides of the seamline, with values from one orthophoto at one side of the seamline and values from the other orthophoto at the other side of the seamline. Then the gradient is computed between either side of the seamline in one orthophoto, and at last the two gradients are subtracted.

4.9.1.1 Seamline detection

At first the seamlines between the shown orthophotos in the graphical map should be detected. This is done by using the reference map shown in Figure 4.8a, which specifies where each orthophoto is shown in the graphical map.

For each shown orthophoto the seamline around the visible area is found using morphological operations. First a dilation is performed, which adds a pixel everywhere around the area. Then an erosion is performed, which removes the pixels at the border of the area. When the two binary images are subtracted only the border remains and the seamline $\mathcal{S}$ is found. The operations are given by

$$\mathcal{S} = (\mathcal{A} \oplus \mathcal{B}) - (\mathcal{A} \ominus \mathcal{B}) \ , \tag{4.122}$$

where $\mathcal{A}$ is the original area and $\mathcal{B}$ is the structuring element given by

$$\begin{bmatrix} 0 & 1 & 0 \\ 1 & 1 & 1 \\ 0 & 1 & 0 \end{bmatrix} \ . \tag{4.123}$$

$\oplus$ and $\ominus$ denote the dilation and the erosion, respectively and $\mathcal{S}$ is the set of pixels that combined form the seamline of $\mathcal{A}$. The process is illustrated in Figure 4.7.

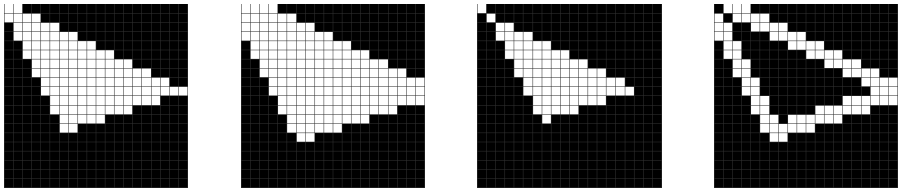

Figure 4.7: *The figure shows an example of the used morphology operations. The four images are (a) the example as a binary area $\mathcal{A}$, (b) the area in (a) after a dilation, (c) the area in (a) after a erosion, and (d) the difference between the dilation in (b) and the erosion in (c).*

Figure 4.7a shows a simple example of a visible area. The dilation and erosion are shown in Figure 4.7b-4.7c, and it can be observed that the dilation is a pixel larger than the visible area, and that the erosion is a pixel smaller than the visible area. The found seamline is shown in Figure 4.7d as the difference between the dilation and the erosion, and it can be observed that it does follow the border of the visible area, as expected.

The seamlines that have been detected using the described process are shown in Figure 4.8b with the reference map. The figure shows that the found seamlines match the position of the seamlines observed in the reference map.

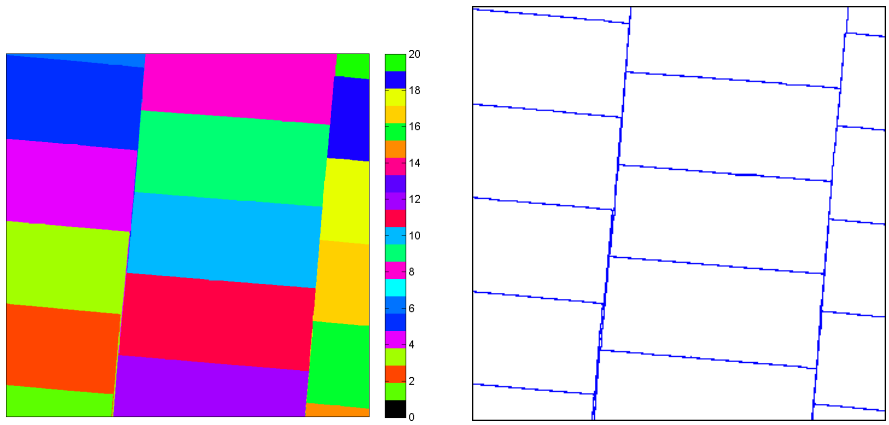

Figure 4.8: *The figure shows (a) the reference map, which specifies where each orthophoto is visible and (b) the detected seamlines in (a).*

4.9.1.2 Seamline measure

Once the seamlines have been detected, the seamline measure is computed. In order to determine the visibility of the seamlines the gradients at the seamlines are used. The gradient uses the difference between the pixels on either side of the seamline while taking the differences along the seamline into account. Therefore the gradients are calculated along the seamline using information from both of the visible orthophotos in question as illustrated in Figure 4.9.

At the seamline at least one of the visible orthophotos O_k are present at both sides of the seamline. The gradients in this orthophoto can be used as comparison of the gradients in the seamline. This is due to the fact that the gradients in O_k are only affected by the objects in the photo. Therefore the gradients are calculated in both the seamline between the two orthophotos and in orthophoto O_k as illustrated in Figure 4.9, and the two results are subtracted.

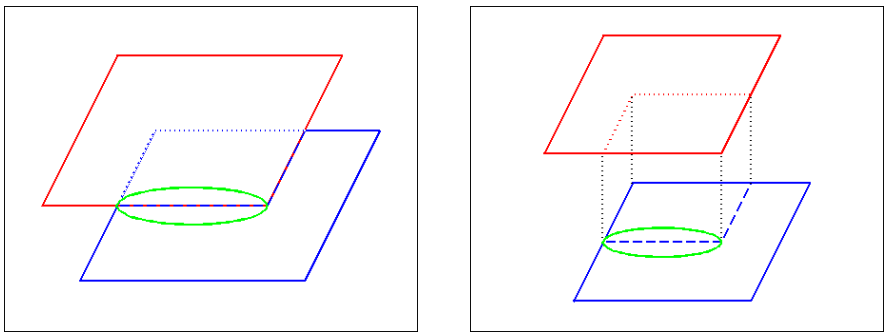

Figure 4.9: *The figure shows a red image, which covers part of a blue image. As the green ellipse illustrates the gradient is calculated (a) at the seamline between the two images and (b) in the blue image at the same positions as the seamline.*

The gradients are calculated by applying a filter based on a Prewitt filter [7] to the image. This filter is given by

$$H = \begin{bmatrix} 1 \\ 0 \\ -1 \end{bmatrix} \quad . \tag{4.124}$$

With this operation the derivative along the vertical axis is obtained. Likewise the derivative along the horizontal axis is computed by using the filter H^T.

The gradient is used since it takes the derivative between either side of the seamline and the derivative along the seamline into account. However, the magnitude g of the gradient can also be calculated simply from the derivatives along the axes since

$$g = \sqrt{d_{||}^2 + d_{\perp}^2} = \sqrt{d_x^2 + d_y^2} \ , \tag{4.125}$$

where $d_{||}$ and $d_{\perp}$ are the derivatives along and orthogonal to the seamline, respectively, d_x and d_y are the derivatives along the respective axes, and g is the magnitude of the gradient.

Once the magnitude of the gradient in the seamline has been calculated for the images in the mosaic and for the orthophoto O_k, the seamline measure of the graphical map is computed by summing the numerical differences Δg. The

seamline measure is thus given by

$$\Delta g = \left| \sqrt{d_{x,s}^2 + d_{y,s}^2} - \sqrt{d_{x,k}^2 + d_{y,k}^2} \right| \Rightarrow \tag{4.126}$$

$$S = \sum_{(x_i,y_i)\in\mathcal{S}} \left| \sqrt{d_{x_i,s}^2 + d_{y_i,s}^2} - \sqrt{d_{x_i,k}^2 + d_{y_i,k}^2} \right| , \tag{4.127}$$

where $d_{x_i,s}$ and $d_{y_i,s}$ are the derivatives in the horizontal and vertical direction, respectively, in pixel i at the seamline, and $d_{x_i,k}$ and $d_{y_i,k}$ are the derivatives in the horizontal and vertical direction, respectively, in pixel i in orthophoto O_k at the position of the seamline.

The advantage of this method is that it quantifies the visual comprehension of the seamlines, since it takes the differences between each side of the seamline into account, and since the difference between the colours in two neighbouring areas is important to the impression of the resulting graphical map.[2]

4.9.1.3 Verification of the seamline measure

Some experiments have been performed in order to determine whether the seamline measure is in fact a measure that determines how visible the seamlines in a graphical map really are. For this purpose a small test area shown in Figure 4.10a is used to construct different situations in order to see the consequences in the seamline measure. The area contains a large homogeneous field, which makes the constructed seamlines very distinct. The examples are constructed such that the upper area of the image marked in Figure 4.10b is transformed using a colour transformation matrix T. An example of the result is shown in Figure 4.10c. This result is used as a controlled example for evaluation of the seamline measure. In this case the transformation matrix is given by

$$T = \begin{bmatrix} 0.6 & 0 & 0 \\ 0 & 1 & 0 \\ 0 & 0 & 1 \end{bmatrix} . \tag{4.128}$$

When the upper area in Figure 4.10c is multiplied by the matrix T, the red band is multiplied by 0.6, while the green and the blue band remain the same. This means that the red colour in the upper area is reduced, while the lower area is unchanged as shown in Figure 4.10c. This creates a colour difference and thereby makes the seamline between them more distinct. This means that the further the diagonal element is from 1, the more distinct is the seamline.

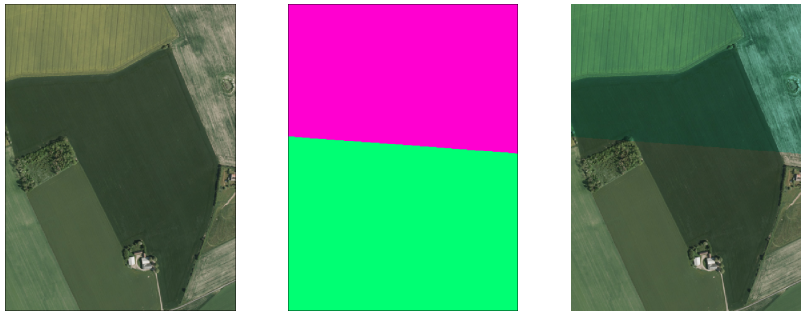

(a) (b) (c)

Figure 4.10: *The figure shows (a) the small test area only showing orthophoto 9, (b) the area which is transformed marked in magenta, and (c) the small test area, but now the upper part of the area has been transformed with a multiplication of the intensity of the red band of 0.6.*

A number of experiments have been performed by systematically computing examples with a change in intensity as the one in Figure 4.10c. The intensity is altered by using the general intensity transformation matrix given by

$$T = \begin{bmatrix} r & 0 & 0 \\ 0 & g & 0 \\ 0 & 0 & b \end{bmatrix} . \tag{4.129}$$

Each of the values r, g, and b different from 1, scales the intensity in the respective colourbands independently, and experiments are made with a change of intensity in one, two, and three bands.

These experiments lead to 7 combinations of a change in intensity in the three bands. The seamline measure is shown in Figure 4.11a as a function of the intensity factor f, where the values r, g, and b that are different from 1 is equal to f. The figure shows that the seamline measure is linearly dependent on the intensity factor, and that it is equal to zero when the intensity factor is 1 in all cases. This is as desired since the transformation matrix is then the identity matrix, which means there is no colour transformation and therefore no seamline. The different positions of the red, green, and blue lines can be explained by the fact that there are different amounts of each colour in the image. Since the image is mostly green, the intensity factor will have a larger impact for green than for red or blue, because it is simply multiplied by higher pixel values.
It can also be observed from the figure that some of the straight lines are sums of other straight lines, for instance the change in intensity in both red and green

marked by the yellow line is the sum of the change in intensity of red and the change in intensity of green. This is due to the fact that the seamline measure is the sum of the difference in gradient in all three colour bands.

The seamline measure is symmetrical around the value one. This means that the seamline measure is the same if the intensity is increased or decreased. This is due to the fact that the seamline measure is calculated using the numerical differences.

Some similar experiments have been performed, where there is a value different from 0 in a single off-diagonal element of the transformation matrix. This means e.g. that a transformation is made on the red band that affects the green band, while the red and the blue band remain unchanged. The transformation matrix is given by

$$T = \begin{bmatrix} 1 & RG & RB \\ GR & 1 & GB \\ BR & BG & 1 \end{bmatrix} , \tag{4.130}$$

where each of the off-diagonal elements are named by their position and effect, for instance is GR the factor, which controls how much the pixels in the red band before the transformation should influence the green band after the transformation.

Experiments have been made with all 6 off-diagonal elements separately and the results are shown in Figure 4.11b. The figure shows that the seamline measure is linearly dependent on the size of the off-diagonal element.

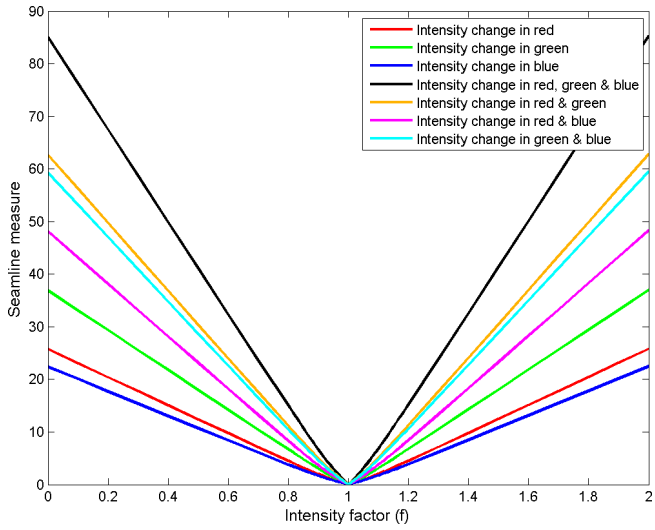

(a)

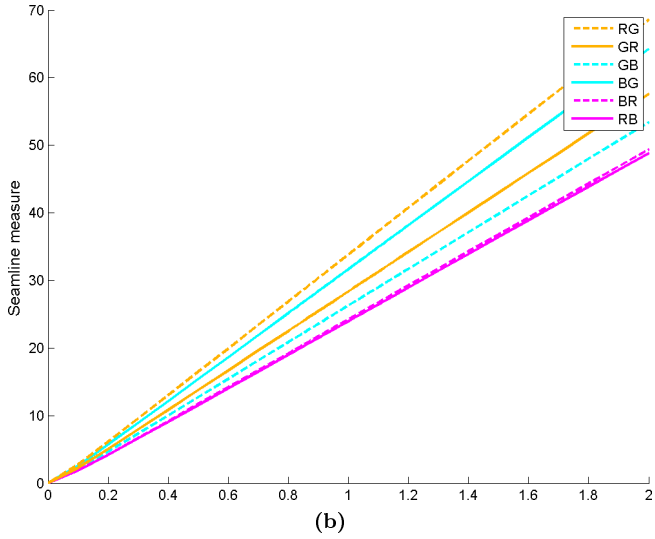

(b)

Figure 4.11: *The figure shows (a) the seamline measure as a function of the intensity factor f of all combinations of the three colour bands and (b) the seamline measure as a function of a change in an element of the off-diagonal of the transformation matrix.*

The examples illustrate that as the intensity f increases or decreases from 1, the seamline measure increases. As described earlier in this section the seamline

becomes more distinct, as f increases or decreases from 1, since this means that the colours of the upper area are further from the original colours. For this reason it can be deduced that a more distinct seamline results in a larger seamline measure, and that a seamline measure close to zero indicates that the seamline is close to invisible. This property is as desired, since it quantifies how visible the seamline is to the observer.

It should be noted that if there is a lot of variation near the seamline, the seamline may not be seen very distinct to the observer, although the seamline measure is high. It should also be noted that the seamline measure only provides a single value for the entire graphical map, which means that some seamlines may look more distinct, but still result in an overall low seamline measure.

4.9.2 Saturation

In order to be able to distinguish different objects e.g. roads, fields, or buildings, it is important that the saturation is high enough. If the saturation is too low, all the colours are more grey, and there will be a greater distance to the natural colours. The saturation is computed, based on the HSV colour space transformation.

The saturation can be computed by exploiting the fact that the image can be transformed such that it is expressed in a different colour space. The graphical map can be transformed from the RGB colour space to the HSV (Hue, Saturation, and Value) colour space [9] & [18].
In this colour space the hue denotes the direction of the colour, which means that it denotes the angle on a colour wheel. It therefore denotes whether the colour is red (axis 1), green (axis 2), blue (axis 3), or a mixture.
The saturation measures the purity of the colour, and is the radius of the colour wheel. With a high saturation the colour will be very pure, and with a low saturation the colour is more greyish.
The value is simply the brightness of the colour, such that it has a clear colour at maximum value and is black at minimum value.

The transformation between the RGB and the HSV colour space is used to compute the saturation of the graphical map, and is given by [9] & [18]

$$H = \begin{cases} \text{undefined} & \text{if} \quad u = v \\ 60° \cdot \frac{g-b}{v-u} + 0° & \text{if} \quad v = r \wedge g \geq b \\ 60° \cdot \frac{g-b}{v-u} + 360° & \text{if} \quad v = r \wedge g < b \\ 60° \cdot \frac{b-r}{v-u} + 120° & \text{if} \quad v = g \\ 60° \cdot \frac{r-g}{v-u} + 240° & \text{if} \quad v = b \end{cases} \tag{4.131}$$

$$S = \begin{cases} 0 & \text{if } v = 0 \\ \frac{v-u}{v} & \text{otherwise} \end{cases} \tag{4.132}$$

$$V = v \ , \tag{4.133}$$

where H, S, and V are hues, saturation, and value, respectively. The two variables used are $u = \min(r, g, b)$ and $v = \max(r, g, b)$, and r, g, and b are the red, green, and blue values in each pixel. The transformation between the two colour spaces is non-linear, but it can be reversed.

The saturation is computed for each pixel i in the graphical map and denoted S_i. The values are summed and the result is normalized by dividing with the number of pixels, such that the saturation measure is given by

$$M_S = \frac{1}{n} \sum_{i=1}^{n} S_i \ , \tag{4.134}$$

where n is the number of pixels in the graphical map.

In order to ensure that the different objects in the image are distinguishable, it is important that the saturation is not too low. Therefore the saturation can be used as a measure of quality.

4.9.3 Contrast

Another property that also gives important information about the quality of a graphical map is contrast. The contrast is computed as a root mean square of the pixel values.

The contrast is important in order to be able to distinguish different objects in the image. If the contrast is too high the shadows in the image may become too dark and if the contrast is too small the image will appear flat and dreary. When the image appears flat it can also be harder to tell different objects apart. [10]

There are different methods, which can be used to calculate the contrast. In this case the Root Mean Square (RMS) contrast has been chosen, which is simply defined as the standard deviation of the pixel intensities given by [19]

$$RMS = \sqrt{\frac{1}{n}\sum_{i=1}^{n}\left(I_i - \bar{I}\right)^2}\ , \tag{4.135}$$

where n is the number of pixels in the graphical map, I_i is the intensity in a pixel, and $\bar{I}$ is the average of all intensities in the graphical map.

The contrast is used since it determines how great differences in light intensity are. This is highly relevant, since it is hard to use an image, where it is difficult to identify the different objects.

4.9.4 Trade-off

The three measures can be used as measures of quality in order to compare different results and thus determine whether a new approach to the problem has been fruitful. It can therefore be used to determine how much impact e.g. use of change detection has on the result.

The three measures can also be used to choose the appropriate parameters, for instance, when choosing the damping parameter in global histogram matching. This is done by making a trade-off of the three measures of the result.

The three measures, the seamline measure, the saturation, and the contrast are illustrated in Section 5.4.

4.10 Residuals

The three measures described in section 4.9 each give a single value for the entire graphical map. This is not always desirable since it reveals nothing about which part of the graphical map that has the largest influence on the quality of the graphical map. Therefore another way should be found to visualize the quality of a graphical map in each pixel individually.
In order to test the quality of the graphical map, the orthophotos are compared. Due to the many overlaps it is not practical to simply subtract each pair of overlapping orthophotos. Therefore the standard deviation is calculated instead.

For each pixel, all orthophotos, which overlap in the pixel, are considered. The colour value of the pixel in each of the orthophotos is found, and the standard deviation is calculated for each colour band: Red, green, and blue. In this way a measure is obtained, which determines the difference between the colours of the orthophotos in each pixel. The calculated standard deviations are then visualized in a combined RGB image.

The residual image has darker colours where there is little difference between the orthophotos and brighter colours where the orthophotos have different values. This means that if the residual image of the transformed orthophotos is very dark, the colours in the orthophotos match very well. However, even with a perfect colour correction some areas will always have a high standard deviation. This is due to the fact that trees and buildings cast shadows, which vary during the day, and that they can appear differently from different angles. This is illustrated in Figure 4.12. The figure shows that since the orthophotos are taken from different angles, the shadows vary between the images.

(a) **(b)** *Orthophoto 9* **(c)** *Orthophoto 19*

Figure 4.12: *The figure shows (a) the standard deviation of tile* $d_{8,32}$*, (b) tile* $d_{8,32}$ *from set 9, and (c) tile* $d_{8,32}$ *from set 19.*

The residuals of the entire orginal test area are described in Section 5.1

4.11 Computational Optimization

Due to the large amount of data necessary measures are taken to reduce the computational time. Here three different methods are used: Parallel programming used in model estimation, parallel programming used in image transformation, and downsampling. In this section these three methods are described using global histogram matching, but they are also used for global pixelwise matching

and global gradual matching.

Each tile consists of 625×625 pixels, and the entire test area consists of 32×32 tiles from 22 different orthophotos. This makes the global histogram matching algorithm computationally heavy, and even just showing the test area may be very time consuming. Therefore steps are taken to optimize the implementation.

The global histogram matching algorithm has been optimized, by ensuring that MatLab divides the iterative process of calculating the histogram matching between pairs of orthophotos parallelly as opposed to making the calculations sequentially. In this way MatLab takes advantage of the computers ability to use several kernels simultaneously. Table 4.2 shows the running time for global histogram matching with sequential and parallel programming. It is seen that parallel programming is approximately 4 times faster than sequential.

Parallel programming has also been used to optimize the transformation. This is done by transforming each row of tiles parallelly. Table 4.2 illustrates that parallel programming makes an improvement of approximately a factor of 5.

The third optimization step, that has been performed, is downsampling. This can be done when the system of linear equations for the global histogram matching is computed, since it would have little effect on the histograms, and consequently little effect on the transformations matrices. Another use of downsampling is when the orthophotos are transformed. This has great effect on the quality of the resulting graphical map, and is mostly used in the developing phase. Therefore downsampling has been used in both cases in these examples.

	Sequential	Parallel
Global histogram matching	114 sec. / 106 sec.	27 sec. / 26 sec.
Transformation	30 sec. / 29 sec.	6 sec. / 6 sec.

Table 4.2: *The table shows the running time of the global histogram matching and the transformation with sequential and parallel programming. The tests are made using a part of the test area with a downsampling factor of* $\frac{1}{10}$ *in each direction.*

Parallel programming and downsampling reduces the computational time significantly, and this is therefore implemented in the described colour correction algorighms.

Chapter 5

Results

Examples are computed in order to study residuals, neighbourhoods, and change detection. A demonstration of three measures for quantification is made, and the three colour correction methods are investigated.

5.1 Residuals

The residual image, shown for the orginal graphical map, is investigated.

The residuals are described in Section 4.10. In order to have a reference for the residuals of the results, the residuals of the original test data is shown in Figure 5.2. It can be observed from the figure that there is a green zone in the top of the image from left to right. This represents the trees seen in the original graphical map in this position as shown in Figure 5.1. This is due to the fact that since the trees are tall objects, they will look different from different angles. It can also be observed that there are some large residuals at the houses in the lower part of the image for the same reason. Furthermore there are bright zones at the left and at the right part of the image. At these positions the overlaps between the three flight lanes are situated, and therefore the residuals are high due to the large light change between the lanes. If the resulting images have had an improvement in the colouring, these two zones will be darker.

In order to be able to make the residuals visible a factor is multiplied to the values. In Figure 5.2 this factor is 5.

Figure 5.1: *The original test data*

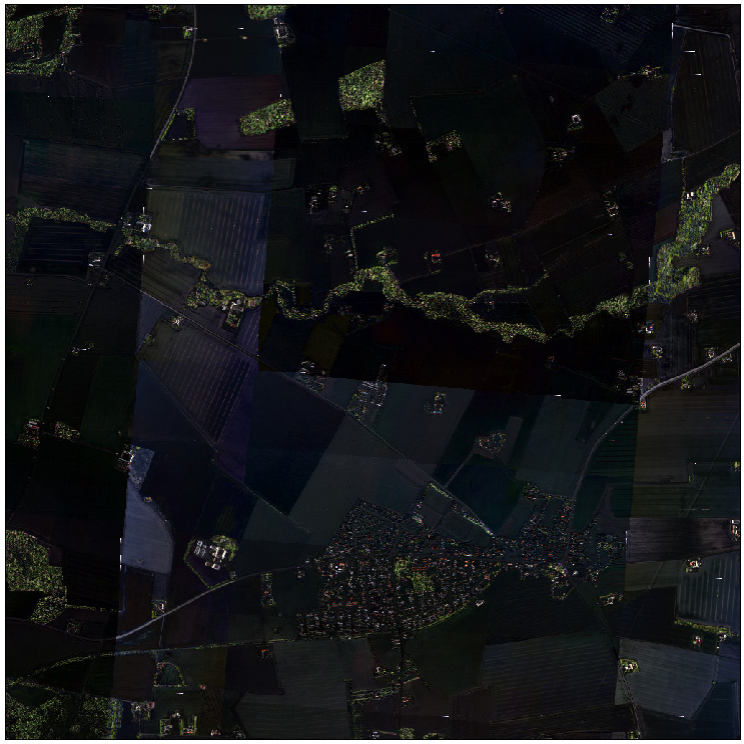

Figure 5.2: *Residuals of the original test data with a factor 5*

5.2 Neighbourhood

As described in Section 4.2 only a small number of the available overlaps are used. Experiments have been made using global histogram matching with both 4-neighbourhood and 8-neighbourhood, and the results are shown in Figure 5.3.

In comparison the result of global histogram matching using 4-neighbourhood in Figure 5.3c has more distinct seamlines than when 8-neighbourhood is used as in Figure 5.3d. This is as expected, since the latter is based on more information.

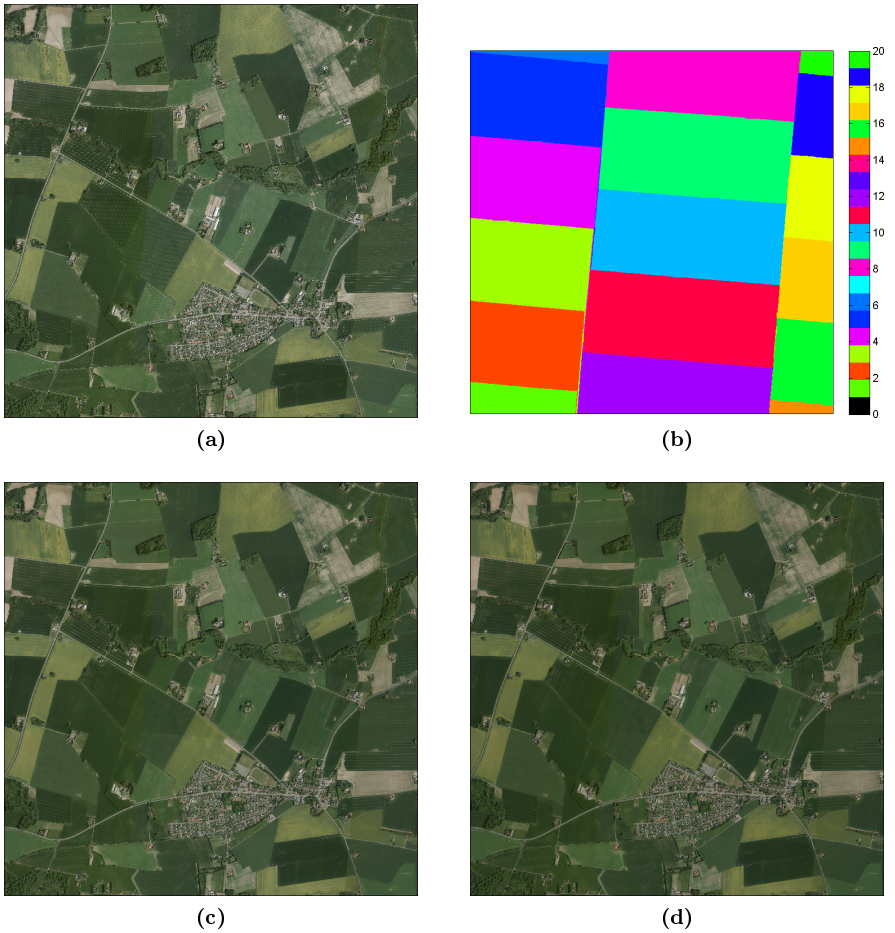

(a) (b)

(c) (d)

Figure 5.3: *The figure shows (a) the test area, (b) the corresponding reference map, (c) the result of a global histogram matching using 4-neighbourhood with a damping parameter of* $\lambda = 0.01$ *and (d) the result of a global histogram matching using 8-neighbourhood with a damping parameter of* $\lambda = 0.01$.

Since the differences in Figure 5.3c and 5.3d are very small, the residual images are computed and shown in Figure 5.4. The figure shows that the difference between using 4-neighbourhood and 8-neighbourhood is very small in this case.

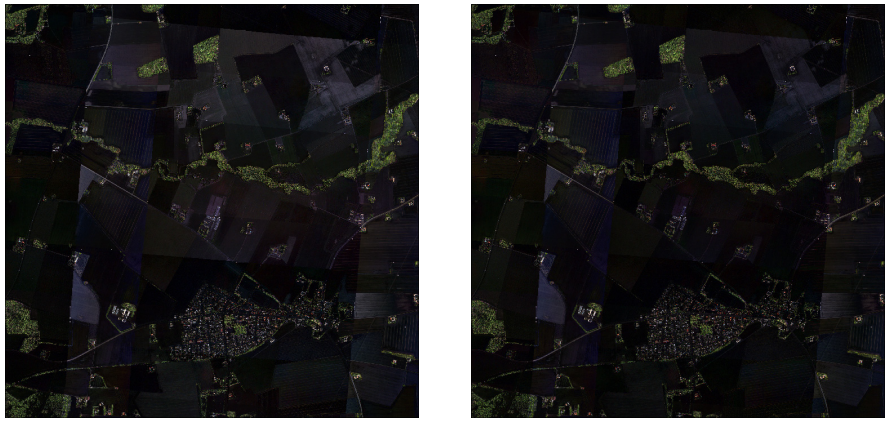

(a) *4-neighbourhood* **(b)** *8-neighbourhood*

Figure 5.4: *The figure shows the residual values for the results obtained using global histogram matching with (a) 4-neighbourhood and (b) 8-neighbourhood. In both cases a damping parameter of* $\lambda = 0.01$ *is used.*

The results are quantified in Table 5.1. The three measures confirm the observations, but they also show that while the result using 8-neighbourhood result has less distinct seamlines, it is at the expense of the contrast, which has decreased slightly.

	4-neighourhood	8-neighbourhood	original
Seamline measure	13.09	11.63	14.45
Saturation	0.36	0.38	0.32
Contrast	0.10	0.09	0.12

Table 5.1: *The table contains the seamline measure, saturation, and contrast for the result from global histogram matching with 4-neighbourhood and 8-neighbourhood, respectively, and a damping parameter of* $\lambda = 0.01$. *The measurements for the original graphical map are also stated in the table.*

The results show that when 8-neighbourhood is used, the seamlines are a little less distinct, and the saturation is increased, than when 4-neighbourhood is used, which is as wanted. However, the contrast is decreased, and the computational time is increased.

5.3 Change Detection

In order to investigate the effect of change detection several experiments have been performed, using global histogram matching.

Initially many examples have been computed for different values of the change detection threshold α and then compared. Then the connection between the change detection threshold α and the amount of remaining pixels is examined. Subsequently the change detection convergence limit ϵ is studied, and in the next example the change detection weights are discussed. Afterwards an example of global histogram matching with and without change detection is compared. Next, an example is shown with two different values of the change detection threshold α and a low value of the damping parameter λ. Finally an investigation is performed to examine the influence of the change detection threshold α on the three measures.

Change detection is, as described in Section 4.8, used to remove the pixels, which have the highest changes in an overlap. This means that e.g. trees, buildings, and other tall objects are removed, because of observation angles, shadows etc. Some examples are computed to investigate the effect of using change detection. In this section the results are based on the global histogram matching algorithm, but change detection can also be used with global pixelwise matching or global gradual matching.

5.3.1 Threshold, High Damping Parameter

The effect of the change detection threshold α has been investigated in several experiments. The results of the global histogram matching with change detection for a high value of λ and for different values of α are shown in Figure 5.5.

(a) $\alpha = 0.1$ (b) $\alpha = 0.2$ (c) $\alpha = 0.3$

(d) $\alpha = 0.4$ (e) $\alpha = 0.5$ (f) $\alpha = 0.6$

(g) $\alpha = 0.7$ (h) $\alpha = 0.8$ (i) $\alpha = 0.9$

Figure 5.5: *The figure shows the result of using global histogram matching with a regularization damping parameter $\lambda = 0.5$, 8-neighbourhood, a change detection convergence limit of $\epsilon = 10^{-2}$, and different change detection weight thresholds α.*

The figure shows that the change detection does not seem to have a high influence of the visibility of the seamlines for a high value of λ. However, there is a slight change in the colouring in some areas, when Figure 5.5a and 5.5i are compared.

5.3.2 Pixel Ratio and Threshold

The impact of the change detection threshold α on the amount of pixels used in the histogram matching is investigated. For each overlap the percentage of pixels left after the change detection is calculated for different values of α, and the result is shown in Figure 5.6. The figure shows that the threshold value should not be very large, since this will remove too much of the information from the histogram matching.

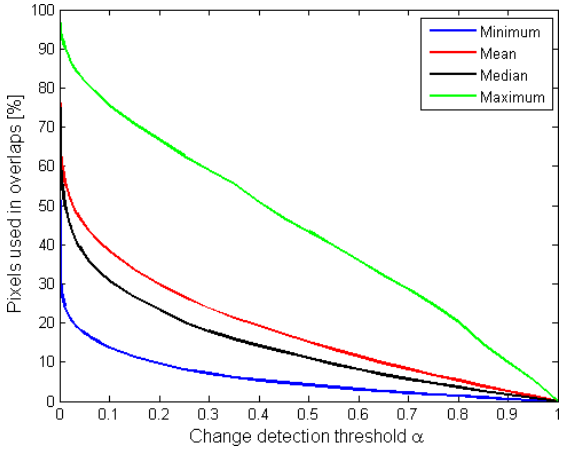

Figure 5.6: *The figure shows the percentage of pixels left in the overlaps after change detection has been performed, as a functions of the change detection threshold α.*

5.3.3 Convergence Limit

Experiments have also been performed in order to test the effect of the change detection convergence limit ϵ. The results are shown in Figure 5.7. There is not much difference between the results, which is as expected, since ϵ is only a limit of the convergence, and only determines how far the result is from the theoretical optimal solution.

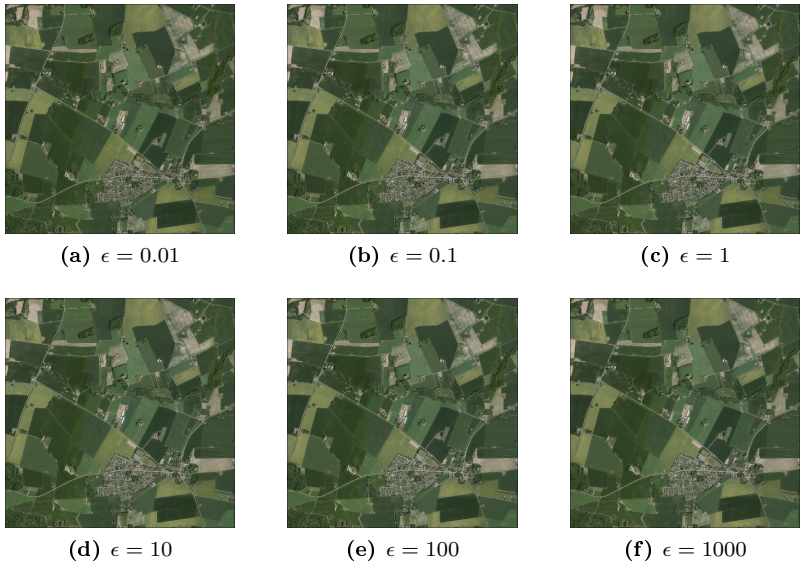

(a) $\epsilon = 0.01$ **(b)** $\epsilon = 0.1$ **(c)** $\epsilon = 1$

(d) $\epsilon = 10$ **(e)** $\epsilon = 100$ **(f)** $\epsilon = 1000$

Figure 5.7: *The figure shows the result of using global histogram matching with a regularization damping parameter* $\lambda = 0.5$*, 8-neighbourhood, a change detection weight thresholds* $\alpha = 0.6$ *and different change detection convergence limits* ϵ*.*

5.3.4 Change Detection Weights

The result of the change detection is investigated in order to determine whether the desired effect is obtained. This is illustrated by showing the weights on the final iteration of change detection for all the overlaps in a single image in Figure 5.8, by showing the sum of the weights from all the overlaps. The figure shows that in some areas the pixel values are very low, e.g. in the area, covered by the narrow zone of trees going from the left to the right in the test area and in the parts of the area covered by the town as seen in Figure 5.1 in Section 5.1. This is as wanted, since these areas are covered by tall objects, which may cast shadows and appear differently from different positions.

Figure 5.8: *The figure shows the final weights calculated in the change detection algorithm for each pair of neighbours using 4-neighbourhood. The dark pixels in each overlap are removed in the final thresholding.*

5.3.5 Examples with and without Change Detection

The effect of the change detection is investigated by comparing the result of the global histogram matching with and without change detection, shown in Figure 5.9, with the corresponding standard deviation images. The figure shows that there are differences in the standard deviations, but it is difficult to get a clear impression of which orthophotos that have been affected. Therefore the difference between the two standard deviation images is computed and shown in Figure 5.10. The difference image shows that the largest difference in the standard deviations is present in the orthophotos that contain areas with buildings and trees as expected.

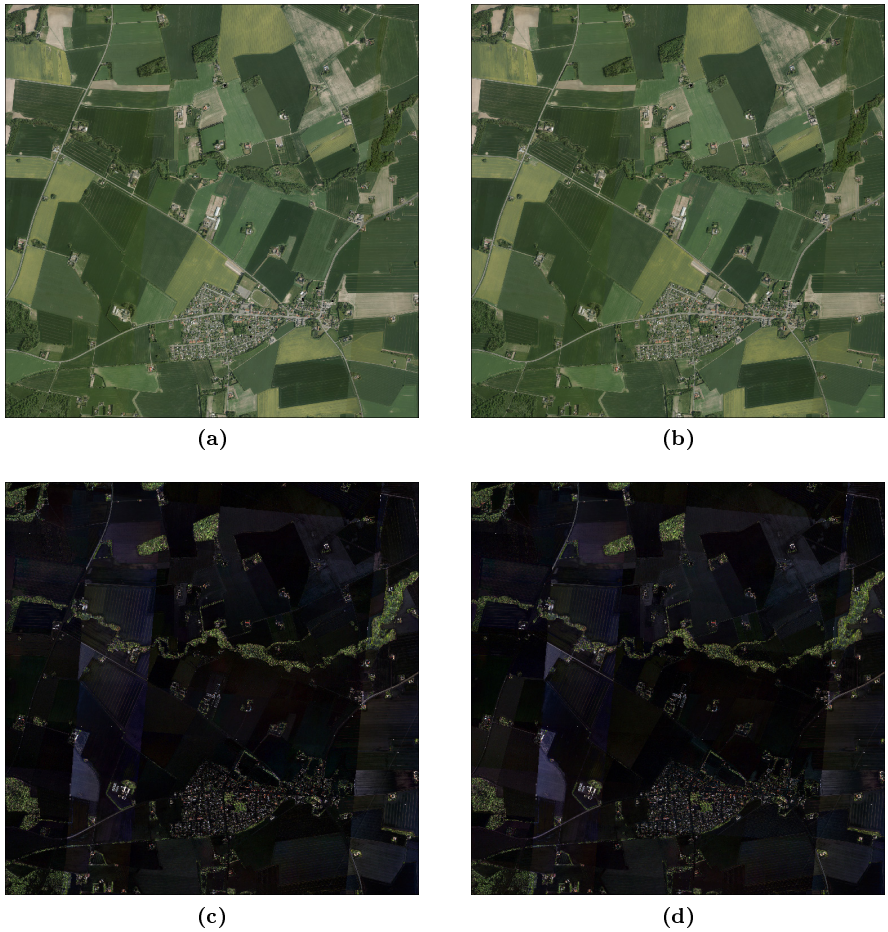

(a) (b)

(c) (d)

Figure 5.9: *The figure shows (a) the result from using global histogram matching, (b) the result from using global histogram matching with change detection with a threshold value of* $\alpha = 0.6$ *and a convergence limit of* $\epsilon = 0.01$*, (c) the standard deviations of the result in (a) and (d) the standard deviations of the results in (b). In both cases a damping parameter of* $\lambda = 0.5$ *and 8-neighbourhood is used. In both the standard deviation images the values have been multiplied by a factor of 5 in order to make the differences in the images more visible.*

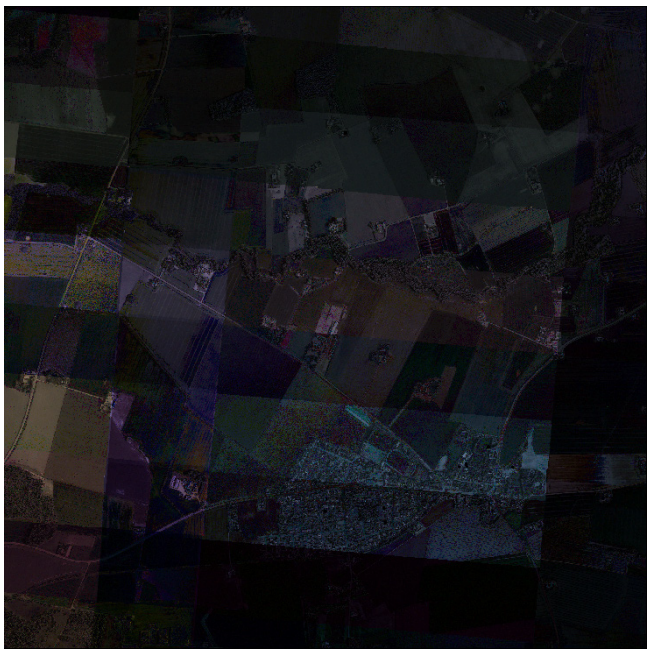

Figure 5.10: *The figure shows the numerical difference between the standard deviation images shown in Figure 5.9c and 5.9d, respectively. The values have been multiplied by a factor of 25 in order to make the differences in the images more visible.*

5.3.6 Threshold, Low Damping Parameter

Due to the small effect of the change detection in the examples in Section 5.3.1, experiments are performed using different values of the damping parameter λ. It appears that the results from using a damping parameter of $\lambda = 0.01$ is more affected by change detection than the result from using a damping parameter of $\lambda = 0.5$. The following experiments are therefore performed using $\lambda = 0.01$.

Figure 5.11 shows two examples of global histogram matching with change detection with different values of the change detection threshold α. It can be observed that the seamlines are more distinct in Figure 5.11a which uses $\alpha = 0.1$ than in Figure 5.11b which uses $\alpha = 0.9$.

(a) $\alpha = 0.1$

(b) $\alpha = 0.9$

Figure 5.11: *The figure shows two examples of the result obtained using global histogram matching with damping parameter* $\lambda = 0.01$*, 8-neighbourhood, and change detection with a convergence limit of* $\epsilon = 0.01$ *for two different values of the change detection threshold* α*.*

5.3.7 Quantification of Change Detection

In order to get an overview of how the change detection threshold affects the seamlines, several tests are made, and the three measures are calculated. The result is shown in Figure 5.12.

The seamline measure has at $\alpha = 0$ the same value as the measure of the global histogram matching without change detection marked by the black horizontal line in Figure 5.12. This is due to the fact that all the pixels in the image that has a weight larger than α are included as stated in Section 4.8, which means that all of the pixels are included at $\alpha = 0$ as is confirmed by Figure 5.6. At the maximum value of α the seamline measure goes towards 0 when α goes towards 1 as expected.
The contrast and the saturation are at $\alpha = 0$ also equal to the measurement obtained when global histogram matching is performed without change detection, as expected. As the change detection threshold goes towards 1, the saturation increases and the contrast decreases. This is as expected, since at $\alpha = 1$ all the pixels are removed.

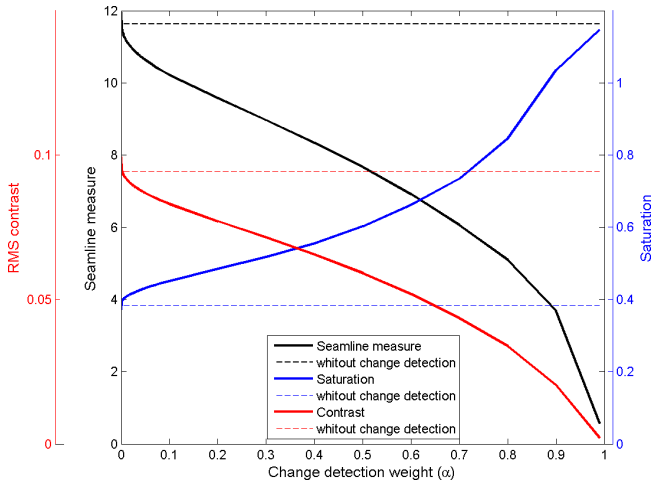

Figure 5.12: *The figure shows the three measures as a function of the change detection threshold α with the results from global histogram matching without change detection, marked by a dashed line. The lines and the respective axes are marked by corresponding colours. 8-neighbourhood and a damping parameter of $\lambda = 0.01$ and a convergence limit of $\epsilon = 0.01$ have been used.*

5.4 Quantification

Three measures have been defined: The seamline measure, the saturation, and the contrast. These measures are used to quantify the quality of the results. The measures are described in Section 4.9.

In order to illustrate the three described measures, three examples have been made, and are shown in Figure 5.13. The figure shows three results from global histogram matching with three different values of the damping parameter. The three different measures are shown in Table 5.2 for each of the three results.

It can be observed from the figure that the result in Figure 5.13a that the seamlines are much less visible than is the case in Figure 5.13c. This is in accordance with the seamline measurements in the table. The table also states that the results with a large damping parameter has a small saturation. This is also illustrated in the figure, since it can be observed that the result shown in Figure 5.13c looks more grey than the result in Figure 5.13a.

It is also seen that the contrast is low, when the damping parameter is low, and high, when the damping parameter is high according to the table. This is confirmed by the figure, since it can be observed that the contrast is higher in Figure 5.13c and lower in Figure 5.13a.

(a) $\lambda = 0.001$ **(b)** $\lambda = 0.003$ **(c)** $\lambda = 0.08$

Figure 5.13: *The figure shows the result from global histogram matching with 8-neighbourhood and three different values of the damping parameter.*

λ	0.001	0.003	0.08	Original
Seamline measure	5.74	8.75	13.68	14.45
Saturation	0.67	0.49	0.33	0.32
Contrast	0.04	0.07	0.11	0.12

Table 5.2: *The table contains some examples of the seamline measure, saturation, and contrast of a few results from global histogram matching with different values of the damping parameter λ.*

5.5 Histogram Matching

Initially histogram matching is tested on a single overlap between two neighbouring orthophotos. The overlap is constructed by loading and concatenating the corresponding tiles. The overlapping orthophotos do not form a precise rectangle, compared to the chessboard pattern, the tiles are divided in. Therefore a mask is made, that removes the areas that do not contain data in both images. Histogram matching is performed on the intersection, and an example of the overlap between orthophoto 1 and 14 is shown in Figure 5.14a and 5.14b.

In order to perform a histogram matching the histograms of the input and output images are calculated. From this, the cumulative histograms are calculated, and a lookup table is created as described in Section 4.3.

The input images are transformed using the estimated models and the results are shown in Figure 5.14c and 5.14d.

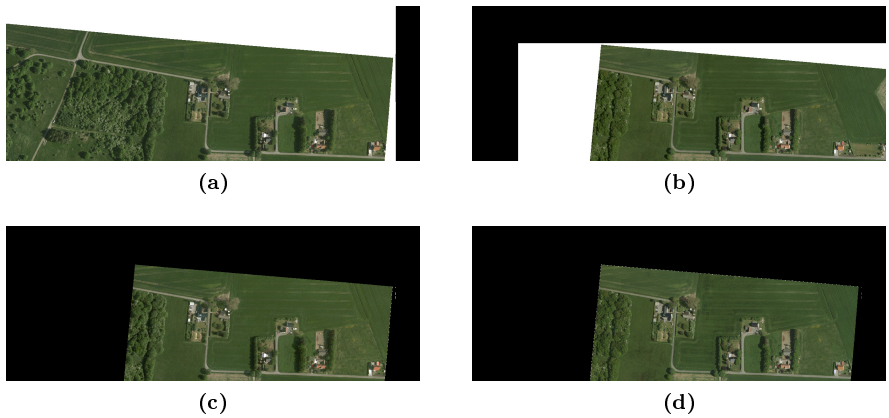

Figure 5.14: *The figure shows the overlap between orthophoto 1 and 14 before the transformation; (a) $X_{1,14}$ and (b) $X_{14,1}$ and after the transformation; (c) $Y_{1,14}$ and (d) $Y_{14,1}$.*

In this example there is e.g. a road a the bottom which is a little brighter in Figure 5.14a than in Figure 5.14b. In the transformed images the road has become darker in Figure 5.14c and brighter in Figure 5.14d. This is as expected, since the histogram of the image in Figure 5.14a is transformed to match the histogram in Figure 5.14b, and vice versa.

5.6 Global Histogram Matching

Experiments are performed to study the results from global histogram matching. Different levels of regularization are used, and the results are compared with the three measures. An analysis is made of the influence of the damping parameter on the three measures, and the residuals are compared.

5.6.1 Regularization

As described in Section 4.4.2 a regularization term has been inserted in the global histogram matching algorithm using the damping parameter λ. Experiments have been performed in order to determine the effect of the value of the damping parameter. The four results are shown in Figure 5.15 and 5.16.

(a) $\lambda = 0.001$

(b) $\lambda = 0.005$

Figure 5.15: *The figure shows the resulting images after using global histogram matching using 8-neighbourhood and two different values of the damping parameter.*

(a) $\lambda = 0.01$

(b) $\lambda = 0.1$

Figure 5.16: *The figure shows the resulting images after using global histogram matching using 8-neighbourhood and two different values of the damping parameter.*

The examples illustrate that a small damping parameter results in a dark image, while a large damping parameter results in an image with colours closer to the original colours, but where the seamlines are more visible. This effect is due to the fact that the damping parameter is used to penalize the term $\lambda \|I - A_i\|_2^2$, which means that the distance between the original and the resulting images is penalized. However, if the resulting images are too close to the original images, the seamlines are more visible.

The three different measures, the seamline measure, the saturation, and the contrast, described in Section 4.9, are shown in Table 5.3 for each of the four graphical maps.

It can be observed from the result in Figure 5.15a that the seamlines are much less visible than is the case in Figure 5.16a. This is in accordance with the seamline measurements shown in the table. The table also states that the results with a large damping parameter has a small saturation.

It is also seen that the contrast is low, when the damping parameter is low, and high, when the damping parameter is high according to the table. This is confirmed by the figure, since it can be observed that the contrast is higher in Figure 5.16b and lower in Figure 5.15a.

λ	0.001	0.005	0.01	0.1	Original
Seamline measure	5.69	10.03	11.53	13.59	14.23
Saturation	0.765	0.433	0.384	0.328	0.316
Contrast	0.0406	0.811	0.0944	0.112	0.115

Table 5.3: *The table contains the seamline measure, saturation, and contrast of a few examples of results from global histogram matching with different values of the damping parameter λ.*

The examples show that if a small damping parameter is used, the seamlines are less distinct, but the result is very dark. For a high value of the damping parameter the results are very similar to the original colours.

The described examples suggest that there is a correlation between the damping parameter and each of the three measures. This is investigated in Section 5.6.2.

5.6.2 Quantification

The damping parameter has a large impact on the result of the global histogram matching as demonstrated in the previous section. It is therefore vital that

the appropriate value is chosen dependent on the utilisation of the result. For this purpose each of the three measures is computed for different values of the damping parameter. The results are shown as functions of the damping parameter, which makes it easier to choose a suitable value.

Initially the seamline measure is investigated, and it is computed as a function of the damping parameter. Then the saturation is examined and mapped as a function of the damping parameter, and in the next section the contrast is examined and mapped as a function of the damping parameter. Finally all three measures are considered simultaneously.

5.6.2.1 Gradient based quantification of seamlines

In order to see the effect the damping parameter has on the result several tests are made, and the seamline measure is computed every time. The results are shown in Figure 5.17. The figure shows that the curve has a horizontal asymptote marked by the red line. This is the seamline measure of the original test data before any transformation. This is reasonable since a large damping parameter λ will penalize the distance from the original images. Therefore, as the damping parameter goes towards infinity, the result will go towards the original images, and therefore towards the original seamline measure.

It can also be observed from the figure that the vertical axis is a tangent to the curve, and the it touches where the seamline measure is 0. The curve has a very steep descent as it approaches the vertical axis. It should be noted that although the seamlines are less visible it does not necessarily mean that the image is better. A smaller damping parameter penalizes the distance to the original images less, but if the damping parameter is too small the result will be very dark. Therefore the small values of λ will automatically have less visible seamlines, since the result is too dark. The curve touches the y-axis at zero, because at $\lambda = 0$ the resulting images are black, and the seamlines are therefore invisible.

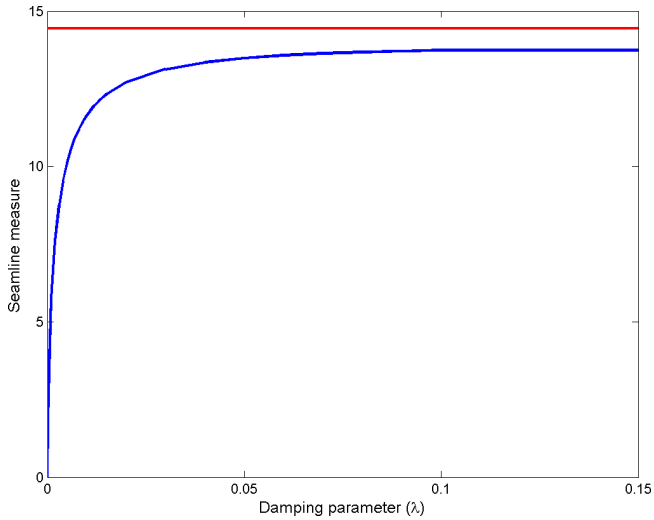

Figure 5.17: *The figure shows the seamline measure as a function of the damping parameter. The results are obtained by making a global histogram matching of the entire test area with 8-neighbourhood. The red line marks the seamline measure of the test area without any colour transformation.*

5.6.2.2 Saturation

The saturation has been computed for the result obtained when global histogram matching with 8-neighbourhood is performed for different values of the damping parameter λ. The result is shown in Figure 5.18. The figure shows that the curve seems to have a vertical asymptote in $\lambda = 0$, and furthermore it has values above 1. This is not as expected, because of the definition of the saturation. This occurs, because some of the pixel values, for very low values of the damping parameter, become negative. This is due to the fact that in the optimization problem, stated in (4.16) in Section 4.4, there is no constraint, to ensure that the pixel values are non-negative. For this reason it is not applicable to use very low values of the damping parameter, but since the resulting graphical map would be black in this case, very low values of the damping parameter would not be used anyway.

The saturation curve has a horizontal asymptote in the saturation value for the original graphical map. It is as expected, since as the damping parameter goes towards infinity, the result goes towards the original graphical map.

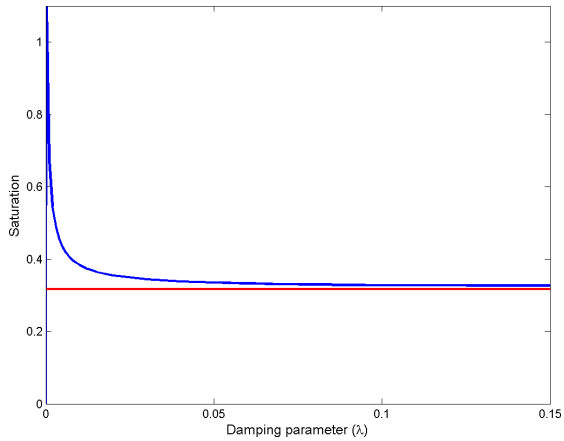

Figure 5.18: *The figure shows the saturation as a function of the damping parameter λ used in global histogram matching with 8-neighbourhood. The red line marks the saturation of the original test set.*

5.6.2.3 Contrast

The Root Mean Square contrast has also been calculated for a number of resulting images from global histogram matching with different values of the damping parameter. The result is shown in Figure 5.19. Like the results in Figure 5.17, the contrast is zero at $\lambda = 0$, since the graphical map is all black. Figure 5.19 also shows that the contrast has a corresponding horizontal asymptote in the contrast of the original graphical map.

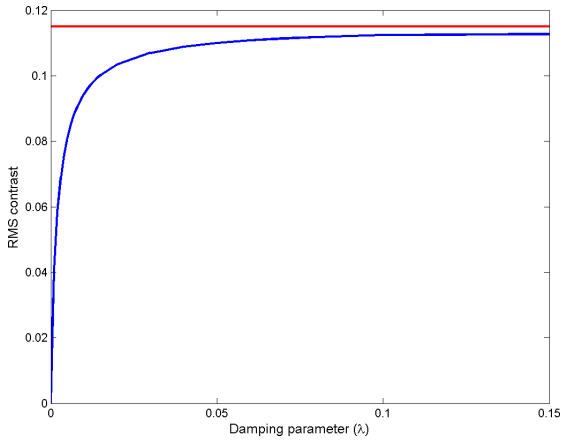

Figure 5.19: *The figure shows the RMS contrast as a function of the damping parameter λ used in global histogram matching with 8-neighbourhood. The red line marks the RMS contrast of the original test set.*

5.6.2.4 Trade-off

The optimal value of the damping parameter can be chosen by making a trade-off of the three measures dependent on the situation. This makes it possible to choose e.g. how important it is to remove the seamlines compared to how much of the contrast can be lost. To help choosing the appropriate damping parameter the three measures are gathered in Figure 5.20 as a function of the damping parameter.
It should be noted that while the seamline measure should be as small as possible, the saturation and the contrast should be as large as possible and that the result is improved with a larger damping parameter in regards to the contrast, but diminished in regards to the seamline measure and the saturation. This is preferred since it means that neither of the two extremes (a damping parameter of 0 or ∞) is optimal, when all three measures are considered.

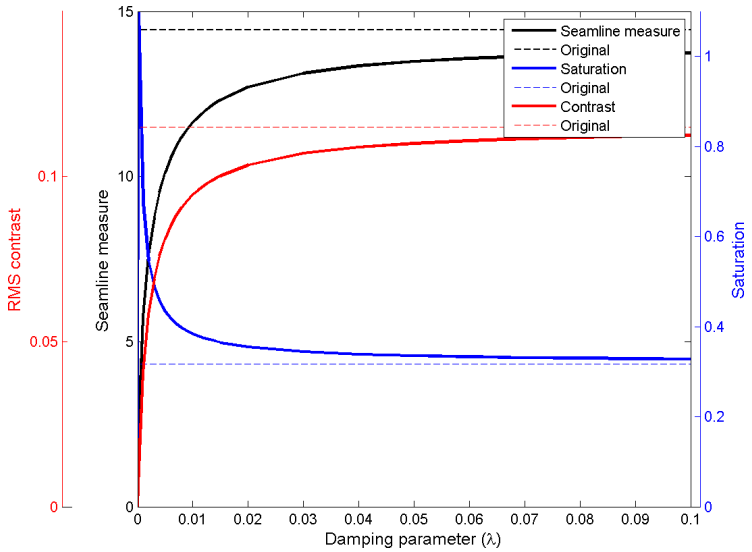

Figure 5.20: *The figure shows the three measures as a function of the damping parameter λ used in global histogram matching with 8-neighbourhood. Each of the measures are shown with the value in the original test area, and their respective vertical axis in corresponding colour.*

5.6.3 Residuals

In order to determine the effect of the damping parameter locally, the residuals of the four examples in Section 5.6.1 are computed. The resulting images are shown in Figure 5.21.

The four images in the figure should be compared to the residuals of the original test area shown in Section 5.1. The standard deviation between the orthophotos is very large in the original image, as expected. The standard deviation is lower for the results of the global histogram matching, and increases as the damping parameter λ increases, as shown in Figures 5.21a-5.21d. This is because the damping parameter penalizes the difference between the transformation matrices and the identity matrix. Therefore the transformation matrices cannot match the colours as well, which results in a high standard deviation.

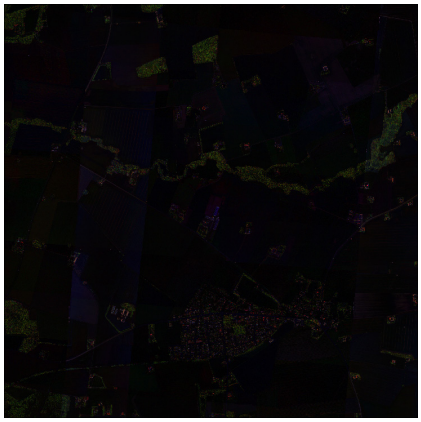

(a) $\lambda = 0.001$

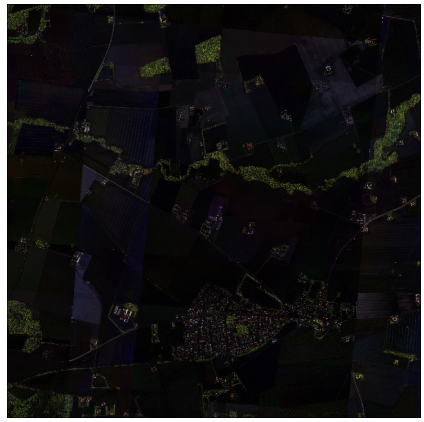

(b) $\lambda = 0.005$

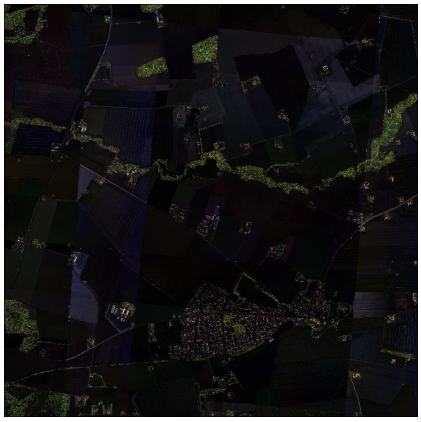

(c) $\lambda = 0.01$

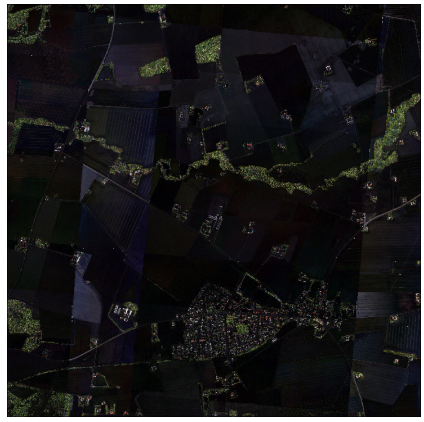

(d) $\lambda = 0.1$

Figure 5.21: *The figure shows the standard deviation of the overlapping orthophotos of (a) the result using global histogram matching with no reference image and damping parameter* $\lambda = 0.001$*, (b) the result using a damping parameter of* $\lambda = 0.005$ *(c) the result using a damping parameter of* $\lambda = 0.01$*, and (d) the result using a damping parameter of* $\lambda = 0.1$*. In order to make the differences in the images more visible, the respective standard deviations have been multiplied by a factor 5.*

It can be observed from Figure 5.21 that the residuals generally become brighter and brighter as the damping parameter increases, which means that the residuals increase as the damping parameter increases. This is as expected, since the result approaches the original data, as the damping parameter increases.

5.7 Global Pixelwise Matching

In pixelwise matching each pixel in the two overlapping orthophotos are matched as described in Section 4.5. An example is computed and the result is compared to the result from global histogram matching.

The result from using global pixelwise matching is shown in Figure 5.22 with the results obtained from using global histogram matching along with the corresponding images of the standard deviation. There is no apparent difference between the two results, and the standard deviation images also appear to be close to identical. Therefore the difference between the two standard deviation images has been computed and is shown in Figure 5.23. The figure shows that there is some difference between the images, however the difference image has been multiplied by 25 in order to make the differences in the images visible.
The three measures described in Section 4.9 are computed and shown in Table 5.4. It is observed that the seamline measure is smaller than for the original graphical map, and that there is only little difference in the measure between the two methods. The difference in the saturation and the contrast is also very small.

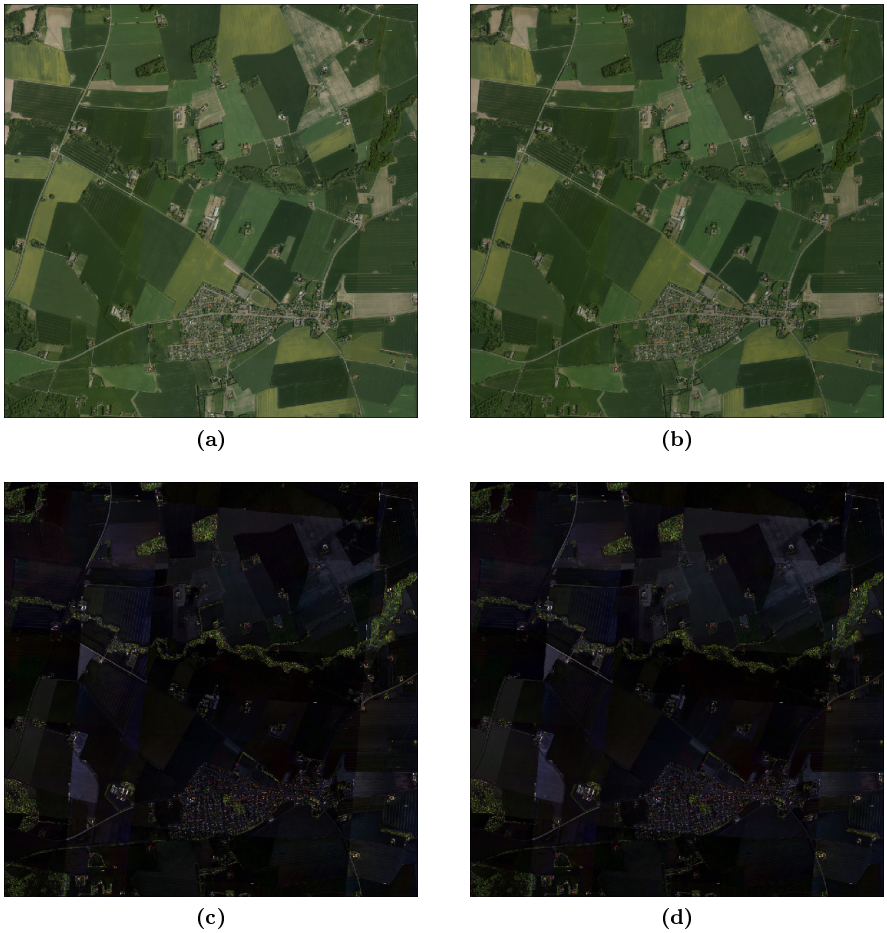

(a) (b)

(c) (d)

Figure 5.22: *The figure shows (a) the result from using global histogram matching, (b) the result from using pixelwise matching, (c) the standard deviations of the result in (a) and (d) the standard deviations of the results in (b). In both cases a damping parameter of* $\lambda = 0.05$ *and 8-neighbourhood is used. In both the standard deviation images the values have been multiplied by a factor of 5 in order to make the differences in the images more visible.*

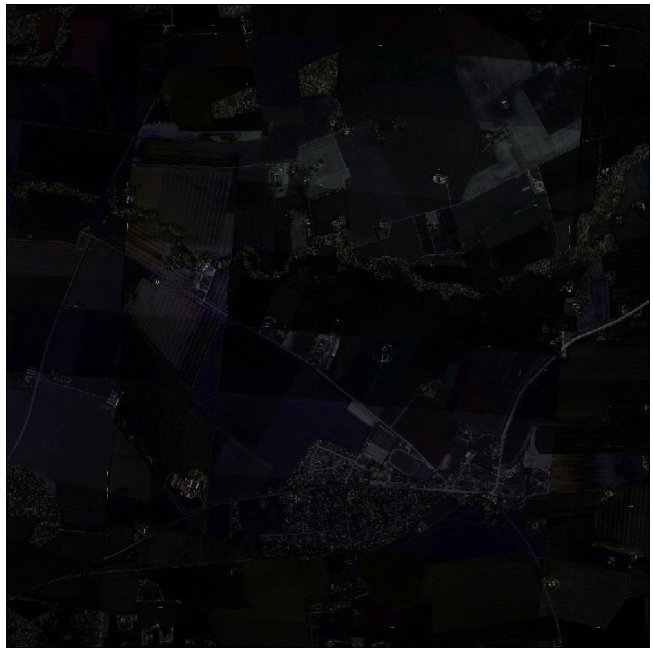

Figure 5.23: *The figure shows the numerical difference between the standard deviation images shown in Figure 5.22c and 5.22d, respectively. The values have been multiplied by a factor of 25 in order to make the differences in the images visible.*

	Histogram Matching	Pixelwise Matching	Original
Seamline measure	13.35	13.41	14.35
Saturation	0.335	0.343	0.316
Contrast	0.110	0.107	0.115

Table 5.4: *The table contains the seamline measure, saturation, and contrast of an example of results from global histogram matching and global pixelwise matching with damping parameter* $\lambda = 0.05$ *and 8-neighbourhood.*

The results shown in Figure 5.22 and 5.23 and the corresponding measurements in Table 5.4 only demonstrate the difference at a single example of the damping parameter, and may just be a single deviation. Therefore the global pixelwise matching has been performed several times, and is quantified by calculating the three measures like it was done for the global histogram matching in Figure 5.20. These results are shown in Figure 5.24 along with the measurements computed from the global pixelwise matching.

It can be observed from the figure that the saturation is a little higher for the

case using global pixelwise matching in the low values of the damping parameter. Simultaneously, the results from the global pixelwise matching has a smaller contrast than the results from the global histogram matching.
The seamlines of the results from the global pixelwise matching are less visible than from the global histogram matching for low values of the damping parameter. However, at approximately $\lambda = 0.045$ this is reversed. This change is likely dependent on the data, since a different dataset will have seamlines at different areas, and they consequently cover different colours and texture, have different lengths etc.
It should be noted that the differences in the three sets of curves are very small, and may depend on the data.

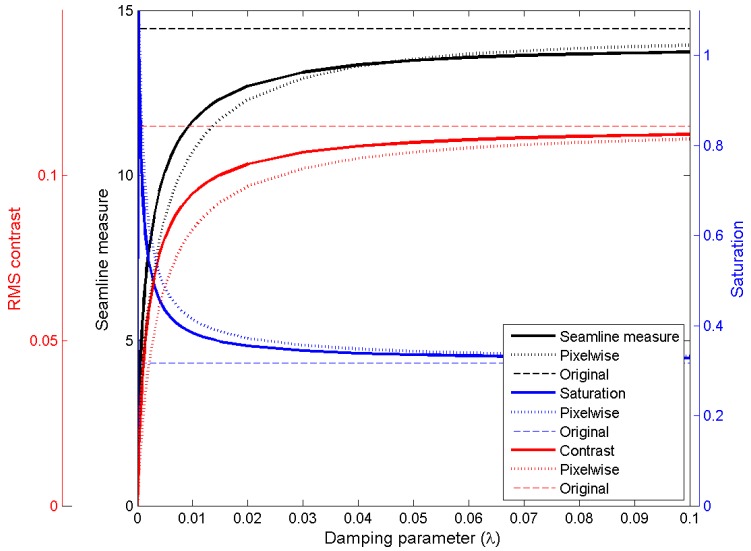

Figure 5.24: *The figure shows the three different measures as functions of the damping parameter. The solid lines are the measures computed of the result of a global histogram matching with 8-neighbourhood, the dotted lines are computed from the results of the pixelwise matching, and the dashed lines mark the measures of the original graphical map. The seamline measure, the saturation, and the contrast are marked with their axes in black, blue, and red, respectively.*

The conclusion from the shown example and the three measures shown in Figure 5.24 is that there is not much difference in the quality of the result from using global histogram matching rather than using global pixelwise matching. This may be because the test area is mostly covered by fields.

5.8 Global Gradual Matching

At first a simple example of global gradual matching using the multiplication method is presented. Afterwards the division method is investigated, first with a one dimensional signal, then with a constructed example with only two orthophotos, and finally with the entire test area.

5.8.1 Multiplication Method

A test example is made by dividing an orthophoto into two overlapping images. The right part of the orthophoto is altered by a gradual transformation given by

$$f(x,y) = \frac{1}{2}x + 1 \ . \tag{5.1}$$

Orthophoto 10 is used in this example. In Figure 5.25 the original orthophoto is shown. This orthophoto is divided into images shown in Figure 5.26, where image 10a is the left part of orthophoto 10 with the original colours, and image 10b is the right part with the given transformation.

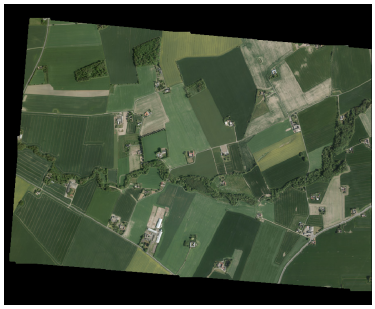

Figure 5.25: *The figure shows orthophoto 10.*

(a) (b)

Figure 5.26: *Orthophoto 10a and orthophoto 10b.*

Global gradual matching is performed on the example, and the result is shown in Figure 5.27b. The figure shows that the seamline between the two images is visible, but not very distinct. The difference between the result and the original orthophoto 10 is shown in Figure 5.28.

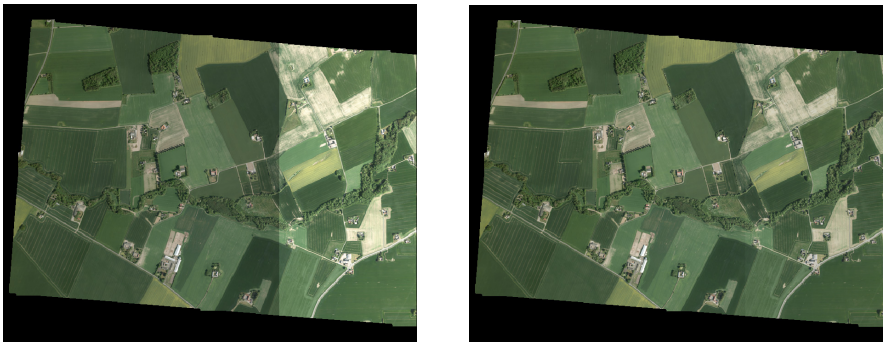

(a) (b)

Figure 5.27: *The figure shows (a) orthophoto 10a and 10b before the transformation, and (b) the result from global gradual transformation of orthophoto 10a and orthophoto 10b with damping parameters* $w_a = w_b = w_c = 500$ *and 4-neighbourhood.*

Figure 5.28: *The numerical difference between of the original orthophoto 10 and the result shown in Figure 5.27b.*

The difference image shown in Figure 5.28 illustrates that the difference in each pixel is still depending on the original colours, i.e. fields, houses etc. are visible. It can also be observed from the figure that the difference in orthophoto 10b is larger than the difference in orthophoto 10a. However, if the images are perfectly matched, the difference would be gradual from left to right, and the seamline should not be visible. This is due to the non-linearity of the resulting images as described in Section 4.6.2.

5.8.2 Division Method

At first, global gradual matching using the division method is used on two one-dimensional signals.

The global gradual matching division method is described in Section 4.6.5. In the following pages a number of experiments are shown in order to determine the effect of the method.

5.8.2.1 One Dimensional Signal

Figure 5.29a shows an example using two one-dimensional signals similar to the ones used in Figure 4.6 in Section 4.6.2. The signals are made by computing 100 random values between 0 and 1, and multiplying with the respective signal magnitudes given by $0.1x + 2$ for signal A and $0.3x + 5$ for signal B, where $x = 1, \ldots, 100$.

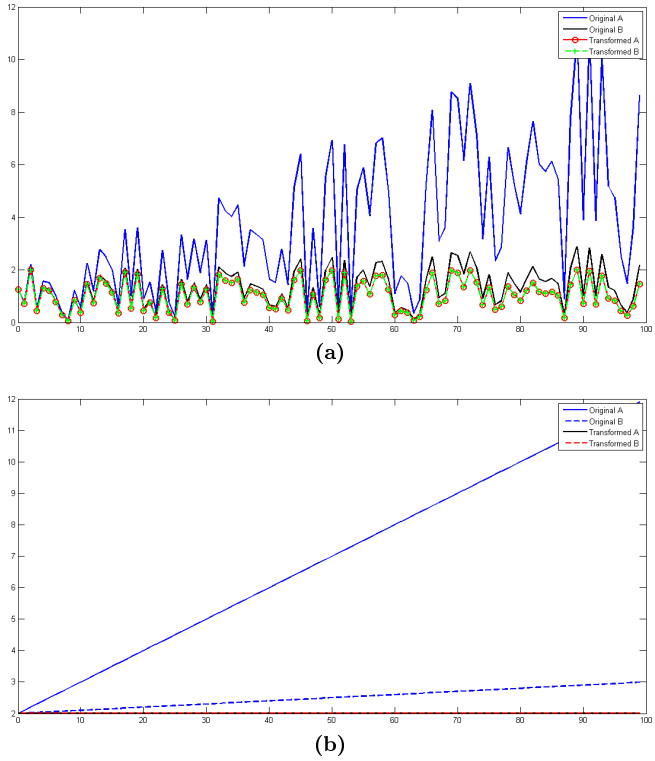

Figure 5.29: *The figure shows (a) the two signals A and B, and their transformed signals using global gradual matching with the division method, and (b) the signal magnitude for signal A, B, and their transformed signals.*

The results are also shown in Figure 5.29a, and it can be observed that the two transformed signals are coinciding as wanted. The signal magnitudes before and after the transformation are shown in Figure 5.29b. In comparison to Figure 4.6b, where the transformed signal magnitudes are quadratic, the signal magnitudes after the transformation using the division method are straight lines as wanted.

5.8.2.2 Constructed Example with two Orthophotos

In order to demonstrate whether the division method removes gradual change in light, the constructed example discussed in Section 5.8.1 is used. The test images before the transformation are shown in Figure 5.26 and 5.27a.

The test images are matched using the division method, and the result is shown in Figure 5.30. The figure shows that the seamline is almost invisible. The difference between the orthophotos in the overlap is computed and shown before and after the transformation in Figure 5.31a and 5.31b, respectively. It can be observed from the figures that there is a large difference in the overlap before the transformation, and that the differences are very small after the transformation. The small differences after the transformation may be due to rounding errors.

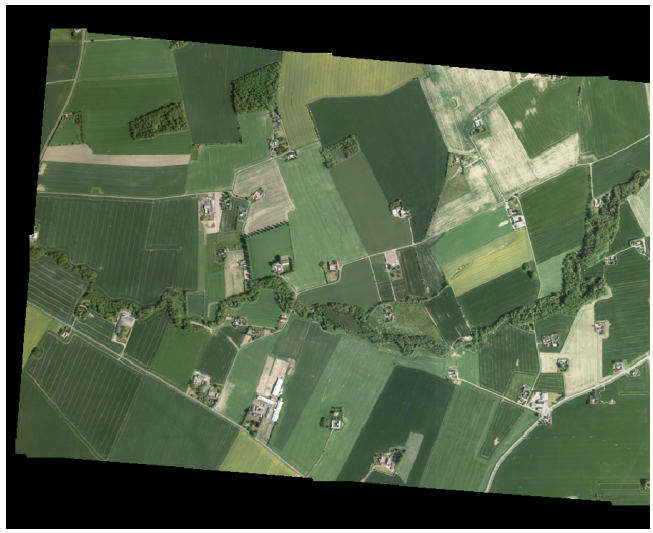

Figure 5.30: *Orthophoto 10a and 10b after the transformation using global gradual matching with the division method. Damping parameters of* $w_a = w_b = w_c = 0.001$.

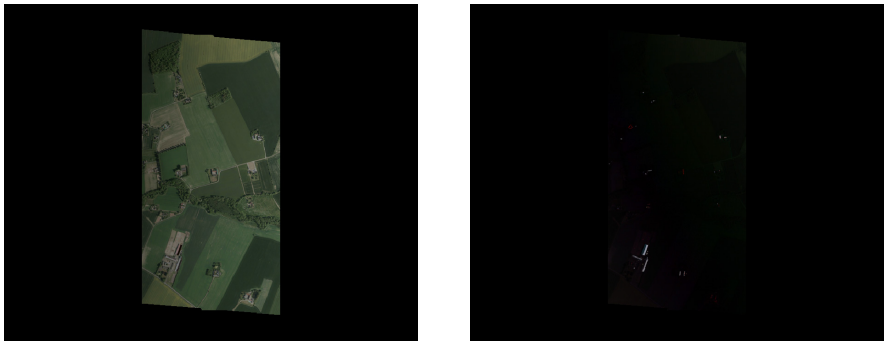

(a) (b)

Figure 5.31: *The figure shows (a) the difference in the overlap between orthophoto 10a and 10b and (b) the difference in the overlap between orthophoto 10a and 10b after the transformation using global gradual matching with the division method and damping parameters of* $w_a = w_b = w_c = 0.001$.

5.8.2.3 Entire Test Area

A number of experiments are performed on the entire test area. Two examples with different damping parameters are investigated, both bandwise and with all three colour bands simultaneously. Then the damping parameter is analysed with respect to the three measures. The use of change detection is studied by comparing the result obtained with and without change detection. Then boundary conditions are examined. This is done by initially comparing several examples with different combinations of parameters, then the effect of the damping parameter is examined with respect to the three measures with constant boundary condition parameters. This shows that there is a value of the damping parameters, where the seamline measure is minimized, and the result from this parameter is studied. Finally a result is shown, which uses both change detection and boundary conditions.

Experiments have been performed on the entire test area shown in Figure 5.1. Two of the results are shown in Figure 5.32 for different values of the damping parameters. The figure shows that there is very little difference between the result using damping parameters of $w_a = w_b = w_c = 0.01$ and the original graphical map. There is a larger difference for the result using damping parameters of $w_a = w_b = w_c = 0.001$. In some areas the seamlines are less distinct, and in some areas they are more distinct. In order to investigate this each colour band is regarded separately. Each colour band for the two results are shown

in Figure 5.33 and 5.34, respectively, along with each band of the original test area. Three areas in the figures are marked by ellipsis, to be used, when the images are compared.

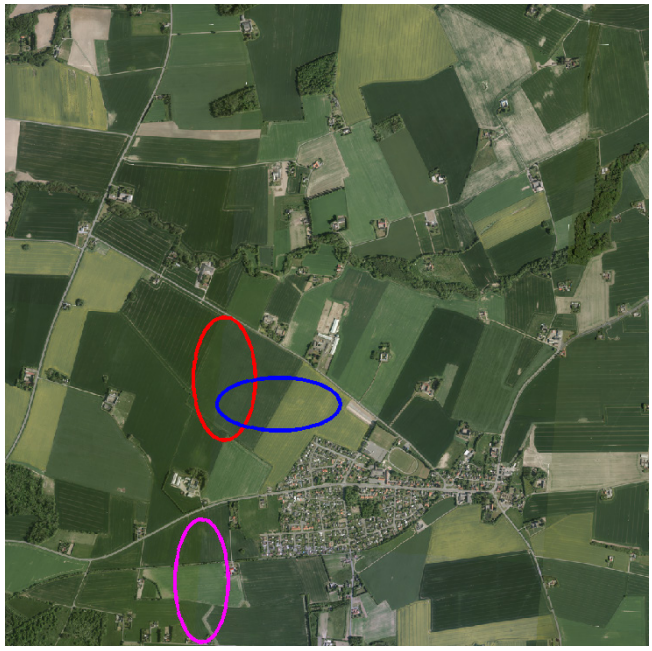

(a) $w_a = w_b = w_c = 0.01$

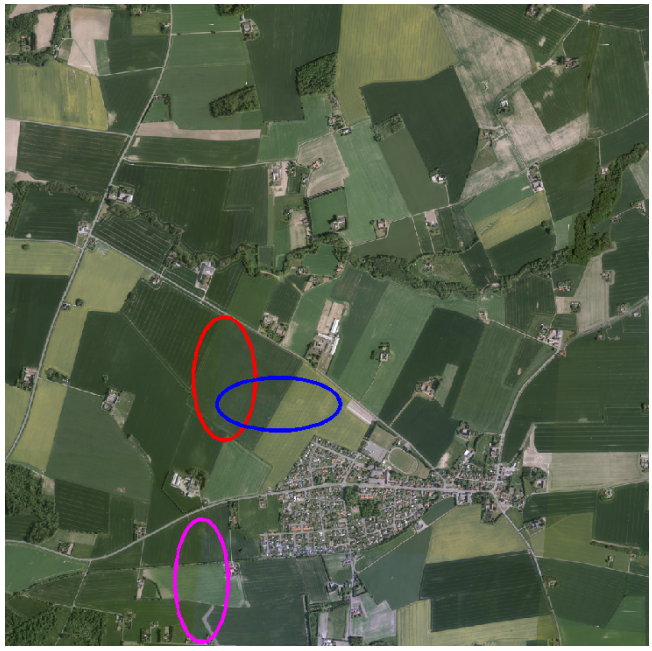

(b) $w_a = w_b = w_c = 0.001$

Figure 5.32: *The figure shows the result from the global gradual matching with the division method using 8-neighbourhood and (a)* $w_a = w_b = w_c = 0.01$ *and (b)* $w_a = w_b = w_c = 0.001$. *Ellipse 1 (red), ellipse 2 (blue), ellipse 3 (magenta).*

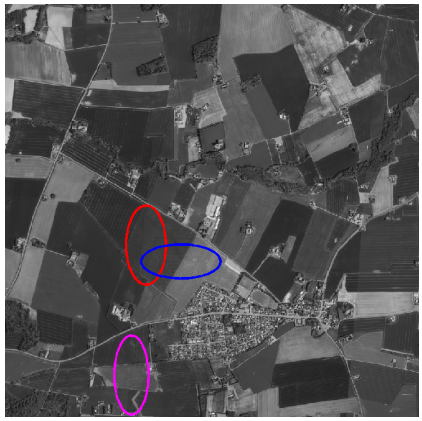

(a) *Original red band*

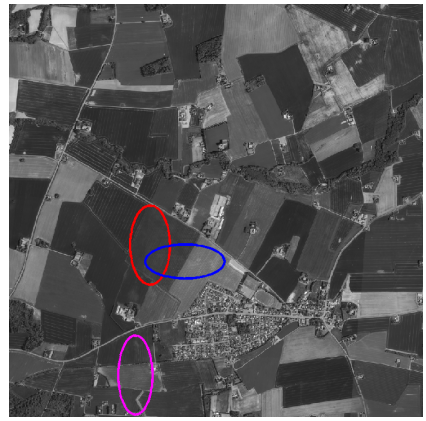

(b) *Result red band*

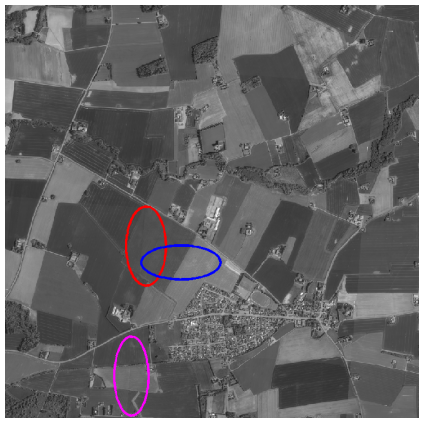

(c) *Original green band*

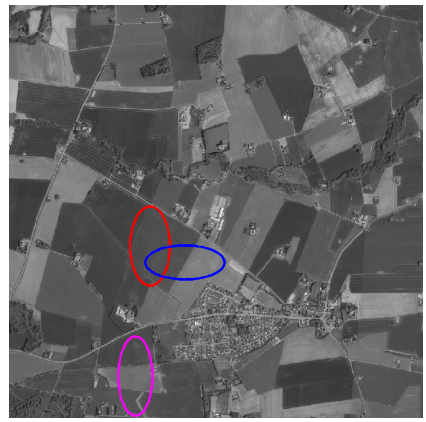

(d) *Result green band*

(e) *Original blue band*

(f) *Result blue band*

Figure 5.33: *The figure shows each band of the original test area on the left and each band of the results from global gradual matching using the division method with damping parameters* $w_a = w_b = w_c = 0.01$ *and 8-neighbourhood. Ellipse 1 (red), ellipse 2 (blue), ellipse 3 (magenta).*

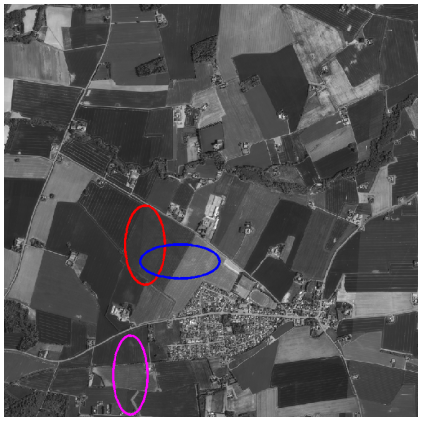

(a) *Original red band*

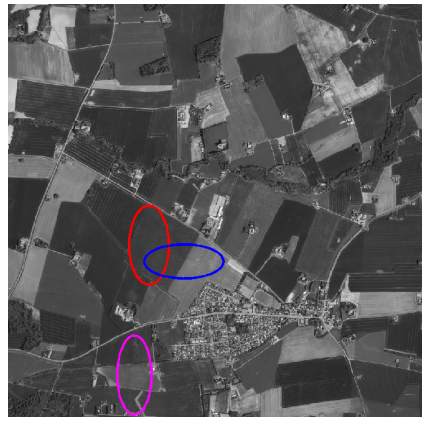

(b) *Result red band*

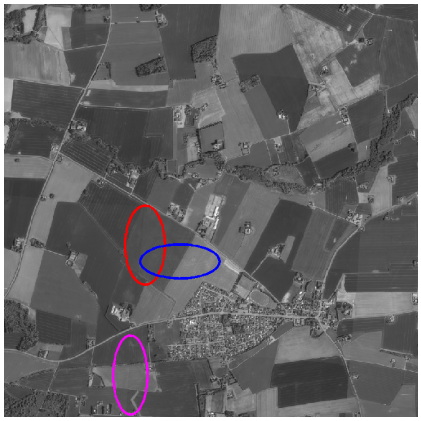

(c) *Original green band*

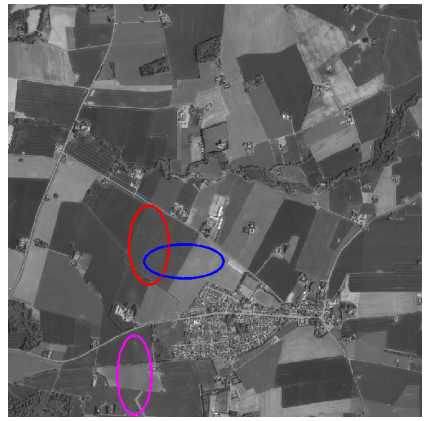

(d) *Result green band*

(e) *Original blue band*

(f) *Result blue band*

Figure 5.34: *The figure shows each band of the original test area on the left and each band of the results from global gradual matching using the division method with damping parameters* $w_a = w_b = w_c = 0.001$ *and 8-neighbourhood. Ellipse 1 (red), ellipse 2 (blue), ellipse 3 (magenta).*

It can be observed from Figure 5.33a, 5.33b, and 5.34b that there is an improvement in the red colour band in ellipse 1 and ellipse 3. The same is the case for the green band shown in Figure 5.33c, 5.33d, and 5.34d. For damping parameters of 0.01 the improvement is larger in ellipse 3, but smaller in ellipse 1 than for 0.001 for both the red and the green colour band. There is no visible change in ellipse 2 in neither the red nor the green band.

The blue band is shown in Figure 5.33e, 5.33f, and 5.34f. The figures show that there is a small improvement in ellipse 1 in both cases. It can also be observed that the seamline in ellipse 2 and 3 are much more distinct than in the original graphical map. The seamline is more distinct for damping parameters of 0.001 in both ellipses. It is thus the change in the blue band that causes the more distinct seamlines, seen in Figure 5.32a and 5.32b.

The three measures described in Section 4.9 are computed and shown in Table 5.5 for the two sets of damping parameters. Here it is seen that in both cases the seamline measure of the result is larger than for the original graphical map, i.e. the seamlines are generally more distinct than originally. It is also seen that in both cases the saturation is smaller than in the original graphical map.

$w_a = w_b = w_c$	0.001	0.01	Original
Seamline measure	17.73	15.45	15.14
Saturation	0.268	0.312	0.315
Contrast	0.119	0.113	0.112

Table 5.5: *The table contains the seamline measure, saturation, and contrast of two examples of results from global gradual matching using the division method with different values of the damping parameters $w_a = w_b = w_c$ and 8-neighbourhood. The results are obtained using a downsampling of 1:20.*

In order to get a clearer overwiev of the quality of the results, several experiments are performed, and the three measures are computed for different values of the damping parameters. The three resulting curves are shown in Figure 5.35. From the figure it can be observed that with smaller values of the damping parameter the larger is the seamline measure. This means that in all cases the seamlines are generally more distinct than in the original graphical map. It is also seen that a smaller value of the damping parameters results in a larger contrast. The saturation initially becomes smaller, but then increases until it reaches the original value, as the damping parameters are increased.

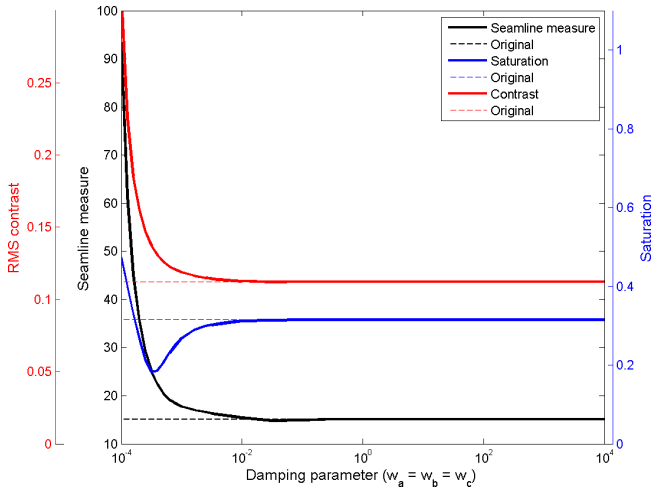

Figure 5.35: *The figure shows the three measures as a function of the damping parameters of same value using the division method and 8-neighbourhood.*

Examples have been made to determine the effect of using change detection in global gradual matching using the division method. The result is shown in Figure 5.36. When the result is compared to the similar result without change detection shown in Figure 5.32b, it can be observed that the seamlines are less distinct, when change detection is used.

Figure 5.36: *The figure shows the result from using global gradual matching with the division method. It was computed using 8-neighbourhood, damping parameters of* $w_a = w_b = w_c = 0.001$*, and change detection with a change detection threshold of* $\alpha = 0.1$*, and change detection convergence limit* $\epsilon = 0.01$*.*

The example in Figure 5.32b shows that the bottom middle orthophoto has become more blue, which is confirmed by the blue band, shown in Figure 5.34f. In order to prevent the colours from becoming too extreme without any further damping on the linear functions, boundary conditions are used as described in Section 4.7. This means that another regularization term is inserted, such that the distance between the original and the resulting colours in the boundary is penalized. An example of this is shown in Figure 5.37.

Figure 5.37: *The figure shows the result from global gradual matching with the division method using 8-neighbourhood, damping parameters of* $w_a = w_b = w_c = 0.01$*, and boundary conditions with damping parameter* $w_B = 10$ *and boundary width* $\delta = 3$*.*

Different experiments have been performed using boundary conditions. Five different parameters have been investigated, the damping parameters w_a, w_b, and w_c, the boundary width δ, and the boundary damping parameter w_B. The values 0, 0.01, and 0.001 have been used for the damping parameters $w_a = w_b = w_c$. The best result obtained was with the value 0.01, see Appendix A.2. The boundary width δ has been investigated by performing experiments with a value of 3 and a value of 50 pixels. It should be noted that these experiments have been performed with a downsampling to a tenth of the original size. This means that the size of the entire test area is 2016×2016 pixels. The experiments showed that a boundary width of 3 gives a better result than 50. The boundary damping parameter w_B has been tested with values of 100, 10, and 0.01. In this case the best result was obtained using a boundary damping parameter w_B of value 10.

The investigations of several combinations showed that the best result was obtained with damping parameters of $w_a = w_b = w_c = 0.01$, and boundary conditions with damping parameter $w_B = 10$ and boundary width $\delta = 3$. This

result is shown in Figure 5.37. Representative results of the other combinations of parameters are shown in Appendix A.2.

Since the result was improved by adding boundary conditions as shown in Figure 5.37, the influence of the damping parameters on the three measures is investigated, now with boundary conditions with a boundary width of $\delta = 3$, and a boundary damping parameter of $w_B = 10$. The resulting curves are shown in Figure 5.38. Here it is shown that there is a minimum value of the seamline measure at approximately $w_a = w_b = w_c = 0.025$. It can also be observed that there is only a small decrease in contrast, and a small increase in saturation, as the damping parameters decrease. The result for the minimum value is shown in Figure 5.39.

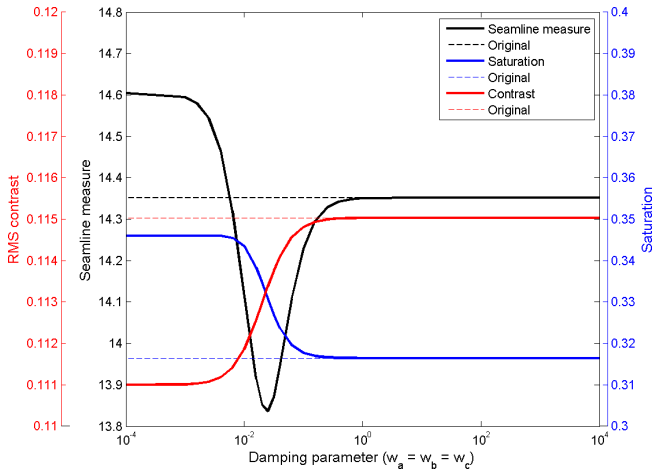

Figure 5.38: *The figure shows the three measures as a function of the damping parameters $w_a = w_b = w_c$ using 8-neighbourhood and boundary conditions with a boundary width of $\delta = 3$, and a boundary damping parameter $w_B = 10$.*

Figure 5.39: *The figure shows the result from global gradual matching with the division method using 8-neighbourhood, damping parameters of* $w_a = w_b = w_c = 0.025$*, and boundary conditions with damping parameter* $w_B = 10$ *and boundary width* $\delta = 3$*.*

The result in Figure 5.39 shows that some of the seamlines are more distinct than in Figure 5.37, and the seamlines in some areas are less distinct. It is not obvious that the result in Figure 5.39 is better than Figure 5.37 to an observer, but the seamline measure computes the sum of the difference in the gradiants in all seamlines, and is not a measure for the individual seamlines.

Finally, a result is computed, which uses both change detection and boundary conditions. A number of experiments have been performed to tune the three sets of parameters: The parameters for the regularisation, the change detection, and the boundary conditions. The tuning has been performed, such that the contribution of each of the three sets of parameters balances. The result is shown in Figure 5.40.

Figure 5.40: *The figure shows the result from global gradual matching with the division method using 8-neighbourhood, damping parameters of* $w_a = w_b = w_c = 0.0001$*, boundary conditions with damping parameter* $w_B = 10^{-6}$ *and boundary width* $\delta = 3$*, and change detection with a change detection threshold parameter of* $\alpha = 0.1$ *and change detection convergence limit* $\epsilon = 0.01$*.*

The result in Figure 5.40 shows that the vertical seamline in the left side of the image is almost invisible, and the colours seem to be closer to the original colours, shown in Figure 5.1, than the result with boundary conditions, but without change detection, in Figure 5.37.

5.8.2.4 Comparison with Global Pixelwise Matching

The result from global gradual matching with the division method and boundary conditions is compared to the results obtained using global pixelwise matching.

The results from the two methods are shon in Figure 5.41.

(a) *Global pixelwise matching using a damping parameter of* $\lambda = 0.05$

(b) *Global gradual matching with the division method using damping parameters of* $w_a = w_b = w_c = 0.01$ *and boundary conditions with damping parameter* $w_B = 10$ *and boundary width* $\delta = 3$

Figure 5.41: *The figure shows a result from (a) global pixelwise matching, and (b) global gradual matching, both using 8-neighbourhood.*

The vertical seamline at the left is highly reduced in the dark green field in both images. The seamline is less distinct in Figure 5.41b than in Figure 5.41a. The colours are darker in Figure 5.41a than in Figure 5.41b, and therefore the seamlines in the right side are less distinct in Figure 5.41a. The dark colours in Figure 5.41a also makes it difficult to distinguish the objects in the image.

Chapter 6

Future Work

In this chapter some suggestions for future investigations are described.

Flight Lanes

The orthophotos are made from a plane flying in parallel lanes. The overlap between subsequent orthophotos within a lane is therefore much larger than the overlap between neighbouring orthophotos in different lanes. Furthermore, the difference in the colours in orthophotos within a lane is much smaller than between lanes. Therefore, more colour correction is needed to match the orthophotos between lanes than matching orthophotos within a lane. However, since there are more pixels in the overlaps within a lane, this has a larger impact on the result. It could therefore be investigated whether the result will be improved, if a global gradual matching is first performed on each lane and then performed between the lanes.

Penalized Areas

When global gradual matching is used, boundary conditions can be added as described in Section 4.7. This method can be modified, such that, in certain areas, the colour differences between the original image and the result are penalized. In this way areas that have suitable colours can be chosen, such that the colour changes in these areas are limited.

This method could be expanded, such that certain areas are initially histogram matched to an ideal colour histogram. In this way the areas to be penalized can be created.

Higher Order Model

An advantage of the global gradual matching algorithm is that it can easily be expanded to use a higher order model, as the $\widetilde{R}_{ij}$ matrix in Equation (4.82) is merely added one or more columns. It could be investigated whether a higher order model gives a better result.

Other Data

The methods presented in this thesis are very dependent on the parameters, and it would therefore be prudent to perform experiments on different data sets. Experiments could be made on data with different content e.g. different ratio between buildings, fields, forests etc. to get a better basis for choosing the appropriate parameters.

It could be prudent to investigate, whether the parameters chosen in this project would give a good result, if the given test area was expanded in all four directions. If the area was expanded, it would be possible to see, if the vertical seamline in the right side of the test area would become less distinct.

The results could be improved by using 16-bit images instead of the current 8-bit images. Thereby the images would contain all the original data, and the matching will be performed based on more information.

The 8-bit data obtained from COWI A/S, has already been colour rectified to remove some of the light differences caused by the position of the sun. It could be investigated, whether the results from global gradual matching could be improved, if the discarded information was available.

A Priori Solution

As described in Section 5.8.2 the enhanced seamlines in the result from global gradual matching shown in Figure 5.34 are caused by a bad solution for the blue band. However, the seamlines in the green band are improved. Therefore

a better solution for the blue band may be found, if the solution for the green band is used as an a priori solution. This means that Equation (4.102) is altered, such that the solution from the green band is used as an initial solution, thus replacing the v vectors.

Chapter 7

Discussion

In Chapter 5 the methods described in Chapter 4 have been investigated by computing several examples, using different parameters. The investigations show that the many different parameters in the methods have influence on the results.

The final graphical map is greatly influenced by the mosaicking method. After the colour correction the seamlines should be placed, such that the remaining colour differences are hidden. This is not done in this thesis, since only the colour transformation is investigated, and a better mosaicking would reduce the visibility of the seamlines, and therefore the visibility of the quality of the colour correction. For the same reason feathering has not been used in this project.

Computational time
Since colour correction in aerial imagery is performed on a lot of data, it is necessary to reduce the used amount of data, in order to reduce the computational time. In this project the computational time is reduced by downsampling the images, and by estimating coefficients on only some of the overlaps. In this case it is done by only using the overlaps of the 4 or the 8 nearest neighbours. The choice of neighbourhood therefore has influence on the result. As shown in Section 5.2, 8-neighbourhood gives better results than 4-neighbourhood, since the coefficient estimation is based on more data. The downside of using 8-neighbourhood is that the computational time is much higher than for 4-neighbourhood.

Methods
In this thesis three colour correction methods are presented: Global histogram matching, global pixelwise matching, and global gradual matching.

Global histogram matching
Global histogram matching was initially used with a reference image. This meant that the solution was pulled in direction of a single image, and therefore it was very dependent on the choice of reference image. Therefore the use of regularization is chosen instead of a reference image.

The results from global histogram matching is greatly influenced by the used damping parameter. A low damping parameter will give less distinct seamlines, but it is at the expense of the contrast of the image. This means that as the damping parameter goes towards zero, the resulting image will become darker and darker. At the same time the saturation is increased as the damping parameter is decreased. As the damping parameter goes towards infinity, the result will go towards the original graphical map. Therefore the damping parameter should be chosen as a trade-off, depending on how important it is to remove seamlines, compared to how much contrast is lost in the process.

As shown in the results from the experiments, global histogram matching can be improved by using change detection. Change detection is highly dependent on the choice of the change detection threshold. This should be chosen in accordance with the data.

Global pixelwise matching
Global pixelwise matching is influenced by the value of the damping parameter and by change detection in the same way as global histogram matching. There is not much difference between the results from the global pixelwise matching and the results from global histogram matching for this test area. This may not always be the case, since pixelwise matching is more dependent on the quality of the georeferencing than histogram matching. The quality of the georeferencing is out of the scope of this thesis.

Since the global histogram matching is performed bandwise, the colour transformation matrix should be a diagonal matrix, because any possible colour dependency between the bands has been removed by the histogram matching. This was discovered very late in the project, and has therefore not been implemented. However, since the off-diagonal elements in the colour transformation matrix are small, this will have little effect on the results. An advantage of using the global pixelwise matching is that the dependency between the colour bands is not removed by the histogram matching, and a full matrix model may be used.

Furthermore, the computational time of the global histogram matching is a little higher than that of the global pixelwise matching, since both methods use the same way of estimating the linear model, but only the global histogram matching computes the histograms and performs the histogram matching.

In the experiments, performed in this thesis, the described issues of the two methods are not significant for the results, and the results of the two methods are almost the same.

Global gradual matching
The global histogram matching algorithm and the global pixelwise matching algorithm estimate a linear colour transformation matrix for each orthophoto. This means that the same colour transformation is performed on the entire orthophoto, which may not always be ideal, since the light conditions may not be constant over the entire orthophoto. The global gradual matching algorithm is therefore based on the assumption, that there is a linear change in the sunlight from one end of the orthophoto to the other.

In the multiplication method a bilinear function is multiplied on the colour values. The downside of this method is that a linear change in light is multiplied on the colour values, and the colour correction therefore introduces a quadratic dependency of the pixel positions. This may introduce very large or very small colour values, and it will make it very difficult to match more than two images. This means that in order to remove a linear function that is multiplied on the actual colours, the image should be divided by a linear function.

Dividing the image by a linear function introduces a non-linearity. This cannot be solved by using the logarithm method, mentioned in Section 4.6.4, since the logarithm itself introduces a non-linearity. Therefore the division method uses the reciprocal colour values in order to make the problem linear.

The global gradual matching with the division method is highly dependent on the three damping parameters, since they determine how large the coefficients of the linear function can be, and therefore how much the images are able to change. Experiments in this thesis show that the global gradual matching algorithm can make some seamlines less distinct while other seamlines become more distinct as shown in Figure 5.32. It can be seen in Figure 5.35 that the seamline measure becomes larger as the damping parameters decrease. This means that in general the seamlines become more distinct, however, the examples show that while they become more distinct in some areas, they become less distinct in other areas. Investigations of the colour bands separately show that it is in the blue band, the seamlines become more distinct. This is because the blue colour values increase in the orthophotos in the bottom of the middle lane in the test area. There is an improvement, when change detection is used, but the result is not as good as desired.

Boundary conditions
The result from global gradual matching is more affected than results from the other two methods by the fact that the orthophotos at the boundaries have

less neighbours, since this may affect the slope of the linear correction function. Therefore boundary conditions are used on global gradual matching to prevent this effect.

The addition of boundary conditions improves the results of the global gradual matching, and the problem with the blue colours, mentioned above, is reduced. Boundary conditions are used to penalize the difference between the original colours and the colours after the transformations in the boundary of the test area. This means that boundary conditions are used to control the solution, without holding the pixels to their original value, as is done, if reference images are used. The result from using boundary conditions then depends on two additional parameters: The boundary width and the boundary damping parameter. If the boundary width is too large, too many pixels have to be closer to the original value, and this will therefore limit the changes, the model is able to make in a larger area. On the other hand, if the boundary is too narrow, it will be highly influenced by possible errors on the boundary. If the boundary damping parameter is too high, the pixels at the boundary are not permitted to change much, and the model will have to adapt. Therefore the model will most likely not be able to change the colours at the boundary orthophotos, and is not able to match these orthophotos to each other. If the boundary damping parameter is too small, the boundary will have no influence on the result.

Figure 5.38 shows that when boundary conditions are used, there is a value of the damping parameters, where the minimum seamline measure is obtained. It can also be deduced from the figure that another advantage of using boundary conditions is that the contrast does not decrease very much, when lower damping parameters are used, but still, the result using the optimal damping parameters shown in Figure 5.39 was not visually better than the solution shown in Figure 5.37. However, since the seamline measure is the sum of the differences in the gradients for all seamlines, all the individual seamlines may not be less distinct to the observer. In order to investigate further the effect, boundary conditions have on the result, more experiments should be made, where the boundary width and the boundary damping parameter vary.

A comparison between the result from global pixelwise matching and global gradual matching with the division method is made in Section 5.8.2.4. It states that seamlines in the left side of the area are less distinct in both cases, and that the result from global pixelwise matching is darker, which makes the seamlines in the right side of the area less distinct, but also makes it harder to distinguish the objects in the image.

Figure 5.40 shows a result from global gradual matching with the division method using both boundary conditions and change detection. This result shows that some of the seamlines are almost invisible, and the colours match the orig-

inal colours much more, than when only boundary conditions were used. In order to find the result with the optimal parameters, a further analysis of the effect of the parameters, when regularization, boundary conditions, and change detection are used simultaneously, should be performed.

It should be noted that the vertical seamline between the middle and the right flight lane has not been removed by any of the experiments. This may be because the colour difference on either side of the seamline is larger than the difference on either side of the seamline between the left and the middle flight lane. This has been independent on which colour correction method is used.

Measures
During the project three measures have been used to quantify the quality of the results. The values of the three measures have been compared to the visible impression of the results throughout the experiments.

The seamline measure is based on the gradient at the seamline. The advantage of this is that a value is obtained, which makes it possible to compare the results mathematically. The downside is that it may not always describe how the seamline is observed. An observer would see a seamline, going through e.g. a field which has very little variation, much clearer than a seamline, going through e.g. a town or a forest with much higher variation. The seamline measure will weigh all areas equally without taking the contents of the image into account.

The contrast measure is based on the difference between the low and high pixel values, and therefore the visible difference between dark and bright areas.

The saturation measure is based on the relative intensity of the three colour bands. If the saturation is small, the colours will be more greyish, which makes it harder to see differences in the image. If the saturation is high, the colours will look more clear, because one or two of the bands are significantly higher than the rest.

The three measures therefore seem like a good way to quantify the quality of the resulting images. However, the seamline measure may not always describe, how distinct an observer will see the different seamlines.

Chapter 8

Conclusion

In this thesis three main methods to perform colour correction on overlapping orthophotos is presented: Global histogram matching, global pixelwise matching, and global gradual matching.

All three methods can be affected by the use of mosaicking, neighbourhood, and change detection.

In addition to the colour correction methods described in this thesis, a better mosaicking method can be a great improvement to the results, but this is outside the scope of this project.

The difference between using 4-neighbourhood and 8-neighbourhood is not very large, but better results are obtained using 8-neighbourhood, since it is based on more information. If it is possible, regarding the computational time, it is better to use 8-neighbourhood or even more overlaps.

Change detection gives an improvement on the results, since it removes pairs of pixels, which are not comparable.

The three methods, global histogram matching, global pixelwise matching, and global gradual matching, have been developed and investigated in experiments.

Global histogram matching reduces the present seamlines, but it is at the expense of the contrast. This is a disadvantage of using this method. It is very dependent on the choice of damping parameter, but shows some improvement, when change detection is used. The amount of change detection used should be

chosen in accordance with the type of area.

The results obtained, using global pixelwise matching, are not much different from the results from global histogram matching. The method is also very dependent on the damping parameters, and obtains less distinct seamlines when the result is darker. It is more dependent on the quality of the georeferencing, but can take possible dependency between the colour bands into account. However, neither of these have caused a visible difference between the results from the two methods for the provided test data.

Global gradual matching with the division method has the advantage that it is not constricted to perform the same colour transformation over the entire orthophoto. This property is contrary to both global histogram matching and global pixelwise matching, which estimate a constant colour transformation matrix for each orthophoto.

Furthermore, global gradual matching can improve the seamlines without much loss in contrast, when boundary conditions are used, despite the fact that the seamline measure shows that the method only makes the seamlines more distinct, when the damping is reduced. As the seamlines improve in one area, when the global gradual matching is used, they may become more distinct in another area. This makes it difficult to choose a set of parameters.

From the experiments performed in this thesis, the results from global pixelwise matching have not appeared to be much different from the results from global histogram matching, but pixelwise matching is preferred, because of the smaller computational time and the fact that the global histogram matching is performed bandwise. However, this does not give as good results as global gradual matching, which is therefore recommended. It is important for good results using global gradual matching that this method is used with boundary conditions and change detection in order to obtain the best results.

Appendix A

Appendix

A.1 Correction to Rasmussen 2010

In [15] the expression is given in (5.14) by

$$\begin{bmatrix} K_{12}+K_{13}+\dots & -L_{12} & -L_{13} & \cdots \\ -L_{21} & K_{21}+K_{23}+\dots & -L_{23} & \cdots \\ -L_{31} & -L_{32} & K_{31}+K_{32}+\dots & \cdots \\ \vdots & \vdots & \vdots & \ddots \end{bmatrix} \begin{bmatrix} A_1 \\ A_2 \\ A_3 \\ \vdots \end{bmatrix} = 0 \ . \tag{A.1}$$

However, since the transformantion matrices are transposed in the expression (5.13) given by

$$\frac{\partial F}{\partial A_i} = \sum_{j \in \mathcal{N}(i)} K_{ij} A_i^T - L_{ij} A_j^T = 0 \ , \tag{A.2}$$

the transformation matrices should also be transposed in the linear system of equations, which yields

$$\begin{bmatrix} K_{12}+K_{13}+\dots & -L_{12} & -L_{13} & \cdots \\ -L_{21} & K_{21}+K_{23}+\dots & -L_{23} & \cdots \\ -L_{31} & -L_{32} & K_{31}+K_{32}+\dots & \cdots \\ \vdots & \vdots & \vdots & \ddots \end{bmatrix} \begin{bmatrix} A_1^T \\ A_2^T \\ A_3^T \\ \vdots \end{bmatrix} = 0 \ . \tag{A.3}$$

A.2 Boundary Conditions

A number of experiments have been performed using global gradual matching with the division method and boundary conditions. The results have been obtained using different values of the damping parameters w_a, w_b, and w_c, the boundary width δ, and the boundary damping parameter w_B.

The results are presented in this section. They are discussed in Section 5.8.2.3.

(a) $w_a = w_b = w_c = 0.01$ $\delta = 3$ $w_B = 10$

(b) $w_a = w_b = w_c = 0$ $\delta = 3$ $w_B = 10$

Figure A.1: *Two results from global gradual matching with the division method using 8-neighbourhood.*

(a) $w_a = w_b = w_c = 0.001$ $\delta = 3$ $w_B = 10$

(b) $w_a = w_b = w_c = 0.01$ $\delta = 50$ $w_B = 10$

Figure A.2: *Two results from global gradual matching with the division method using 8-neighbourhood.*

(a) $w_a = w_b = w_c = 0.01$ $\delta = 3$ $w_B = 0.01$

(b) $w_a = w_b = w_c = 0.01$ $\delta = 3$ $w_B = 100$

Figure A.3: *Two results from global gradual matching with the division method using 8-neighbourhood.*

Bibliography

[1] T. Bjerge. *Lyslære*. Ejnar Munksgaard, 1951.

[2] S. Buch, K. Dueholm, S. Elgaard, A. Flatman, C. Hviid, J. Hohle, H. F. Jepsen, L. T. Jørgensen, V. W. Laursen, P. S. Madsen, and J. M. Sørensen. *Specifikation for ortofotos*. Geoforum Danmark, 2 edition, November 2005.

[3] J. M. Carstensen (Ed.). *Image analysis, vision and computer graphics*. Technical University of Denmark, 2 edition, August 2002.

[4] Lars Elden, Linde Wittmeyer-Koch, and Hans Bruun Nielsen. *Introduction to Numerical Computation - Analysis and MATLAB Illustrations*. Studentlitteratur AB, July 2004.

[5] EXELIS. ENVI Orthorectification Module. `https://www.exelisvis.com/Home/NewsUpdates/TabId/170/ArtMID/735/ArticleID/12404/ENVI-Orthorectification-Module.aspx`, 2013. [Online; accessed 26-December-2013].

[6] Lars Hansen. CDT3 Ltd., Personal communication, 2013.

[7] Per Christian Hansen, James G. Nagy, and Dianne P.O'Leary. *Deblurring Images Matrices: Spectra, and Filtering*. Society of Idustrial and Applied Mathematics, 0 edition, 2006.

[8] Regin Møller Sø rensen. COWI A/S, Personal communication, 2013.

[9] R. Naoum and A. Al-Sabbah. Colour image enhancement using steady state genetic algorithm. *World of Computer Science and Information Technology Journal*, 2(6):184–192, 2012.

[10] Ordnance Survey. The national mapping agency of Great Britain. *Specification for imagery data for the OS MasterMap Imagery Layer*. Corporate Design and Publishing, 3.1 edition, May 2011.

[11] A. A. Nielsen. The regularized iteratively reweighted MAD method for change detection in multi- and hyperspectral data. *IEEE Transactions on Image Processing*, 16(2):463–478, feb 2007.

[12] M. Ø . Nielsen. True orthophoto generation. Master's thesis, Technical University of Denmark, Department of Informatics and Mathematical Modelling, August 2004.

[13] G. Palubinskas, R. Muller, P. Reinartz, and M. Schroeder. Radiometric normalization of sensor scan angle effects in optical remote sensing imagery. *International Journal of Remote Sensing*, 28, October 2007.

[14] Kaare Brandt Petersen and Michael Syskind Pedersen. *The Matrix Cookbook*. DTU IMM, November 2012.

[15] A. T. Rasmussen. Color adjustment of orthophotos. Master's thesis, Technical University of Denmark, Department of Informatics and Mathematical Modelling, March 2010.

[16] Søren Andersen. COWI A/S, Personal communication, 2013.

[17] M. A. Sadeghi, S. M. M. Hejrati, and N. Gheissari. Poisson local color correction for image stitching. pages 275–282, 2008.

[18] C.-M. Tsai and Z.-M. Yeh. Contrast enhancement by automatic and parameter-free piecewise linear transformation for colour images. *IEEE Transactions on Consumer Electronics*, 54(2):213–219, 2008.

[19] Wikipedia. Wikipedia Contrast (vision). `http://en.wikipedia.org/wiki/Contrast_%28vision%29`, 2013. [Online; accessed 26-December-2013].

[20] Wikipedia. Wikipedia Georeference. `http://en.wikipedia.org/wiki/Georeference`, 2013. [Online; accessed 26-December-2013].